CALIFORNIA INSTITUTE OF TECHNOLOGY

CIT - ELECTRON TUBE & MICROWAVE
LABORATORY REPORT

THEORY OF PLASMA WAVE RESONANCES IN A HOT NONUNIFORM PLASMA

by

Jerald V. Parker

Technical Report No. 23

Nonr 220(50)

June 1964

THEORY OF PLASMA WAVE RESONANCES IN A HOT NONUNIFORM PLASMA

by

Jerald V. Parker

Technical Report No. 23
CALIFORNIA INSTITUTE OF TECHNOLOGY
Pasadena, California

A Technical Report to the Office of Naval Research
Contract Nonr 220(50)

June 1964

ABSTRACT

This work is concerned with the resonant motion exhibited by a plasma column which is excited by an oscillating electric field transverse to the column. A theory is considered which includes the effects of electron temperature and of nonuniformities in the plasma electron density. In order to have a quantitative theory, the nonuniform electron densities used are calculated numerically using a theory due to Tonks and Langmuir.

The theory yields a fourth order differential equation which is integrated numerically to find the predicted resonant frequencies. The predictions are compared with experiment and show excellent agreement. It is concluded that the nonuniform electron density plays a crucial role in determining the resonant frequencies.

The effect of an axial magnetic field upon the resonances has been investigated. It is shown that the field causes each resonance to split into a right and left circularly polarized resonance whose frequencies depend on the field strength. These preliminary calculations have been checked with experiment and they give good qualitative agreement.

Possible diagnostic uses of these results are considered.

Table of Contents

SECTION I - INTRODUCTION TO PLASMA WAVE RESONANCES

1.1 Experimental Observations

Several investigations of the response of a mercury positive column to a radio frequency electric field were carried out during the late 1920's and early 1930's. In 1931 Tonks (1,2) reported a series of measurements demonstrating a resonant response associated with the plasma. The occurrence of this resonance was not unexpected because the simple theory describing the positive column as a gas of cold electrons predicted that a resonance should occur. However, Tonks also reported ovserving one or two additional resonances at higher frequencies. Tonks attempted to explain these extra resonances in terms of magnetic effects or nonuniform effects but he was not successful.

No further investigations were made of this phenomenon until the early 1950's. A problem similar to the mercury positive column was encountered in connection with the scattering of radio signals from the ionized trails left by meteors entering the atmosphere. This initiated several experimental investigations of scattering carried out by Denno, et al (3) at 3 cm. wavelength and by Rommel (4) at 30 cm. wavelength. The existence of the several additional resonances was again reported but not explained. Dattner (5) conducted extensive investigations of these additional resonances by observing the scattering of microwave signals in a waveguide which contained a mercury discharge column. He reported not two, but a whole series of additional resonances, each successively higher frequency resonance being weaker until they could no longer be detected.

Because of the current interest in radio scattering in the ionosphere and the defense aspect of scattering from the reentry trails of missiles, several attempts have been made to explain these resonances. Particular interest has been directed toward determining the physical parameters which affect the strength of each resonance, the spacing of the resonant frequencies, and the number of observable resonances. The next section will review the various theories which have been advanced and their predictions.

1.2 Theoretical Investigations

The elementary theory used by Tonks to explain the occurrence of the lowest frequency resonance neglects the effects of electron temperature upon the plasma. The plasma is assumed to be a uniform cold electron gas with a background of fixed ions to provide charge neutrality. In this case the plasma behaves as a dielectric with a permittivity

$$\epsilon = \epsilon_o \left(1 - \frac{\omega_{po}^2}{\omega^2} \right) \tag{I.1}$$

where $\omega_{po}^2 = n_o e^2 / \epsilon_o m_e$ and n_o is the electron density. Figure 1 defines what will be called the cylindrical geometry problem in the remainder of this paper. Because the resonances under investigation occur when the electric field is transverse to the cylinder axis, the problem is essentially a two-dimensional one.

If $\underset{\sim}{E}_{applied}$ is the electric field of an electromagnetic wave it will be assumed that the wavelength is much larger than the dimensions of the cylinder so the $\underset{\sim}{E}_{applied}$ may be taken to be a uniform

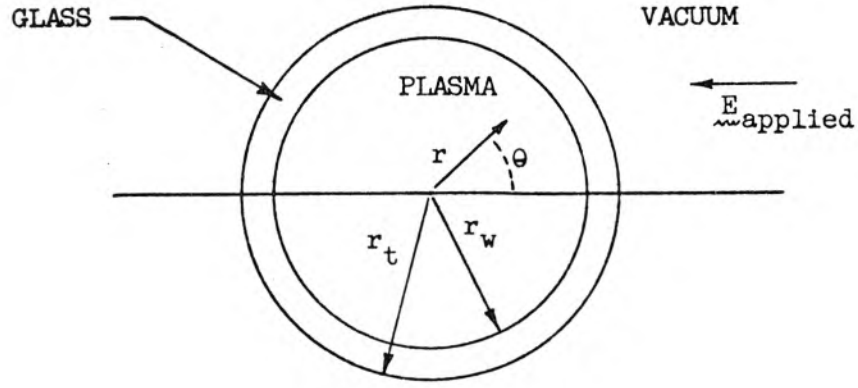

Figure 1.

field*. If the plasma is treated as a dielectric with a permittivity given by Eqn. I.1 and the glass tube is neglected, $r_w = r_t$, then the electric field induced in the plasma is

$$\underset{\sim}{E}_{plasma} = \frac{2\,\underset{\sim}{E}_{applied}}{1 + \epsilon/\epsilon_o} \quad . \tag{I.2}$$

A resonance occurs when $\epsilon = -1$ or when

$$\omega^2 = \omega_{po}^2 / 2 \quad . \tag{I.3}$$

This result will be modified if one takes into account the glass tube, $r_w \neq r_t$. In that case Eqn. I.3 becomes

$$\omega^2 = \omega_{po}^2 /(1 + K_{eff}) \tag{I.4}$$

---

*Later $\underset{\sim}{E}_{applied}$ will be generalized to other inverse multipole fields besides the dipole, but the restriction (wavelength) $\gg r_t$ will always be assumed.

where K_{eff} is the effective dielectric constant of the region exterior to the plasma which depends upon the dielectric constant of the glass and the dimensions r_w and r_t.

Following Tonks' suggestion that the additional resonances might be due to some spatial nonuniformity of the electron density, several workers have extended Eqn. I.4 to the case of a radially nonuniform plasma. As before, only one resonance occurs*; its frequency is given by

$$\omega^2 = \overline{\omega_p^2}/(1 + K_{eff}) \qquad (I.5)$$

where $\overline{\omega_p^2} = \overline{n}\, e^2/\epsilon_o m_e$, n is the electron density at a point r and the bar indicates an average over the cylinder. There is also some enhancement in the scattering cross-section at other frequencies which is related to the steepness of the electron density gradients in the plasma but no other resonances are predicted. Herlofson (6) has pointed out that the resonances with more rapid angular variation such as quadrupole, etc. will occur at lower frequencies than the dipole and hence cannot account for the additional resonances. This was confirmed by Boley (7) who measured the angular dependence of the scattered waves and found all resonances to be of dipole character. At this point it was apparent that some fundamental change or addition was required if an explanation was to be found for the multitude of resonances.

*Kaiser and Closs (17) consider a stepwise approximation to a nonuniform plasma which showed additional resonances; however, it was later shown that these resonances resulted from the discontinuities in the electron density and that they did not occur for a smoothly nonuniform plasma.

A basic property of the plasma which has been neglected to this point is its ability to propagate longitudinal plasma waves. These waves have not entered into the analysis previously because they exist only when the electron temperature is nonzero. Gould (8) proposed a theory in which the effects of electron temperature are approximated by ascribing a pressure to the electron gas, $p_o = nkT$, and a pressure fluctuation which is connected to the electron density fluctuations by an adiabatic law, $p_1 = \gamma kT\, n_1$. Gould's derivation is similar to the one given in Section III with the exception that he treats a spatially uniform plasma. The equation resulting from his analysis can be obtained from Eqn. III-26 by setting $\nabla f = 0$ and $f = 1$. This equation can be rewritten

$$\nabla^2(\nabla^2 + k^2)\phi_1 = 0 \qquad (I.7)$$

where $k^2 = (\frac{\omega^2}{\omega_{po}^2} - 1) / \gamma \lambda_{DO}^2$, $\lambda_{DO}^2 = \epsilon_o kT / n_o e^2$ is the square of the Debye length, and ϕ_1 is the fluctuation in the electric potential induced in the plasma. The solutions to Eqn. I.7 are obviously solutions to

$$\nabla^2\phi_1 = 0 \qquad (I.8a)$$

$$(\nabla^2 + k^2)\phi_1 = 0 \quad . \qquad (I.8b)$$

The solutions to Eqn. I.8a show the dielectric response of the plasma which exists here as well as in the cold plasma. Eqn. I.8b describes the plasma's response as a wave-propagating medium with k

being the magnitude of the wave vector. When the plasma frequency ω_{po}^2 is less than the applied frequency ω^2 then $k^2 > 0$ and longitudinal plasma waves can propagate. Conversely, when $\omega_{po}^2 > \omega^2$ then $k^2 < 0$ and only exponential decaying solutions of Eqn. I.8b can exist. When the solutions to Eqns. I.8 are combined with appropriate boundary conditions, the plasma is found to exhibit an infinite* number of resonances. This is in much better qualitative agreement with experiment than the single resonance of the cold theory. However, the spacing of these resonances is in very poor agreement with experiment. Where theory predicts one resonance at $\omega^2 = \omega_{po}^2/(1 + K_{eff})$ and an infinite number of closely spaced resonances beginning immediately above the plasma frequency ω_{po}, the experimental observations indicated that several resonances could occur below the plasma frequency and that the spacing between resonances was many times that predicted. Gould (9) suggested that better agreement might be obtained by taking into account the nonuniformity in the electron density which is certain to exist in experimental plasmas.

The complications of solving Eqn. III-26 for a nonuniform plasma have led to several approximate attacks on the problem. Gould (27) employed a WKB approach in treating the plane case and Vandenplas (28) formulated a solution to the problem of a parabolic electron density variation, $n_e = n_o(1 - \alpha r^2)$, but did not obtain any results. Weisglas (10) obtained analytic results for the resonances of a plane plasma by assuming a very special electron density $n(x) = n_o[1 + \epsilon + \cos(\frac{\pi x}{a})]$ for a slab of width $2a$. The resulting equation can be transformed

*Presumably only a finite number would be observable if damping were included in this theory.

into a Mathieu equation and explicit solutions exhibited. He finds that the splitting between resonances is much greater than is obtained for a uniform plasma. His result is encouraging in this respect but is far from providing a quantitative test of the validity of the theory. Its greatest drawbacks are the limitations of plane geometry, since all experiments to date have been performed on cylindrical plasmas, and in failing to use an electron density profile which is physically reasonable.

1.3 Outline of the Present Work

It is the purpose of this investigation to overcome the deficiencies of the previous analyses in two respects. First, to calculate the electron density profiles based on a simple physical model and, second, to integrate Eqn. III.26 in cylindrical geometry using the previously calculated density profiles.

Section II will be devoted to a description of the theory used to describe the steady state behavior of the plasma column and a description of the static electron density profiles which have been found. Details of the techniques used in solving the integro-differential equation which describes the plasma will be given in an appendix. Some results on the static electron density profile in plane geometry from the work of Self (13) will also be presented because they will be needed in Section III.

Section III deals with the behavior of a plane or cylindrical plasma when a transverse radio frequency electric field is applied. The equation describing the perturbations induced in the plasma will

be derived and then integrated numerically in both plane and cylindrical geometry. The method of integration will be described. Finally, the results will be compared with experiment to test the validity of the theory. A short description will be given of two alternate assumptions which can be made in deriving the theory and the effect they have upon the agreement between theory and experiment. In this way it will be shown that the approximation of a scalar electron pressure is a reasonable one and cannot be improved upon in any simple way.

The effect of a uniform axial magnetic field upon the spectrum of resonant frequencies will be investigated in Section IV. It will be demonstrated that all of the resonances of a cylindrical plasma column are split into two resonances by the magnetic field. The behavior of the lowest resonance agrees qualitatively with the predictions obtained using a simple dielectric model of the plasma. The higher resonances are shown to exhibit a behavior qualitatively different from that of the lowest resonance.

The results and conclusions of this investigation are summarized in Section V . The adequacy of the models employed in accounting for the experimental observations is discussed and various diagnostic uses of the calculations are outlined.

SECTION II - STATIC ELECTRON DENSITY PROFILE

2.1 Theory

During their early work on the arc discharge Tonks and Langmuir (11) developed a simple model for the steady state behavior of a collisionless plasma. They reasoned as follows: Since the discharge is contained within insulating walls the current flowing into the walls must vanish. Because the thermal speed of the electrons is so much greater than that of the ions, an electric field is created in the plasma to impede the flow of electrons to the wall. This same electric field accelerates the ions toward the wall and thereby increases the ion current. A steady state is reached when the electric field created by charge separation in the plasma is strong enough that the reduced electron current is equal to the enhanced ion current at the wall.

To cast this theory into mathematical terms several simplifying assumptions are made. The plasma is assumed to be only slightly ionized and the neutral gas is assumed to be cold (i.e., room temperature). This implies that ions will be created at a rate proportional to the local electron density (if binary collisions are the dominant ionization mechanism) and that the ions will be created with zero velocity. Next, one assumes that the ion-neutral mean-free path is greater than the radius of the cylinder. As a result, an ion, once created, moves radially under the influence of the internal electric field until it reaches the wall. This allows the ion density at any radius r to be written as an integral over the number of ions created

within that radius weighted by a factor inversely proportional to the ion velocity at r. Finally it is assumed that the electrons possess a Maxwellian velocity distribution. This allows the electron density at any point to be related to the electric potential at that point.

One of the preceding assumptions is of questionable validity. A Maxwellian velocity distribution is usually the result of thermal equilibrium brought about by collisions in the plasma. This seems to contradict the requirement that the plasma be essentially collisionless. Evidence in favor of a Maxwellian velocity distribution can be found, however, in the work of Langmuir and Mott-Smith, Jr. (12) who report extensive probe measurements supporting the Maxwellian distribution.

The mathematical expression of this theory follows directly from the preceding assumptions. The electron density at any radius is related to the electron density at the center, n_{eo}, by

$$n_e(r) = n_{eo} \exp(+ e\phi/kT) \qquad \text{(II.1)}$$

where $\phi(r)$ is the electric potential at radius r and T is the electron temperature. The number of ions created per second per unit volume $S(r)$ is proportional to the local electron density

$$S(r) = \alpha n_e \quad . \qquad \text{(II.2)}$$

The number of ions per unit volume at radius r can be related to the number of ions created within that radius. An ion created at $r' < r$ will pass by the radius r with a velocity

$$v = \sqrt{\frac{2e}{m_i}\left[\phi(r) - \phi(r')\right]}$$

and its contribution to the ion density at r will be proportional to the time it spends near r or inversely proportional to its velocity. Hence

$$n_i(r) = \int_0^r \frac{S(r')r'dr'}{\sqrt{\frac{2e}{m_i}\left[\phi(r) - \phi(r')\right]}} \quad . \tag{II.3}$$

The potential $\phi(r)$ is then related to the ion and electron densities by Poisson's equation

$$\nabla^2\phi = \frac{e}{\epsilon_o}(n_e - n_i) \quad . \tag{II.4}$$

Equations II.2 - II.4 can be combined into a single integro-differential equation for the potential $\phi(r)$. The resulting equation is most clearly written by changing to dimensionless variables,

$$\eta(r) = -\frac{e\phi}{kT} \tag{II.5}$$

$$s = \alpha r/\sqrt{2kT/m_i} \quad . \tag{II.6}$$

The equation in terms of these variables is

$$s\,\frac{d^2\eta}{ds^2} + \frac{d\eta}{ds} = \beta^2\left[\int_0^s \frac{e^{-\eta(\sigma)}\,\sigma\,d\sigma}{\sqrt{\eta(s) - \eta(\sigma)}} - se^{-\eta(s)}\right] \tag{II.7}$$

where $\beta^2 = 2n_{eo}e^2/\epsilon_o m_i \alpha^2$.

If the integral in Eqn. II.7 is to be integrated numerically, then the solution for $\eta(s)$ must begin at the origin and proceed outward until the boundary condition is satisfied. At any point s the current per unit area of ions is given by

$$J_i(s) = \int_0^s S(\sigma) \frac{\sigma}{s} d\sigma \qquad \text{(II.8)}$$

since the total number of ions created per second within radius s must cross the surface of a cylinder of radius s in one second. The electron current density at s can be found by integrating eV_r times the Maxwellian velocity distribution function over all outward directed velocities. This gives

$$J_e(s) = n_e(s) \sqrt{\frac{kT}{2\pi m_e}} \quad . \qquad \text{(II.9)}$$

The boundary condition of zero net current to the wall will be satisfied when the following dimensionless equation is satisfied.

$$e^{\eta(s_w)} \int_0^{s_w} e^{-\eta(\sigma)} \frac{\sigma}{s_w} d\sigma = \sqrt{\frac{m_i}{4\pi m_e}} \quad . \qquad \text{(II.10)}$$

The radius s_w is then the radius at which the wall of the cylinder will occur for that particular ion species. Because s_w is a function of the ion mass m_i the solution to Eqn. II.7 is not uniquely determined by β^2 but depends to a small extent upon the gas which is being used.

Before proceeding to the solution of Eqn. II.7 a comment must be made about the parameter β^2. Since β^2 is a function of α and

α is a very difficult quantity to measure experimentally, it appears that comparison with experiment would be difficult. Actually β^2 can be obtained without any knowledge of α. Using Eqn. II.6 and the definition of β^2 it follows that

$$\beta^2 = \frac{n_{eo}e^2}{m_i \epsilon_o} \frac{m_i}{kT} \left(\frac{r_w}{s_w}\right)^2 = \frac{1}{s_w^2} \left(\frac{r_w^2}{\lambda_{DO}^2}\right) \qquad \text{(II.11)}$$

where $\lambda_{DO}^2 = \epsilon_o kT/n_{eo}e^2$ is the Debye length at the center of the column. Once the solution of Eqn. II.7 is accomplished for a certain gas, it is a simple matter to plot a graph of β^2 versus $s_w^2 \beta^2$. To obtain β^2 for an experimental plasma it is necessary to measure only n_{eo} and T, calculate $r_w^2/\lambda_{DO}^2 = s_w^2\beta^2$ and read β^2 off of the graph.

2.2 Technique for Solving Equation II.7

In their original work on this problem Tonks and Langmuir (11) solved Eqn. II.7 for the special case $\beta^2 = \infty$ or equivalently, $n_e = \infty$. Their method involved a series expansion of s in powers of η. By expanding the argument of the integral in powers of η it can be evaluated term by term and the coefficients of the power series can be determined. This method can also be applied to the more complicated problem when β^2 is finite, however the recursion formula for the power series coefficients becomes quite unmanageable and the number of terms necessary for convergence of the series increases very rapidly as β^2 decreases. A better method with the advent of high speed computers is simply to integrate the equation

numerically, point by point, from the center outward.

This method, which is described in greater detail in Appendix 2, is simple in concept but requires some care in detail if it is to yield accurate results. The greatest source of error arises from the singular nature of the integrand in the integral

$$I(s) = \int_0^s \frac{e^{-\eta(\sigma)}\ \sigma\ d\sigma}{\sqrt{\eta(s) - \eta(\sigma)}} \qquad \text{(II.12)}$$

where the denominator vanishes when $\sigma = s$. Numerical integration at an interval h will make an error $\approx \frac{3}{2}\left(\frac{h}{s}\right)^{1/2}$ if the infinite point at $\sigma = s$ is neglected. A more accurate estimate of $I(s)$ can be obtained if the integrand is divided into two terms, an integrable function containing the singularity and a remainder which is non-singular. For example, Eqn. II.12 can be written

$$I(s) = \frac{e^{-\eta(s)}}{\sqrt{\eta'(s)}} \int_0^s \frac{\sigma\ d\sigma}{\sqrt{s - \sigma}} + \int_0^s \left\{ \frac{e^{-\eta(\sigma)}}{\sqrt{\eta(s) - \eta(\sigma)}} - \frac{e^{-\eta(s)}}{\sqrt{\eta'(s)[s - \sigma]}} \right\} \sigma\ d\sigma \ . \qquad \text{(II.13)}$$

The first integral in Eqn. II.13 is simply $\frac{4}{3} s^{3/2}$. The integrand of the second integral is a function which goes to zero at $\sigma = s$ although its derivatives are still singular. The error now made by ignoring the last point is less than

$$\frac{1}{2}\left(\eta' - \frac{\eta''}{\eta'}\right) h\left(\frac{h}{s}\right)^{1/2}$$

which represents an improvement of a factor of h. This process was carried out twice for the integral in this problem giving an error

proportional to $h^{5/2}$.

The only other important source of error is the numerical differentiation necessary to evaluate η'' and η'. If the interval used in differentiation is too large then the approximation to the actual derivative will be poor. Conversely, if the interval is too small in comparison to the number of significant figures available, then an error results from loss of significance. There is no way to avoid this type of error. The interval must be chosen carefully to insure at least a tolerable error.

Numerical solution of Eqn. II.7 is accomplished using a predictor-corrector method. Assume that the function $\eta(s)$ has been calculated for the values $s = nh$ $(n = 0,1,2,\cdots,N)$, then a prediction η^{p}_{N+1} of the value of η at $s = (N+1)h$ can be made using the known values η_N, η_{N-1}, $\cdots$. Using η^{p}_{N+1} and the table of η the integral and derivatives in Eqn. II.7 can be evaluated. The two sides of the equation will, in general, not be equal as they should because η^{p}_{N+1} is not the correct value for η_{N+1}.

From the error between the two sides of the equation a correction to the value of η^{p}_{N+1} can be derived. This corrected value is η^{c1}_{N+1}. The correction process used to derive η^{c1}_{N+1} from η^{p}_{N+1} can be repeated to obtain η^{c2}_{N+1}, etc. until the two sides of Eqn. II.7 are equal to within some preassigned tolerance. When this happens the current value of η^{c}_{N+1} is entered in the table as η_{N+1} and Eqn. II.10 is evaluated to find if the boundary condition is satisfied. If it is, the calculation is complete; if not, the entire procedure is repeated to find η_{N+2}.

What has been outlined is essentially an inductive procedure to obtain $\eta(s)$ at certain tabular points. As with all inductive procedures, the first one or two steps must be considered separately. Since the table of η_N does not exist when $N = 0$ and is not extensive enough for accurate numerical work when $N < 5\text{-}10$, the first few values of η_N must be calculated by some independent means. Since $0 < N < 10$ represents small values of s, a power series expansion of $\eta(s)$ has proven most convenient. Therefore the calculation is begun by evaluating a simple two-term series for $\eta(s)$ at the first twelve points $(N = 0,1,\cdots,11)$ and the predictor-corrector formula is applied beginning with $N = 11$.

Details of the techniques described above are contained in Appendix 1. This includes the formulas used for prediction, correction, differentiation and integration. The initial power series is derived and, in addition, various minor points such as interval sizes, testing tolerances and expected error are presented.

2.3 Electron Density Profile for Cylindrical Geometry

Solutions to Eqn. II.7 have been obtained for a series of values of β^2 between 10^2 and ∞. The solution for $\beta^2 = \infty$ was checked against the solution of Tonks and Langmuir and was in good agreement. Figure 2 shows the potential $\eta(s)$ as a function of s for several values of β^2. The points marked on each curve indicate the location of the wall for the indicated ion species. Both s_w and $\eta(s_w)$ can be easily obtained from this graph for the five gases shown. It is interesting to note that the potential $\eta(s_w)$ necessary to satisfy

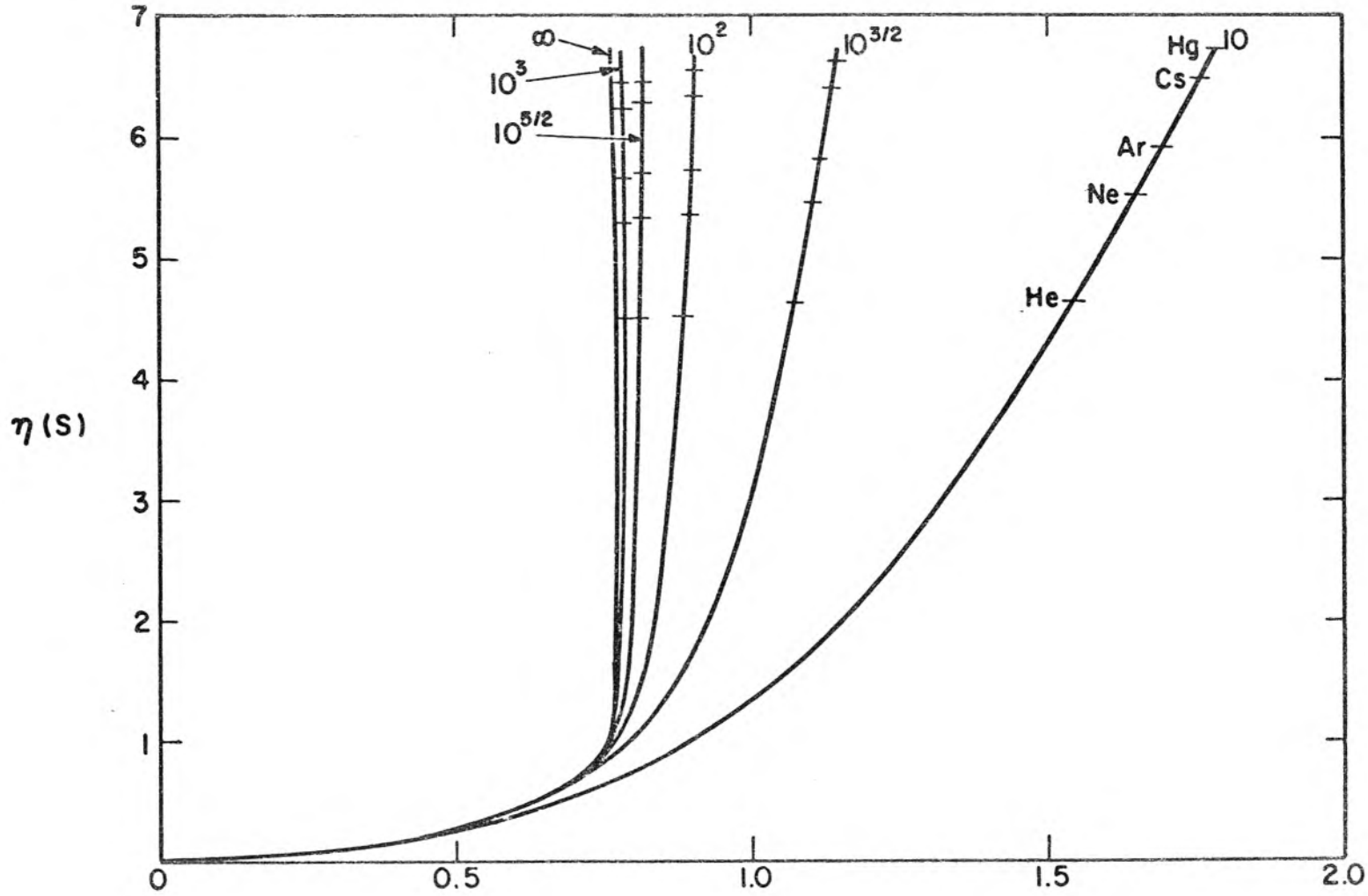

Fig. 2 Potential Function for Several Values of β

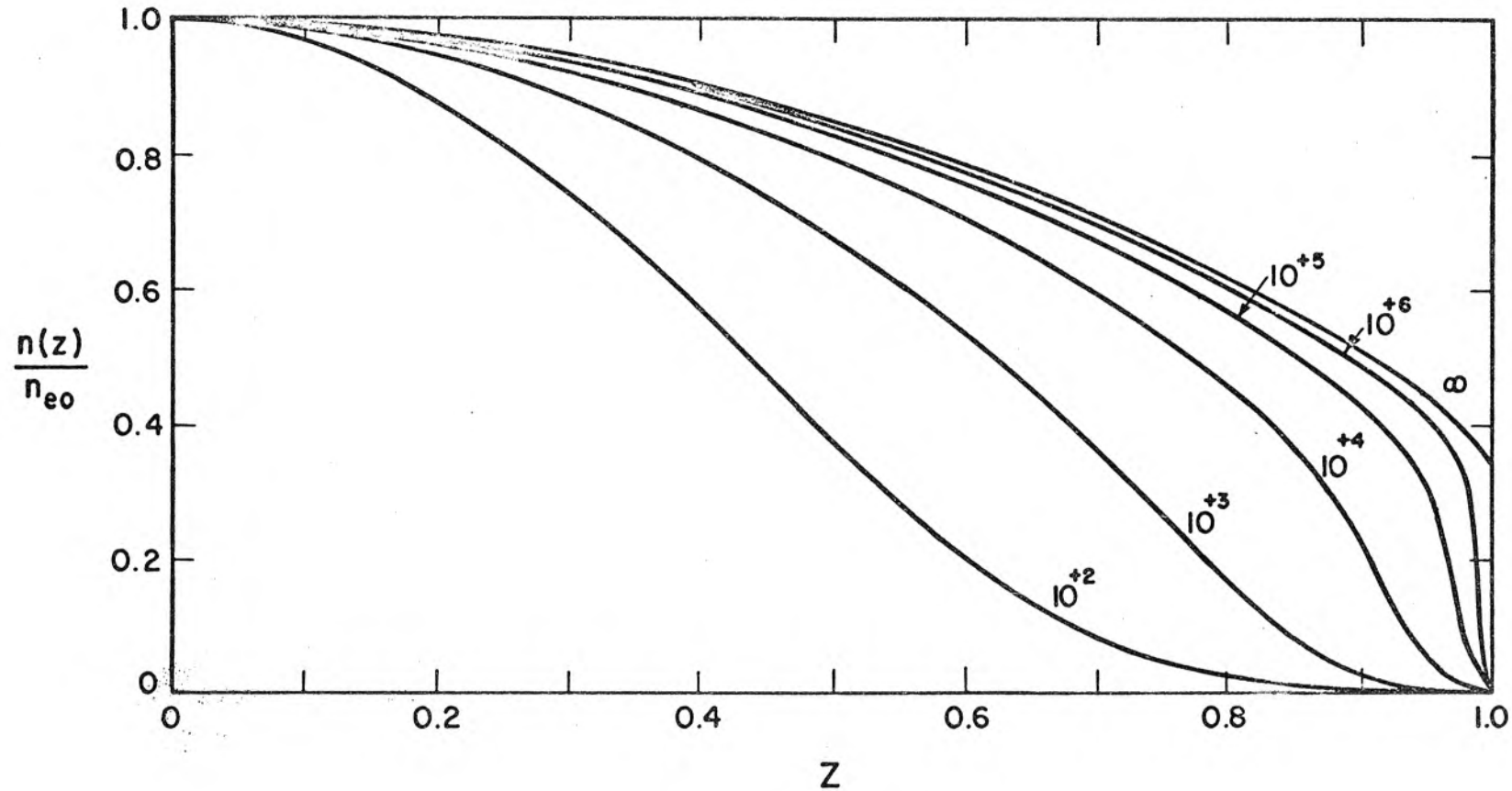

Fig. 3 Electron Density for Mercury Plasma

the boundary conditions is relatively independent of the size of the column compared to the Debye length (i.e., to β^2) but is primarily a function of the ion mass.

Figure 3 shows the electron density profiles

$$\frac{n(z)}{n_{eo}} = e^{-\eta(z)} \qquad \text{(II.14)}$$

where $z = s/s_w = r/r_w$ is the radius of the column normalized to 1 at the wall. The formation of a thin sheath region is quite apparent for $\beta^2 = 10^6$ and when $\beta^2 = 10^2$ the sheath has expanded to fill a large fraction of the column. For computational use the functions $\eta(s)$, $n(s)/n_{eo}$, $\eta'(s)$ and $\eta''(s)$ are tabulated in Appendix III.

From the calculated electron density profiles a useful relation concerning sheath thickness can be derived. Comparing the theoretical sheath thickness to the Debye length an approximate rule can be derived for estimating the sheath thickness. This comparison has been carried out in Table I. For the purposes of this analysis the edge of the sheath was defined to be the point where charge neutrality was violated by 1%.* It is apparent that the sheath thickness is eighteen times the Debye length at the center of the column to within 3%. Note that it is the Debye length at the center of the column for which this simple relation is obeyed and not the Debye length obtained from the average electron density.

---

*For another relation involving sheath thickness which makes use of a different definition, see Table III.

In the following sections it will be necessary to compare theoretical calculations based on these density profiles with experiment. The parameters ω_{po}^2 and λ_{DO}^2 are inconvenient from an experimental viewpoint because n_{eo} is difficult to measure. Since it is quite easy to measure $\bar{n}$, the average electron density, we shall give all theoretical results in terms of the following average quantities.

$$\overline{\omega_p^2} = \bar{n}\, e^2/\epsilon_o m_e = \omega_{po}^2\, \bar{n}/n_{eo} \qquad \text{(II.15)}$$

$$\overline{\lambda_D^2} = \epsilon_o kT/\bar{n}\, e^2 = \lambda_{DO}^2\, n_{eo}/\bar{n} \quad . \qquad \text{(II.16)}$$

To aid in making the connection between average quantities and their on-axis values, Table II has been prepared. For each value of β^2 which is used in this work the following quantities are given: s_w, r_w^2/λ_{DO}^2, $\bar{n}/n_{eo}$, and r_w^2/λ_{DO}^2. This table applies only to mercury plasmas.

TABLE I -- SHEATH THICKNESS

β^2	Sheath length/r_w	λ_{DO}/r_w	Sheath length/λ_{DO}
10^6	2.28×10^{-2}	1.27×10^{-3}	18.0
10^5	7.18×10^{-2}	3.86×10^{-3}	18.6
10^4	2.02×10^{-1}	1.10×10^{-2}	18.4
10^3	4.91×10^{-1}	2.76×10^{-2}	17.8
10^2	1.00	5.60×10^{-2}	17.8

TABLE II -- CONNECTION BETWEEN AVERAGE PARAMETERS AND THEIR VALUES AT THE ORIGIN

β^2	s_w	r_w^2/λ_{DO}^2	$\bar{n}/n_{eo}$	$r_w^2/\bar{\lambda}_D^2$
∞	0.772	∞	.698	∞
10^6	0.789	6.23×10^5	.678	4.22×10^5
10^5	0.822	6.75×10^4	.637	4.30×10^4
10^4	0.910	8.28×10^3	.547	4.53×10^3
$\frac{1}{3} \times 10^4$	0.996	3.31×10^3	.478	1.58×10^3
10^3	1.150	1.32×10^3	.389	5.15×10^2
$\frac{1}{3} \times 10^3$	1.380	6.35×10^2	.305	1.94×10^2
10^2	1.790	3.21×10^2	.224	7.19×10^1

2.4 Electron Density Profiles for Slab Geometry

The theory outlined in Section 2.1 is also applicable to a slab geometry, i.e., a plasma infinite in the y and z directions and bounded by insulating walls at $x = \pm d$. The nonuniformities of the slab plasma will have the same characteristics as those of the cylinder although the details will be different. The mathematical formulation of the theory for slab geometry yields the following equation

$$\frac{d^2\eta}{ds^2} = \beta^2 \left[\int_0^s \frac{e^{-\eta(\sigma)}\, d\sigma}{\sqrt{\eta(s) - \eta(\sigma)}} - e^{-\eta(s)} \right] \qquad \text{(II.17)}$$

where the meaning of all symbols is the same as before with r replaced by x. An extensive treatment of this equation and its

solutions has been given by Self and Kino (13). The density profiles for a slab plasma will be required in the next section, but the resonances of a slab plasma are not of sufficient interest to warrant solving Eqn. II.7 as was done for the cylindrical case. Therefore the results given in Reference (13) have been used. Since Reference (13) does not provide extensive numerical tables of the electron density profiles, it was found most convenient to approximate their calculated $\eta(s)$ by a series of line segments. Let this approximation to $\eta(s)$ be called η_{approx}, then the electron density in a slab plasma is

$$n(z)/n_{eo} = e^{-\eta_{approx}} .$$

These electron density profiles are shown in Figure 4 as a function of the parameter $d^2/\overline{\lambda_D^2}$. The slight discontinuities in the slopes of the curves is the result of the method used in approximating $\eta(s)$.

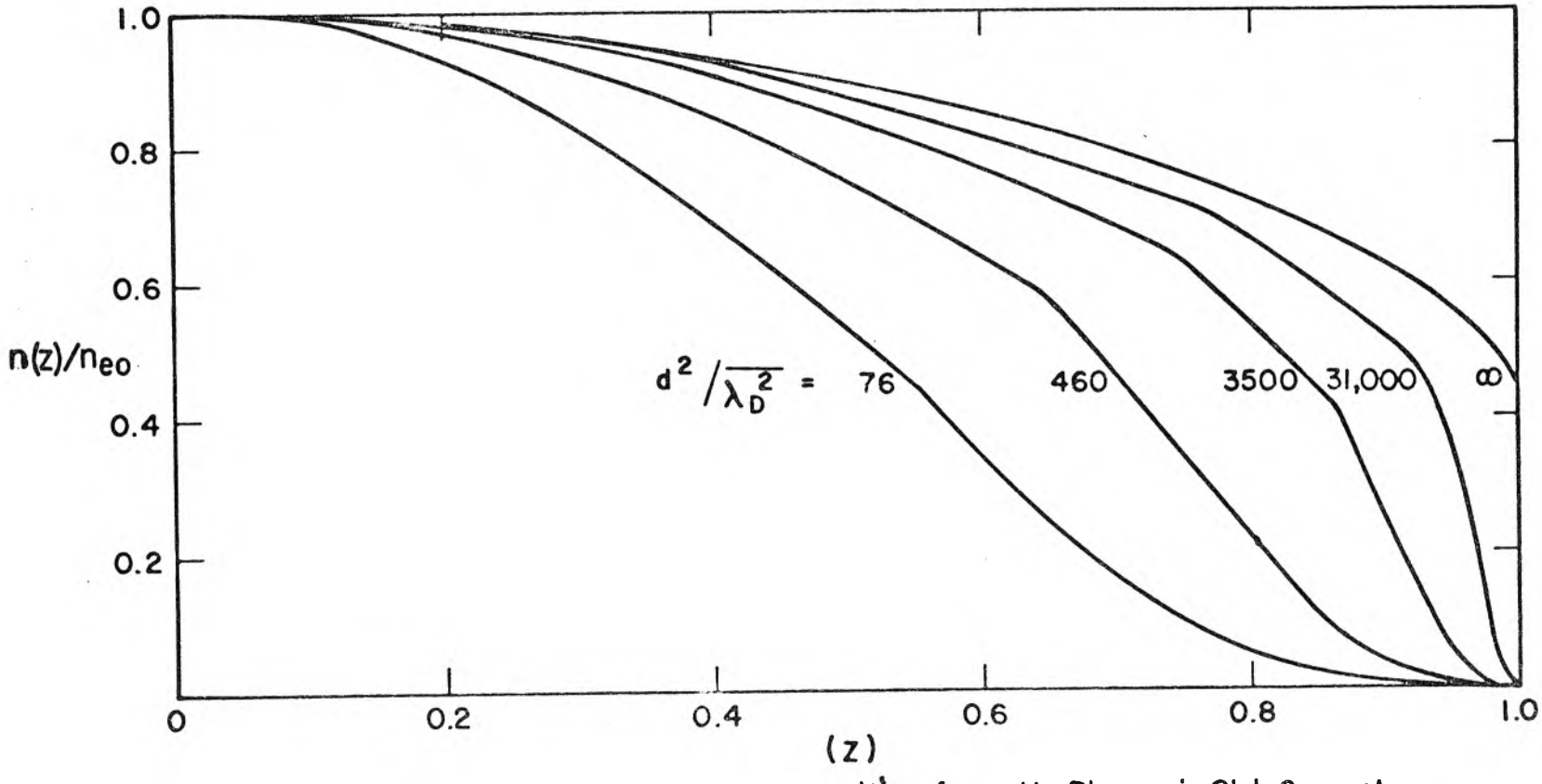

Fig. 4 Approximate Electron Densities for a Hg Plasma in Slab Geometry

SECTION III - PLASMA WAVE RESONANCES IN A NONUNIFORM PLASMA

3.1 Theory

Having determined the theoretical static electron density profiles in Section II the preparations are completed for the study of small perturbations from this steady state. The purpose of this study is to investigate the perturbations which are induced by an electromagnetic wave incident perpendicular to the axis of the plasma column and with its electric vector also transverse to the column axis. In slab geometry the electric field is assumed to be normal to the surface of the plasma.

Certain assumptions will be made concerning the nature of the plasma and the applied field which are well justified for the laboratory plasmas investigated by Tonks (1), Dattner (5), Nickel et al (15) and others. These assumptions are: (1) that the frequency of the applied field is much greater than the electron-ion or electron-neutral collision frequencies, (2) that the wavelength of the incident wave in free space is much greater than any of the relevant physical dimensions, e.g., r_w or λ_{DO}, and (3) that the motion of the ions is negligible. As a result of assumptions 1 and 3, only the motion of the electrons will enter into the analysis and these motions may be described by the collisionless Boltzmann equation.

$$\frac{\partial F(\underset{\sim}{r},\underset{\sim}{v},t)}{\partial t} + \underset{\sim}{v} \cdot \frac{\partial F(\underset{\sim}{r},\underset{\sim}{v},t)}{\partial \underset{\sim}{r}} + \underset{\sim}{A} \cdot \frac{\partial F(\underset{\sim}{r},\underset{\sim}{v},t)}{\partial \underset{\sim}{v}} = 0 \qquad \text{(III.1)}$$

where $F(\underset{\sim}{r},\underset{\sim}{v},t)$ is the electron distribution function in $\underset{\sim}{r},\underset{\sim}{v}$ space and $\underset{\sim}{r},\underset{\sim}{v},\underset{\sim}{A}$ are position, velocity and acceleration respectively.

Eqn. III.1, together with Maxwell's equations, constitute a complete set of equations describing the electron motion. In fact, the complete Maxwell's equations are not needed if assumption 2 is used. The electric potential Φ obeys

$$\left[\nabla^2 - \mu_o \epsilon_o \frac{\partial^2}{\partial t^2}\right] \Phi = - \frac{\rho}{\epsilon_o} \tag{III.2}$$

which can be solved for Φ by Fourier analysis (16) to give

$$\Phi_\omega(r) = \frac{1}{4\pi \epsilon_o} \int \frac{\rho_\omega(r') \, e^{i\underset{\sim}{k} \cdot (\underset{\sim}{r} - \underset{\sim}{r}')}}{|\underset{\sim}{r} - \underset{\sim}{r}'|} \, d^3r' \tag{III.3}$$

If $kr \sim kr' \ll 1$ then $\phi_\omega(r)$ is given approximately by

$$\Phi_\omega(r) \cong \frac{1}{4\pi \epsilon_o} \int \frac{\rho_\omega(r')}{|\underset{\sim}{r} - \underset{\sim}{r}'|} \, d^3r' \tag{III.4}$$

or

$$\Phi(r,t) = \int_{-\infty}^{\infty} \Phi_\omega(r) e^{-i\omega t} d\omega = \frac{1}{4\pi \epsilon_o} \int \frac{\rho(r',t)}{|\underset{\sim}{r} - \underset{\sim}{r}'|} \, d^3r' \tag{III.5}$$

which implies that Φ at time t is the solution to the time independent Maxwell's equations with the source function evaluated at t. Therefore Maxwell's equations for the purposes of this analysis reduce to

$$\nabla^2 \Phi(\underset{\sim}{r},t) = - \rho(\underset{\sim}{r},t)/\epsilon_o \tag{III.6}$$

and

$$\nabla \Phi(\underset{\sim}{r},t) = - \underset{\sim}{E}(\underset{\sim}{r},t) \quad . \tag{III.7}$$

Regrettably, solutions for $F(\underset{\sim}{r},\underset{\sim}{v},t)$ are extremely difficult to obtain for nonuniform plasmas (see Section 3.4). An alternative to finding F is to solve for the velocity moments of F.

The velocity moments about the mean of the function F are defined to be

$$
\begin{aligned}
n_e(\underset{\sim}{r},t) &= \int_{-\infty}^{\infty} F(\underset{\sim}{r},\underset{\sim}{v},t)d^3v \\
u_i(\underset{\sim}{r},t) &= \int_{-\infty}^{\infty} v_i F(\underset{\sim}{r},\underset{\sim}{v},t)d^3v \\
&\vdots \\
M^p_{ij\cdots p} &= \int_{-\infty}^{\infty} c_i c_j \cdots c_p \, F(\underset{\sim}{r},\underset{\sim}{v},t)d^3v
\end{aligned}
\qquad \text{(III.8)}
$$

where $c_i = v_i - u_i$ and where the symbols M^0 and M^1 (the electron density and the average electron velocity) have been replaced by their conventional symbols.

If velocity moments of Eqn. III.1 are taken; that is, $\int_{-\infty}^{\infty} v_i v_j \cdots v_p$ (Eqn III.1)d^3v, an infinite set of coupled equations for the moments M^p results. The first two of these equations are

$$(p = 0) \qquad \frac{\partial n_e}{\partial t} + \nabla \cdot n_e \underset{\sim}{u} = 0 \qquad \text{(III.9)}$$

$$(p = 1) \qquad n_e \frac{\partial \underset{\sim}{u}}{\partial t} + n_e\left[\underset{\sim}{u} \cdot \nabla\right]\underset{\sim}{u} + n_e \underset{\sim}{A} + \nabla \cdot M^2 = 0 \quad . \qquad \text{(III.10)}$$

Clearly, Eqn. III.9 gives n_e if $\underset{\sim}{u}$ is known and Eqns. III.9 and III.10 give $\underset{\sim}{u}$ if M^2 is known, and so forth. To avoid solving an infinite set of equations it is common practice to arbitrarily set $M^j = 0$ for some j. A discussion of the validity of this process for the present problem is given in Appendix 2. In this case $j = 3$ was chosen which leaves Eqns. III.9 and III.10 plus an additional equation relating M^2 to n_e and $\underset{\sim}{u}$. This set of equations will be discussed in Section 3.4 where it is called the tensor pressure theory. For the present a simplification will be made by replacing $\nabla \cdot M^2$ in Eqn. III.10 by a term $\frac{1}{m_e} \nabla p$. Physically M^2 is proportional to the tensor electron pressure and the simplification replaces the divergence of the tensor pressure by the gradient of a scalar pressure. This approximation would be exact in the case of a uniform Maxwellian plasma and seems to be adequate for the nonuniform plasma.

The final form of the equations describing the plasma are arrived at by writing for the acceleration $\underset{\sim}{A}$ the force acting on an electron divided by its mass, $\underset{\sim}{A} = e\,\underset{\sim}{E}/m_e$. Then

$$\frac{dn_e}{dt} + \nabla \cdot n_e \underset{\sim}{u} = 0 \qquad \text{(III.11)}$$

$$\frac{d\underset{\sim}{u}}{dt} + \left[\underset{\sim}{u} \cdot \nabla\right]\underset{\sim}{u} = -\frac{e}{m_e}\underset{\sim}{E} - \frac{1}{m_e n_e}\nabla p \qquad \text{(III.12)}$$

$$\nabla^2 \Phi = -\frac{\rho}{\epsilon_o} \qquad \text{(III.13)}$$

$$\nabla \Phi = -\underset{\sim}{E} \quad . \qquad \text{(III.14)}$$

To solve for perturbations from the steady state each quantity is written as a steady state term (subscript zero) and a small time-dependent perturbation (subscript one).

$$n_e(\underset{\sim}{r},t) = n_{eo}\, f(\underset{\sim}{r}) + n_1(\underset{\sim}{r})\, e^{-i\omega t} \tag{III.15}$$

$$\underset{\sim}{u}(\underset{\sim}{r},t) = \underset{\sim}{u}_1(\underset{\sim}{r})\, e^{-i\omega t} \tag{III.16}$$

$$\Phi(\underset{\sim}{r},t) = \phi_o(\underset{\sim}{r}) + \phi_1(\underset{\sim}{r})\, e^{-i\omega t} \tag{III.17}$$

$$\underset{\sim}{E}(\underset{\sim}{r},t) = \underset{\sim}{E}_o(\underset{\sim}{r}) + \underset{\sim}{E}_1(\underset{\sim}{r})\, e^{-i\omega t} \tag{III.18}$$

$f(\underset{\sim}{r})$ describes the nonuniformity of the plasma, $f(0) \equiv 1$.

Eqns. III.11 through III.14 are not complete unless p is related in some way to the other physical quantities. For a Maxwellian electron gas it is simple to show that the static pressure p_o is proportional to the electron density $n_{eo}\, f(r)$. If a pressure disturbance occurs in the electron gas it will be proportional to a density disturbance but the proportionality constant depends upon the way in which the disturbance is made. If a one-dimensional adiabatic variation is assumed, then the gradient of the pressure may be written

$$\nabla p(\underset{\sim}{r},t) = kT\, n_{eo}\, \nabla f(\underset{\sim}{r}) + \gamma kT\, \nabla\, n_1(\underset{\sim}{r})\, e^{-i\omega t} \tag{III.19}$$

with $\gamma = 3$.

Inserting the definitions III.15 through III.19 into Eqns. III.11 - III.14 gives two equations for the steady state*

---

*Note that Eqns. III.20-21 are identically satisfied for the steady state solutions previously discussed; Eqn. III.20 is derivable from Eqn. II.1.

$$kT\, n_{eo}\, \nabla f(\underset{\sim}{r}) = - e n_{eo}\, f(\underset{\sim}{r})\, \underset{\sim}{E}_o(\underset{\sim}{r}) \tag{III.20}$$

$$\nabla \cdot \underset{\sim}{E}_o = \frac{e}{\epsilon_o}\left[n_{io} - n_{eo}\, f(\underset{\sim}{r}) \right] \tag{III.21}$$

and four equations first order in the perturbation

$$i\omega n_1 = n_{eo}\, \nabla \cdot \left[f\, \underset{\sim}{u}_1 \right] \tag{III.22}$$

$$i\omega m_e n_{eo}\, f\, \underset{\sim}{u}_1 = e n_1 \underset{\sim}{E}_o + e n_{eo}\, f \underset{\sim}{E}_1 + \gamma kT\, \nabla n_1 \tag{III.23}$$

$$\nabla^2 \phi_1 = \frac{e}{\epsilon_o} n_1 \tag{III.24}$$

$$\nabla \phi_1 = - \underset{\sim}{E}_1 \quad . \tag{III.25}$$

Combining Eqns. III-22-25 and using III.20 to define E_o leads to a single fourth order differential equation in ϕ_1, the perturbation electric potential.

$$\nabla^2 \nabla^2 \phi_1 - \frac{\nabla f}{\gamma f} \cdot \nabla \nabla^2 \phi_1 + \left[\frac{1}{\gamma \lambda_{DO}^2} \left(\frac{\omega^2}{\omega_{po}^2} - f \right) - \nabla \cdot \left(\frac{\nabla f}{\gamma f} \right) \right] \nabla^2 \phi_1$$

$$- \frac{1}{\gamma} \nabla f \cdot \nabla \phi_1 = 0 \quad . \tag{III.26}$$

It is convenient for numerical computation to have this equation in dimensionless form. This is accomplished by introducing a new independent variable $\underset{\sim}{z} = \underset{\sim}{r}/r_w$ or $\underset{\sim}{z} = \underset{\sim}{r}/d$ in slab geometry. With this change of variables the differential equation depends only upon the two dimensionless parameters r_w^2/λ_{DO}^2 and ω^2/ω_{po}^2. It is important to note that r_w^2/λ_{DO}^2 is the same parameter which was derived from β^2 in Section 2.1. This makes it very easy to choose the correct

density profile $f(\underset{\sim}{r})$ when integrating Eqn. III.26.

3.2 Numerical Solutions for a Slab Plasma

In its general form Eqn. III.26 is a fourth order partial differential equation. Only in special geometries is the equation separable into ordinary differential equations and of the separable geometries only the one-dimensional problem of a slab reduces to a simple differential equation. Although the slab plasma has never been investigated experimentally, the theoretical predictions of the resonant frequencies are of interest because they yield insight into the solutions which will be obtained in more complicated geometries. It is instructive therefore to calculate the solutions to Eqn. III.26 for a slab plasma before proceeding to the more useful problem of a cylindrical plasma.

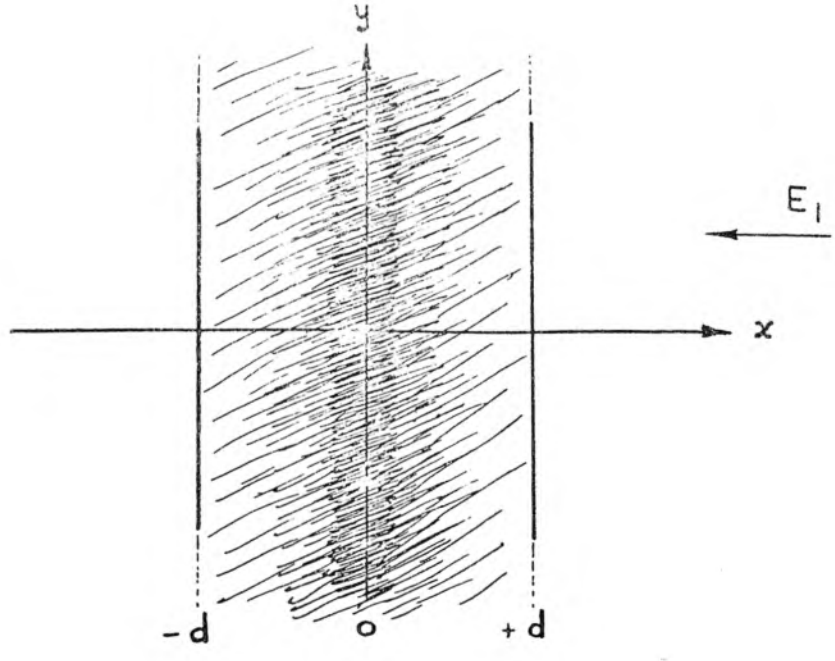

Figure 5. The Slab Plasma

The geometry of the slab plasma is shown in Figure 5 and the direction of the applied field is indicated. Since E_1 is a function of x only, the operator $\nabla^n = d^n/dz^n$ so that Eqn. III.26 becomes an ordinary differential equation in the variable x (or $z = x/d$ when changed to dimensionless variables). It can be reduced to an ordinary second order differential equation by two changes. First the dependent variable is changed from ϕ_1 to $E_1 = -\phi_1'$ ($'$ denotes d/dz) which gives

$$E_1''' - \frac{1}{\gamma}\frac{f'}{f}E_1'' + \frac{1}{\gamma}\left[\frac{d^2}{\lambda_{DO}^2}\left(\frac{\omega^2}{\omega_{po}^2} - f\right) - \left(\frac{f'}{f}\right)'\right]E_1' - \frac{f'}{\gamma}E_1 = 0 . \quad \text{(III.27)}$$

This can be written as a perfect differential

$$\frac{d}{dz}\left[E_1'' - \frac{f'}{\gamma f}E_1' + \frac{1}{\gamma}\frac{d^2}{\lambda_{DO}^2}\left(\frac{\omega^2}{\omega_{po}^2} - f\right)E_1\right] = 0 \quad \text{(III.28)}$$

which yields upon integration the inhomogeneous equation

$$E_1'' - \frac{f'}{\gamma f}E_1' + \frac{d^2}{\gamma\lambda_{DO}^2}\left(\frac{\omega^2}{\omega_{po}^2} - f\right)E_1 = C \quad \text{(III.29)}$$

The constant can be evaluated by using the boundary condition which is discussed next.

Boundary Conditions. A unique solution $E_1(z)$ to Eqn. III.29 requires the specification of two boundary conditions plus specification of the integration constant C. One boundary condition is clearly an arbitrary scale factor multiplying the solution. A second condition can be derived from conservation of the electric displacement

vector which requires that $\epsilon_o E_1(1) = \epsilon_o E_1(-1)$. Since Eqn. III.29 is unchanged by the inversion $z \to -z$, the solution $E_1(z)$ must be symmetric about the origin. Simply stated, the second boundary condition is therefore $E_1'(0) = 0$. Evaluation of the constant C requires a knowledge of the left hand side of Eqn. III.29 at some point in the plasma. Referring back to Eqn. III.20 which defines the velocity u_1 and making the substitutions $E_o = -\frac{kT}{e}\frac{f'}{f}$ and $n_1 = -\frac{\epsilon_o}{e}\nabla \cdot E_1$, an expression similar to Eqn. III.29 is obtained.

$$E_1'' - \frac{f'}{\gamma f} E_1' - \frac{1}{\gamma \lambda_{DO}^2} f E_1 = -\frac{i\omega m_e}{e} f \frac{d^2}{\gamma \lambda_{DO}^2} u_1 \quad . \tag{III.30}$$

Gould (8) and Weisglas (10) have used the condition $u_1 = 0$ at $z = 1$ as a boundary condition. This boundary condition is based on the following argument: Since all laboratory plasmas are contained in vessels with glass walls, there can be no current flow to the walls, but the current is simply $J = en_{eo} f u_1$ so $J = 0$ is equivalent to $u_1 = 0$. There is some question about the validity of this boundary condition (see Section 3.4 for a discussion of this point), but it will be used here because it is convenient and it appears to give good results. Evaluating Eqns. III.29-30 at $z = 1$ and using the condition $u_1(1) = 0$ an expression can be derived for C .

$$C = \frac{1}{\gamma}\frac{d^2}{\lambda_{DO}^2}\frac{\omega^2}{\omega_{po}^2} E_1(1) \tag{III.31}$$

The nature of the slab resonance problem. The experimental quantity which is most easily measured in these experiments is the frequency at which a resonance occurs. In a cylindrical plasma a resonance is understood to mean a peak in the scattering or the frequency at which motion is induced in the plasma with vanishingly small applied field. The analog of this in slab geometry defines a resonance as the frequency at which motion can occur in the plasma with no applied field, i.e., $E_1(1) = 0$. This is a convenient condition because if only the resonant frequencies are of interest, then Eqn. III.29 becomes a homogeneous equation and the problem becomes one of determining the frequencies ω_i $(i = 0,1,2,\cdots)$ for which Eqn. III.29 (with $C = 0$) has a solution that satisfies $E_1(1) = 0$ and $E_1'(0) = 0$.

Although it appears simple enough to find such solutions by trial and error, there is a complicating factor. In the introduction (Section 1.2) it was pointed out that the solutions to Eqn. I.7 were of an exponential nature if $\omega^2/\omega_{po}^2 < 1$. Similarly Eqn. III.29 has exponential solutions whenever $\omega^2/\omega_{po}^2 < f(z)$ and the exponential length L_e (i.e., $E_1 \propto e^{z/L_e}$) is given by

$$k_e = L_e^{-1} = \frac{d}{r^{1/2}\lambda_{DO}} \sqrt{f(z) - \frac{\omega^2}{\omega_{po}^2}} \qquad \text{(III.32)}$$

where $d/r^{1/2}\lambda_{DO}$ varies between 7 and 40 in these calculations. Of course the physical behavior of the plasma causes the fields to decay as the negative exponential in the nonpropagating region $(\omega_p^2 > \omega^2)$

however, the positive exponential solution exists mathematically and magnifies numerical errors until the correct solution is completely hidden. The best way to overcome this difficulty is to begin the numerical integration at $z = 1$ where the function $E_1(z)$ is oscillatory and then stop when the solution begins to exhibit exponential behavior. Figure 6 shows the results of this procedure carried out for several different frequencies near a resonance. It is apparent that the resonant frequency lies between .612 and .614 because at other frequencies there is a strong positive exponential behavior. The dotted curve shows the actual function $E_1(z)$ which would be obtained exactly at resonance.

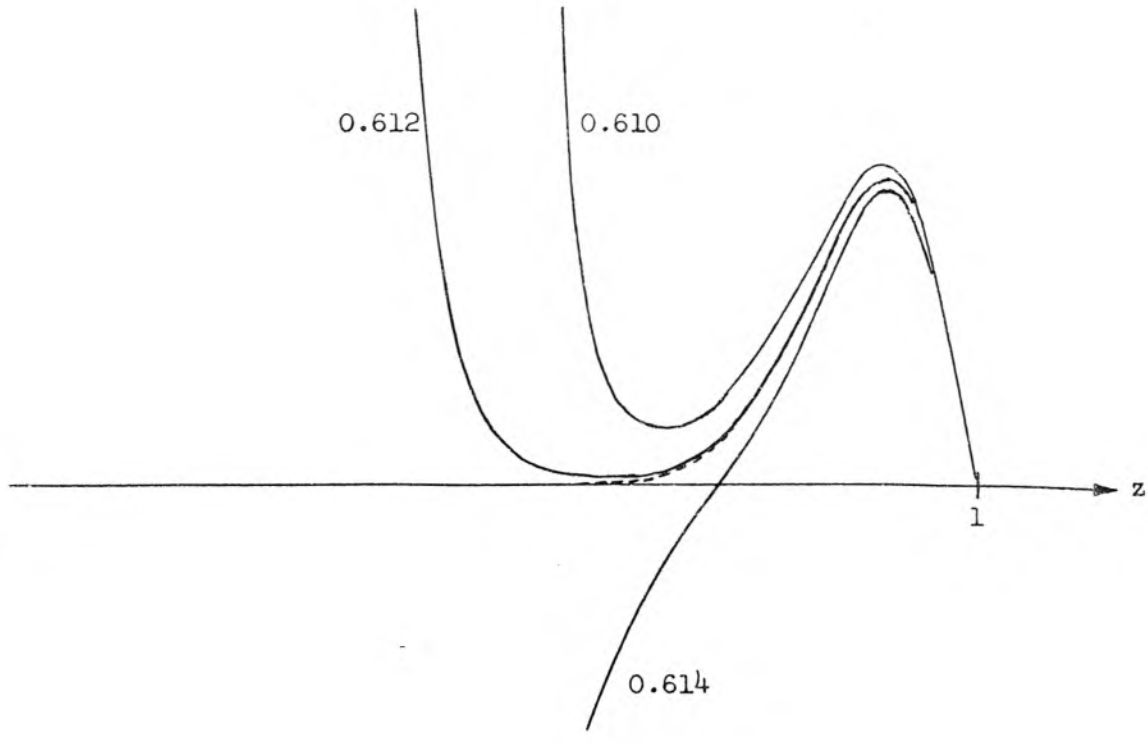

Figure 6. Solutions to Eqn. III.29 for three values of ω^2/ω_{po}^2

Numerical Integration. Integration of Eqn. III.29 has been performed numerically using a fourth order Runge-Kutta (RK) integration method. RK integration is normally applied to a system of N first order differential equations of the form

$$\frac{dy_j}{dx} = g_j(x,y_1, \cdots, y_N) \quad , \quad (j = 1,2,\cdots,N) \quad . \tag{III.33}$$

The RK equation will give the value of the dependent variables y_j at the point $x = (k+1)h$ given the values y_j at $x = kh$. Since Eqn. III.29 is a second order differential equation it must be rewritten as two first order equations.

$$E_1' = F = g_1(z,E_1,F) \tag{III.34}$$

$$F' = \frac{1}{\gamma}\frac{f'}{f}F - \frac{1}{\gamma}\frac{d^2}{\lambda_{DO}^2}\left(\frac{\omega^2}{\omega_{po}^2} - f\right)E_1 = g_2(z,E_1,F) \quad . \tag{III.35}$$

The RK integration formula is

$$y_j^{k+1} = y_j^k + \frac{1}{6}h(\ell_{1j} + 2\ell_{2j} + 2\ell_{3j} + \ell_{4j}) \tag{III.36}$$

where $y^k \equiv y(kh)$

$$\ell_{1j} = g_j\left[kh, y^k\right]$$

$$\ell_{2j} = g_j\left[(k+\tfrac{1}{2})h, y^k + \tfrac{1}{2}h\ell_1\right]$$

$$\ell_{3j} = g_j\left[(k+\tfrac{1}{2})h, y^k + \tfrac{1}{2}h\ell_2\right]$$

$$\ell_{4j} = g_j\left[(k+1)h, y^k + h\ell_3\right] \quad .$$

Errors. The RK formula (Eqn. III.36) gives a fourth order approximation to the correct solution. That is, starting with the correct solution $y^k = y(kh)$ at the point k, then the value of y^{k+1} computed from Eqn. III.36 will differ from the correct value $y[(k+1)h]$ by an amount of order h^{4+1}. This is called truncation error. The total error after n steps will be the sum of the truncation error in the last integration step plus some fraction of all the error committed in previous steps. The fraction of the total error at step n which is carried forward to step $n+1$ is called the propagating error and it depends strongly on the form of the differential equation being integrated. Todd (14) gives an approximate expression for these errors. Letting $r(x_n,h)$ denote the truncation error and $\epsilon_n \equiv y^n - y(nh)$, the total error at point n is

$$\epsilon_{n+1} = \left[I + h \frac{\partial g}{\partial y} \right] \epsilon_n + r(nh,h) \quad . \tag{III.37}$$

For a system of equations $I + h \frac{\partial g}{\partial y}$ is a matrix and ϵ is a vector giving the error in each component. Whether the total error increases depends on the eigenvalues of the matrix $M = I + h \frac{\partial g}{\partial y}$. If all the eigenvalues are less than one, the error decreases; if any are greater than one, then some part of the error increases. For Eqn. III.29 the eigenvalues are

$$\lambda_m^{\ell} \simeq 1 \pm h\, k_e^{\ell} \tag{III.38}$$

at the point ℓh and the total error after n steps will be

$$\epsilon_n \approx \lambda_m^0 \cdot \lambda_M^1 \cdots \lambda_M^{n-1} \epsilon_o \approx \exp\left[nh\left(\frac{k_e^0 + k_e^1 + \cdots + k_e^{n-1}}{n}\right)\right]$$

or

$$\epsilon_n \approx \exp\left[nh\, \bar{k}_e\right] . \tag{III.39}$$

The error grows exponentially at some average rate $\bar{k}_e$ when $\bar{k}_e$ is real. In the oscillatory region of the plasma $\bar{k}_e$ is imaginary and the error does not grow as rapidly. To illustrate this let $hk_e = ih\delta$ where $h\delta$ is a small, real constant. Then

$$\epsilon_n \approx (1 + i\delta h)^n \epsilon_o \approx (1 + h^2\delta^2)^{n/2} e^{in\delta} \epsilon_o \tag{III.40}$$

and

$$|\epsilon_n| \approx e^{nh\frac{h\delta^2}{2}} \epsilon_o . \tag{III.41}$$

Since $|\bar{k}_e| \propto \delta \gg (\frac{h\delta}{2})\delta$ the error increases more slowly in the oscillatory region.

Typical values of $\bar{k}_e$ range from 3 to 20 and nh varies from .7 to .3 so that the worst error magnification is about e^{14} or about 10^6. This illustrates the earlier remark that integration into the exponential region is sometimes prohibited by the errors involved. In the oscillatory region, however, $h\delta/2 < .02$ and the errors are multiplied by vactors of $e^{.4}$ which is negligible.

The truncation error $r(nh,h)$ can be estimated by noting that Eqn. III.36 reduces to Simpson's rule if g is independent of y. The truncation error for Simpson's rule is

$$|r(nh,h)| \leq \frac{\max|g^{(4)}|\, h^5}{2880} \qquad \text{(III.42)}$$

and for the worst combination of parameters considered here gives $|r| \leq 10^{-7}$. Trial integrations of Eqn. III.29 for a uniform plasma where the solutions are tabulated functions, indicate that the actual truncation errors are of this magnitude.

Results. Calculations of the resonant frequencies were carried out for four values of the parameter d^2/λ_{DO}^2. For each value of d^2/λ_{DO}^2 the four lowest resonant frequencies ω_i^2 $(i = 0,1,2,3)$ were determined. The results are shown in Figure 7 where $\omega_i^2/\overline{\omega_p^2}$ is given as a function of $d^2/\overline{\lambda_D^2}$. The circled points indicate calculated resonances; the connecting lines represent interpolation between these points and not the results of calculation. As explained in Section 2.3 all parameters are expressed in terms of the average electron density because it is more easily measured. The average electron density is, however, shown in Figure 7 so that either parameter may be converted to its value at $r = 0$ with the aid of Eqns. II.15-16.

The points marked by triangles in Figure 7 were obtained by WKB solutions. This was necessitated by the very large value of $d^2/\gamma\lambda_{DO}^2 \sim 4 \times 10^4$ which made numerical integration impractical. Eqn. III.29 can be put into standard WKB form, that is

$$\psi'' + [k^2 - U(x)]\psi = 0 \qquad \text{(III.43)}$$

by the change of variables $E_1 = f^{1/2\gamma}\psi$. The function $U(x)$ is

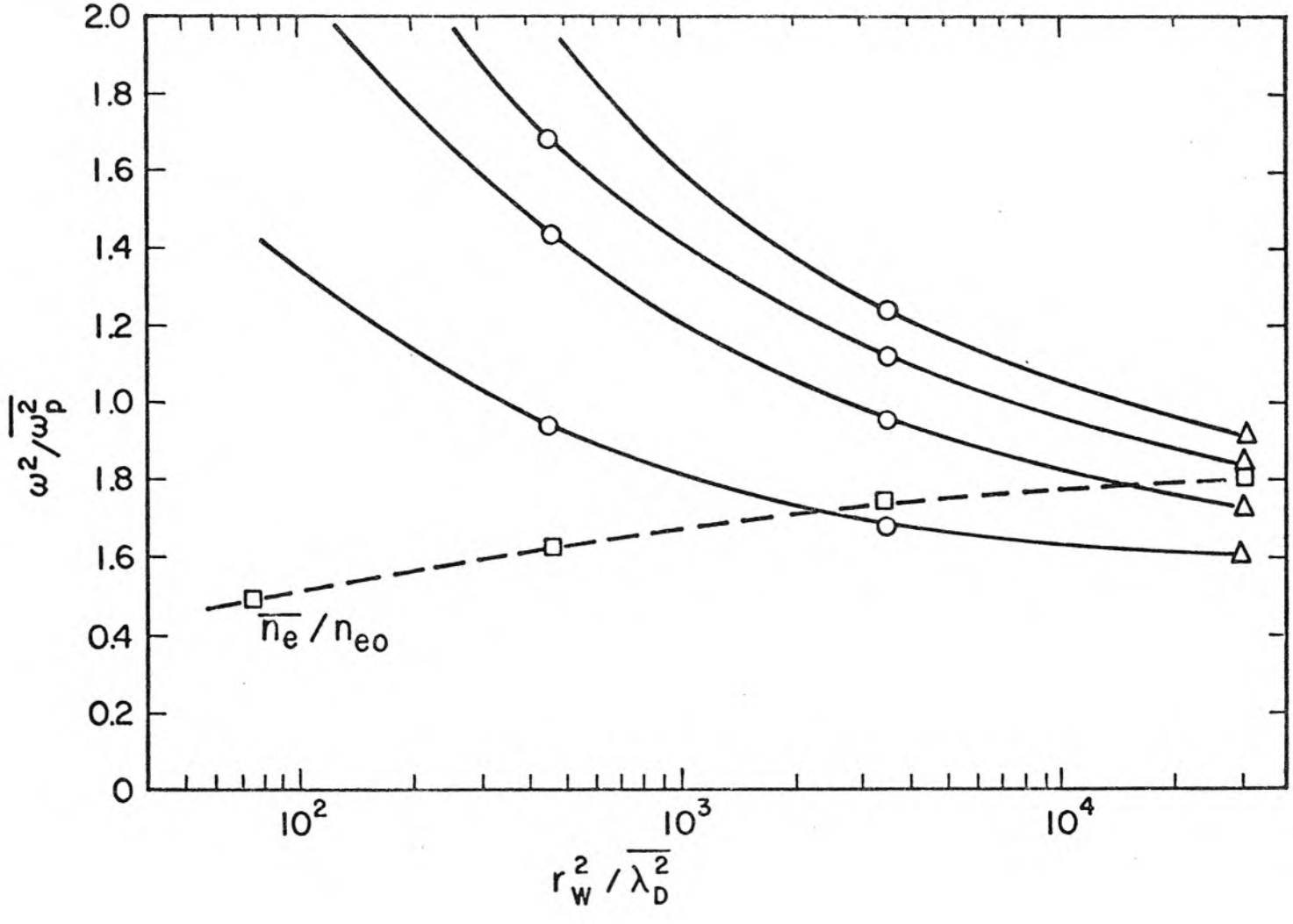

Fig. 7 - Resonant Frequencies for Slab Geometry

$$U(x) = \frac{1}{\gamma}\frac{d^2}{\lambda_{DO}^2} f + \frac{7}{4}\left(\frac{f'}{\gamma f}\right)^2 - \frac{1}{2}\frac{f''}{\gamma f} \qquad \text{(III.44)}$$

and

$$k^2 = \frac{1}{\gamma}\left(\frac{d^2}{\lambda_{DO}^2}\right)\left(\frac{\omega^2}{\omega_{po}^2}\right) \quad . \qquad \text{(III.45)}$$

A straightforward application of the WKB method for boundary conditions of $\psi(1) = 0$ and decaying exponential in the cutoff region leads to the results shown (see, for instance, Morse and Feshbach (18)). By applying the WKB method for values of $(d^2/\gamma\lambda_{DO}^2)$ already treated, it was estimated that the error in the triangle points is within $\pm$ 5% .

It is clear from Figure 7 that the resonant frequencies are quite widely spaced which is in qualitative agreement with the experiment. It is also notable that the spacing depends upon (d^2/λ_{DO}^2) . This is encouraging because measurements on cylindrical plasmas (15) indicates that the relative spacings of the resonant frequencies are indeed functions of the plasma density. A discussion of the physical reasons for these effects will be deferred until the results have been presented for the cylindrical plasma.

3.3 Numerical Solutions for a Cylindrical Plasma

The theory derived in Section 3.1 is, of course, valid in any geometry. In particular Eqn. III.26 describes the perturbations induced in a cylindrical plasma if the various vector operators are expressed in cylindrical coordinates. The difficulty of integrating Eqn. III.26 to find the resonant frequencies, however, increases enormously with this minor change in geometry. The next few

paragraphs will describe in more detail these added difficulties.

Most important, the reduction of Eqn. III.26 to an ordinary second order differential equation which was accomplished for a plasma slab is impossible for the plasma column. This means that a more complex system of four first order differential equations must be integrated with an attendant increase in computational problems, e.g., greater round-off errors, greater truncation errors, and several new boundary conditions.

The four independent solutions to Eqn. III.26 will certainly exhibit some of the characteristics of the solutions to Eqns. I.8a,b the uniform cylindrical plasma equations. Eqns. I.8 each have one regular and one singular solution at the origin. Therefore two of the boundary conditions in cylindrical geometry are simply the requirement that the function $\phi_1(0) = 0$. The only convenient way to use this condition is to begin the integration of Eqn. III.26 at the origin.

Integration was begun at the wall for the slab plasma because the exponential nature of the solutions in the interior of the plasma made integration outward impossible. Since boundary conditions at the origin force the integration to go outward, it will be necessary in some cases to use double precision (16 digit) calculations to preserve accuracy.

In practice the numerical integration cannot begin at the point $z = 0$ because the differential equation III.26 has a singular point there and the numerical integration formulas make large errors. This requires that $\phi_1(z)$ be developed in a power series about the

origin and evaluated at a point z' far enough removed from $z = 0$ to eliminate this source of error.

Finally, the condition for resonance to occur becomes more complicated. In the region exterior to the plasma $\phi_1(z)$ obeys the static Maxwell's equations with no sources.

$$\nabla^2 \phi_1^{ext} = 0 \tag{III.46}$$

the solution to Eqn. III.46 is

$$\phi_1^{ext}(z) = \sum_{\ell} (A_\ell Z^\ell + \frac{B_\ell}{Z^\ell}) \cos \ell\theta \tag{III.47}$$

where $\ell = 1,2,\cdots$ gives the dipole fields, quadrupole field, and so forth. A third boundary condition for this problem is ϕ_1 and ϕ_1' continuous (or equivalently ϕ'/ϕ continuous) in the absence of surface charges. A resonance occurs when the applied field $A_\ell Z^\ell \cos(\ell\theta)$ becomes zero while the scattered field $B_\ell Z^{-\ell} \cos(\ell\theta)$ remains finite. This implies that

$$\frac{\phi_1'^{ext}}{\phi_1^{ext}} = \frac{\phi_1'}{\phi_1} = -\ell \qquad (z = 1) \tag{III.48}$$

is the condition for resonance. Reference to Figure 1 will quickly show that this is not the most general resonance condition. It was tacitly assumed above that the plasma was surrounded by a vacuum. If a glass tube of arbitrary thickness and dielectric constant surrounds the plasma, then the preceding analysis must be repeated. The effect

of the glass tube is to modify Eqn. III.48 to

$$\frac{\phi_1'}{\phi_1} = - \ell K_{eff} \qquad \text{(III.49)}$$

where K_{eff} is an effective dielectric constant which depends on the properties of the glass tube. Details of K_{eff} are available in the works of Nickel (20) and Crawford (19). Because one boundary condition depends upon the experimental apparatus, it is not possible to speak of the resonant frequencies. The only remedy for this is to calculate and plot ϕ_1'/ϕ_1 versus $\omega^2/\overline{\omega_p^2}$ so that the resonant frequencies for a given value of K_{eff} can be easily determined.

Numerical Treatment. Numerical integration is carried out with the RK formula, Eqn. III.36. The functions y and g are now four component vectors rather than two component vectors. The system of four first order differential equations will be derived directly from Eqns. III.22 - III.25 rather than using the various derivatives of ϕ_1 as dependent variables. These particular equations have the advantage of using physically interesting quantities for the dependent variables, i.e., electron density, radial electron velocity, potential and electric field. They also have the advantage of slightly greater computational speed.

Eqns. III.22-25 can be written in dimensionless form by introducing the following variables

$$N_1(z) \cos m\theta = n_1(z)/n_{eo} f \qquad \text{(III.50)}$$

$$\Phi(z)\cos m\theta = e\phi_1(\underset{\sim}{z})/kT \qquad \Phi^*(z)\cos m\theta = e\phi_1'(\underset{\sim}{z}) \cdot z/kT$$

$$v_r(z)\cos m\theta = u_{1r}(z)/i\omega r_w \qquad v_\theta(z)\sin m\theta = u_{1\theta}(\underset{\sim}{z})/i\omega r_w$$

where $z = |\underset{\sim}{z}| = |\underset{\sim}{r}/r_w|$ for the cylindrical problem. When the definitions III.50 are substituted in Eqns. III.22-25, it results in four first order differential equations and one algebraic equation. The algebraic equation can be used to eliminate v_θ from the system, yielding

$$v_r' = N_1\left[1 - \gamma m^2/ABz^2\right] + m^2\,\Phi/ABz^2 - \left(\frac{1}{z} + \frac{f'}{f}\right)v_r \qquad \text{(III.51)}$$

$$N_1' = \frac{1}{\gamma}\left[\Phi^*/z - ABv_r + (1-\gamma)\,\frac{f'}{f}\,N_1\right] \qquad \text{(III.52)}$$

$$\Phi^{*\prime} = Afz\,N_1 + m^2\,\Phi/z \qquad \text{(III.53)}$$

$$\Phi' = \Phi^*/z \qquad \text{(III.54)}$$

where $A \equiv r_w^2/\lambda_{DO}^2$ and $B = \omega^2/\omega_{po}^2$. Eqns. III.51-54 are in the form of Eqn. III.33 for RK integration if the vector variable $y \equiv (v_r, N_1, \Phi^*, \Phi)$.

As mentioned earlier the singular point at $z = 0$ requires that y be developed in a power series about the origin. Since the differential equation is in the form of 4 linear equations, it is convenient to derive a matrix power series for y. Assume a power series expansion of the form

$$y(z) = \sum_{k=0}^{\infty} \begin{pmatrix} y_k^1 z^{k+t-1} \\ y_k^2 z^{k+t} \\ y_k^3 z^{k+t} \\ y_k^4 z^{k+t} \end{pmatrix} \quad y_o \neq 0 \qquad \text{(III.55)}$$

with an arbitrary index t . Substitute definition III.55 into Eqns. III.51-54 and replace the electron density functions $f(z)$ and f'/f by the following approximations which are valid for small z ,

$$f(z) = 1 - \alpha z^2 \qquad \text{(III.56)}$$

$$f'/f = - 2\alpha z - 2\alpha^2 z^3 \qquad \text{(III.57)}$$

Then collecting terms containing like powers of z gives a matrix recursion formula for the coefficients y_k .

$$K\, y_k = K2\, y_{k-2} + K4\, y_{k-4} \quad (k = 0,1,2,\cdots) \qquad \text{(III.58)}$$

The matrices K , $K2$ and $K4$ are

$$K = \begin{pmatrix} k + t & \gamma m^2/AB & 0 & -m^2/AB \\ AB/\gamma & k + t & -1/\gamma & 0 \\ 0 & 0 & k + t & -m^2 \\ 0 & 0 & -1 & k + t \end{pmatrix}$$

$$K2 = \begin{pmatrix} 2\alpha & 1 & 0 & 0 \\ 0 & (\gamma - 1/\gamma)2\alpha & 0 & 0 \\ 0 & A & 0 & 0 \\ 0 & 0 & 0 & 0 \end{pmatrix}$$

$$K4 = \begin{pmatrix} 2\alpha^2 & 0 & 0 & 0 \\ 0 & (\gamma - 1/\gamma)2\alpha^2 & 0 & 0 \\ 0 & -\alpha A & 0 & 0 \\ 0 & 0 & 0 & 0 \end{pmatrix} .$$

It is assumed that $y_i = 0$ if $i < 0$ so that Eqn. III.58 for $k = 0$ becomes

$$K\, y_o = 0 \qquad (y_o \neq 0) \tag{III.59}$$

which does not have a solution unless Det $K = 0$. This condition is equivalent to the indicial equation for a single differential equation and serves to determine the allowed values of t . Eqn. III.59 can be rewritten

$$(K - tI)\, y_o = -t\, y_o \qquad (k = 0) \tag{III.60}$$

showing that t is the negative of the eigenvalues of the matrix $(K - tI)$. The four independent eigenvectors of $(K - tI)$ are the initial conditions for the four independent solutions to Eqns. III.51-54.

The eigenvalues are $t = \pm m, \pm m$. The two eigenvalues $t = -m$ give solutions which are singular at $z = 0$ and are therefore discarded. Since the eigenvectors $t = m$ are degenerate, there is some choice in the eigenvectors y_{01} and y_{02} . The eigenvectors used in the present work are

$$y_{01} = \begin{pmatrix} m/AB \\ 0 \\ m \\ 1 \end{pmatrix} \qquad y_{02} = \begin{pmatrix} m/A \\ (1-B)/3 \\ m \\ 1 \end{pmatrix} \tag{III.61}$$

because they generate the functions $\phi_1(z) \propto z$ and $\phi_1(z) \propto J_m(\sqrt{A(1-B)}\, z)$ in the limit $\alpha = 0$ (uniform plasma). Of course any linear combination of y_{01} and y_{02} is also a valid eigenvector.

With this preliminary work accomplished the calculation of ϕ_1'/ϕ_1 versus $\omega^2/\overline{\omega_p^2}$ proceeds straightforwardly. For a given value of A and B the recursion relation III.58 is used to generate two sets of coefficients y_{k1} and y_{k2} for the power series III.55. The two power series are then evaluated at some point z' far enough from the origin to avoid numerical errors. Usually this was $z' = 10h$ or about $z = .02$. Starting with $y_1(z')$ and $y_2(z')$ the RK integration formula is used to carry out the integration of Eqn. III.51-54 to obtain $y_1(1)$ and $y_2(1)$. At this point the remaining boundary condition must be used to determine the linear combination of y_1 and y_2 which is a solution to the problem. That is,

$$y(z) = \beta_1 y_1(z) + \beta_2 y_2(z) \tag{III.62}$$

The discussion of boundary conditions for a slab plasma in Section 3.2 is applicable here also. One condition is simply a scale factor which is chosen to make $\Phi(1) = 1$. The second boundary condition requires that the radial component of the electron velocity equal zero at the wall, $v_r(1) = 0$. Therefore, solving

$$\beta_1 v_{r1}(1) + \beta_2 v_{r2}(1) = 0$$

$$\beta_1 \Phi_1(1) + \beta_2 \Phi_2(1) = 1 \qquad \text{(III.63)}$$

for β_1 and β_2 and calculating

$$\frac{\phi_1'}{\phi_1} = \frac{\Phi^*(1)}{\Phi(1)} = \beta_1 \Phi_1^*(1) + \beta_2 \Phi_2^*(1) \qquad \text{(III.64)}$$

completes the solution. For certain combinations of large A and small B some of these steps must be carried out in doublt precision arithmetic for reasons already explained. In particular, the RK integration and Eqn. III.63 require double precision but the power series calculations do not.

Errors. The discussion of truncation and propagation error in Section 3.2 is independent of geometry. However, the actual error estimates become very complicated as the number of equations increases. Rather than estimating the errors analytically, sample calculations were made for a uniform plasma where the correct solutions are known. Checks of this nature indicate a relative accuracy better than 10^{-4} and usually 10^{-5}. Errors committed in evaluating the power series are completely negligible. An important potential source of error is

the determination of β_1 and β_2 from Eqn. III.63. Because the functions $y_1(z)$ and $y_2(z)$ both show strongly exponential behavior in the cutoff region of the plasma and the correct solution $y(z)$ does not, it may happen that y_1 and y_2 are not independent when only eight significant figures are available. This will result in incorrect values of β_1 and β_2. A special check was made every few calculations to avoid this error. The check consisted of repeating the RK integration with the initial condition $y_c(z') = \beta_1 y_1(z') + \beta_2 y_2(z')$. If β_1 and β_2 are correct, then $y_c(1)$ should have $\Phi = 1$ and $v_r = 0$.

Results. Numerical calculations were performed on the IBM7090 computer. The program of calculation called for detailed curves of ϕ_1'/ϕ_1 versus ω^2/ω_{po}^2 for both dipole and quadrupole modes at five logarithmically spaced values of r_w^2/λ_{DO}^2. In all cases values of ω^2/ω_{po}^2 ranged from 0 to above the third resonance. These are shown in Figures A3.1-10 (Appendix 3). The parameters ω^2/ω_{po}^2 and r_w^2/λ_{DO}^2 have been converted to $\omega^2/\overline{\omega^2}_p$ and $r_w^2/\overline{\lambda^2}_D$ with the aid of Table II. Because the results presented in Figures A3.1-10 will be useful to experimentalists and because they require considerable time and expense to calculate*, the figures have been drawn in full detail so that they may be read to 1% or better.

To obtain a theoretical resonance spectrum for a given experimental plasma column the number K_{eff} of Eqn. III.49 must be known.

---

*The average time to compute one value of ϕ'/ϕ is 6 sec (single precision) or 20 sec (double precision).

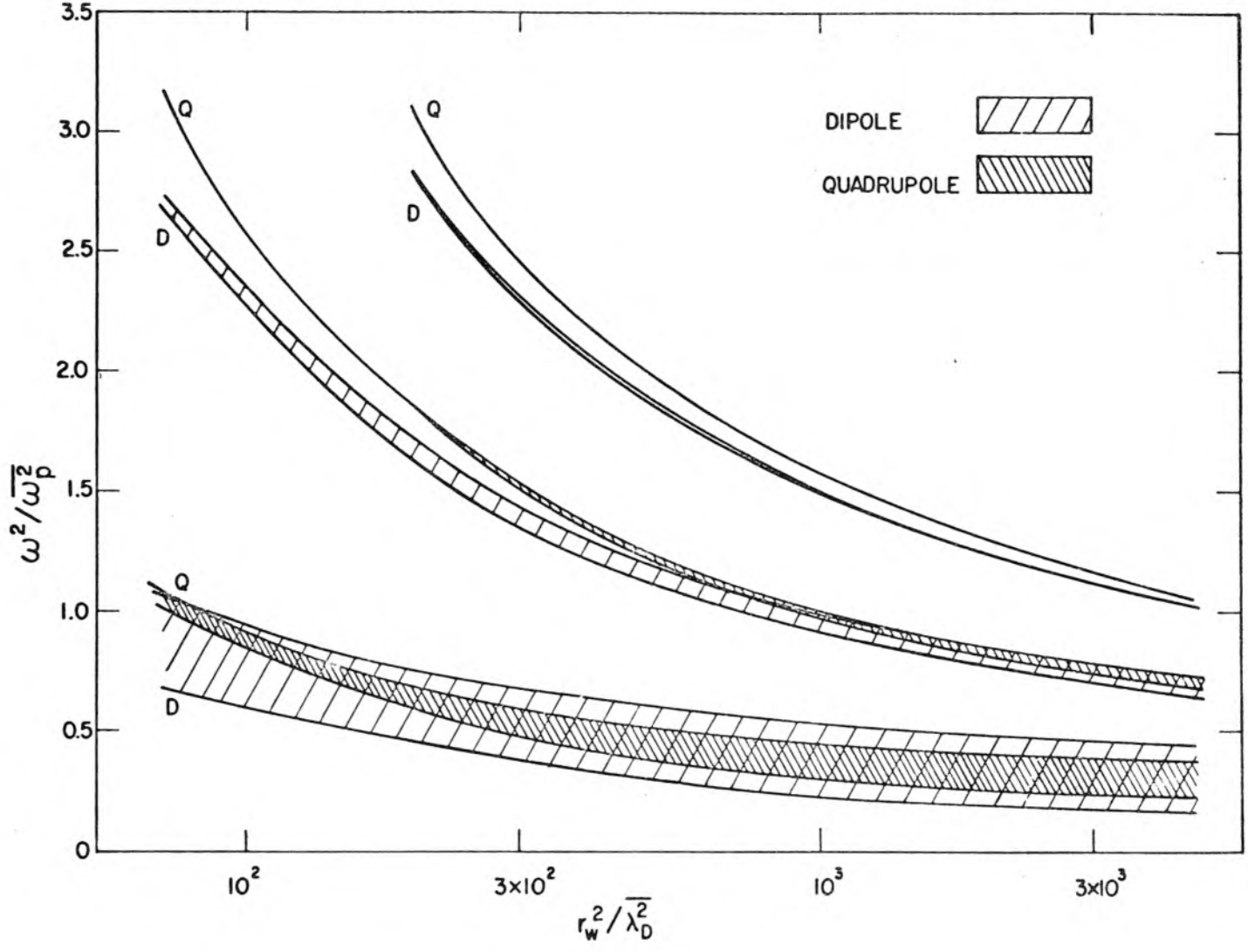

Fig.8 Range of Resonant Frequencies for a Mercury Discharge Column

Nickel (20) has derived formulas for K_{eff} which include the effects of the external exciting apparatus as well as the effects of the glass tube enclosing the plasma. If a line $\phi'/\phi = -m\, K_{eff}$ is drawn on any of the figures A3.1-10, it will intersect the curve $\phi'/\phi(\omega^2/\overline{\omega_p^2})$ at the resonant frequencies. This is illustrated in Figure A3.1 for an assumed value of $K_{eff} = 2.5$ ($m = 1$ since it is a dipole mode. Because any value of K_{eff} between 1 and ∞ is possible, the resonant frequencies can be varied over a range of frequencies. In Figure 8 the resonant frequencies for $K_{eff} = 1$ and $K_{eff} = \infty$ have been plotted as a function of $r_w^2/\overline{\lambda_D^2}$ for both dipole and quadrupole resonances. The shaded areas between the points indicate the range of resonant frequencies that can be obtained for any plasma column by varying the external conditions.

A convenient analytical approximation exists for the functions ϕ'/ϕ . It is apparent from Figures A3.1-10 that the function ϕ'/ϕ has a series of simple poles beginning at some low value of $\omega^2/\overline{\omega_p^2}$ and continuing to infinity. It is also clear that the higher poles have a small residue and hence will not affect the function ϕ_1'/ϕ_1 except near the pole. If ϕ'/ϕ is represented by a series of the form

$$\frac{\phi_1'}{\phi_1} \approx 1 + \sum_{i=1}^{N} \frac{A_i}{\omega_i^2/\overline{\omega_p^2} - \omega^2/\overline{\omega_p^2}} \qquad \text{(III.65)}$$

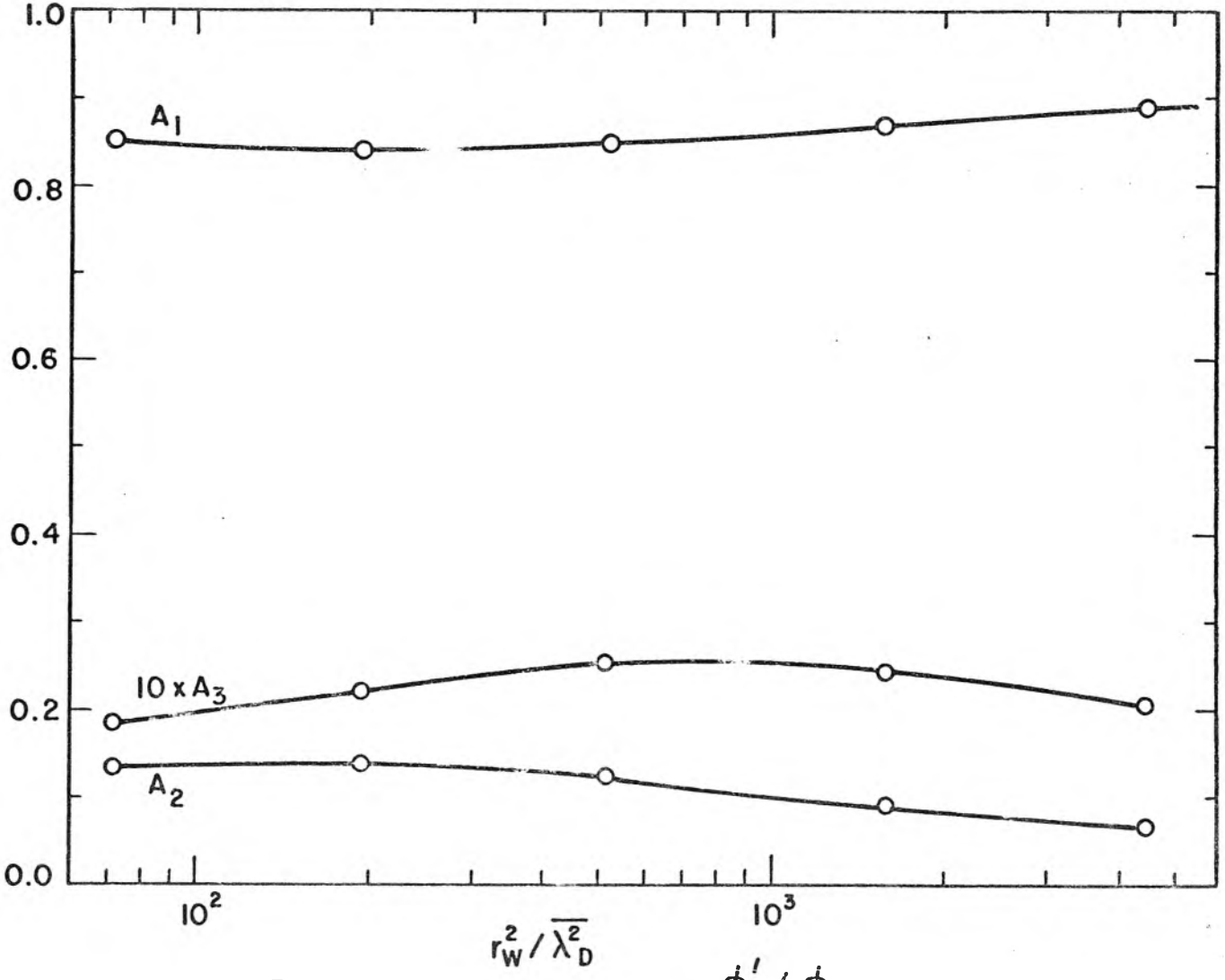

Fig. 9 Residue of the Poles of ϕ_1' / ϕ_1

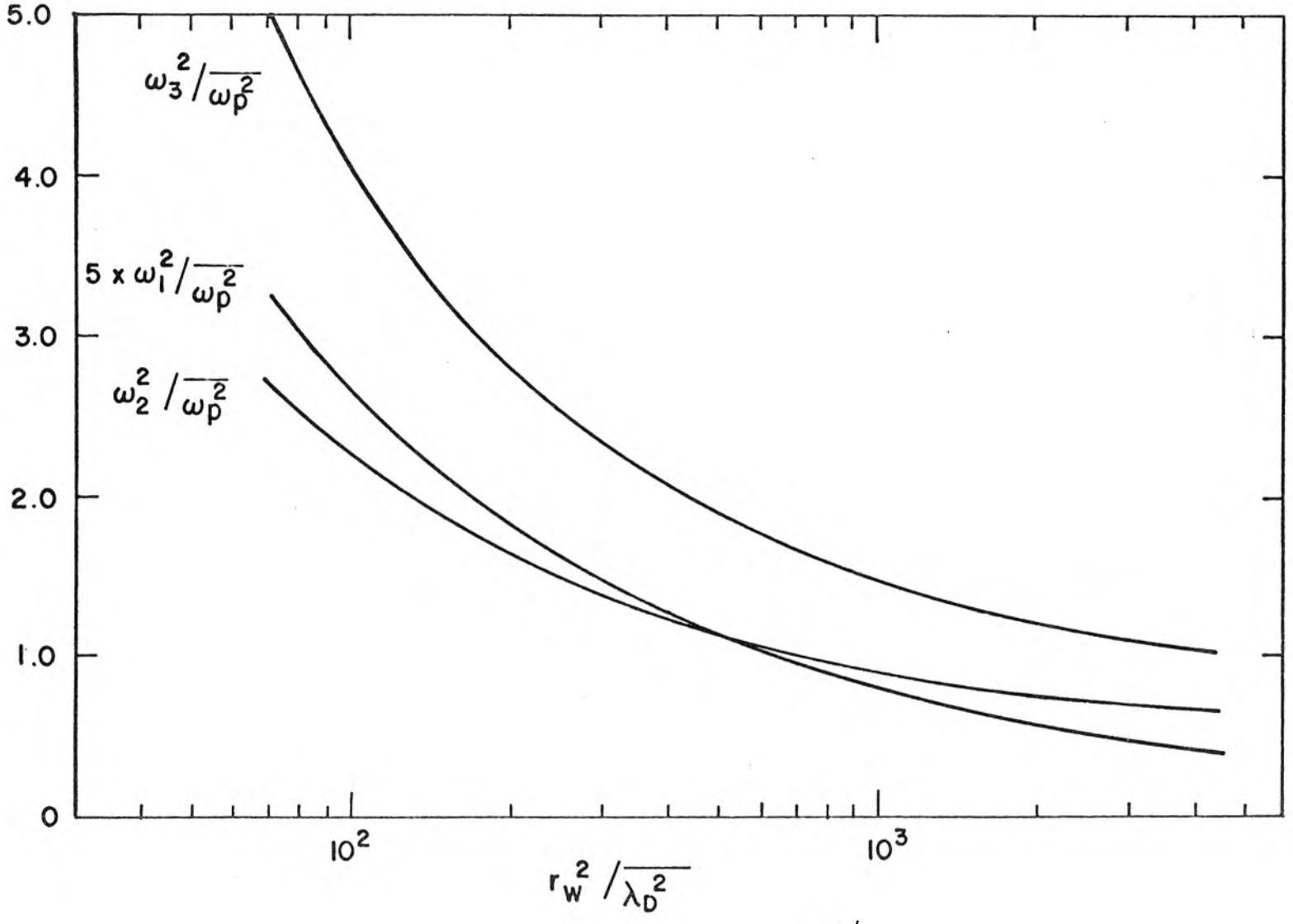

Fig. 10 – Location of the Poles of ϕ_1'/ϕ_1

where $\omega_i^2/\overline{\omega_p^2}$ $(i = 1,2,\cdots,N)$ are the location of the first N poles, then the series will approximate ϕ_1'/ϕ_1 accurately up to the N^{th} pole and beyond with the exception of the vicinity of ω_i^2 $(i = N+1, \cdots, \infty)$. The constants A_i and $\omega_i^2/\overline{\omega_p^2}$ have been evaluated for the dipole data presented in Figures A3.1-5 and are presented in Figures 9 and 10. N has been taken equal to 3 which provides a reasonable fit since the residue of the higher poles decreases rapidly. For the values of $r_w^2/\overline{\lambda_D^2}$ which are marked on Figures 9 and 10, the expression III.65 fits ϕ_1'/ϕ_1 to within 1-2%, and there is reason to believe that the points on the interpolated curves will have similar accuracy. It should be noted that the sum of the A_i's for any given $r_w^2/\overline{\lambda_D^2}$ is very nearly equal to 1. This means that for $\omega^2 \gg \omega_i^2$ the logarithmic derivative obeys the relation

$$\phi_1'/\phi_1 \approx 1 - \overline{\omega_p^2}/\omega^2 \qquad \text{(III.66)}$$

This same relation can be derived by ignoring the effects of electron temperature which implies that at high frequencies the plasma waves are very poorly coupled to the external fields and the plasma

behaves primarily as a dielectric.

It has been pointed out by Gould (21) that the plasma behaves at low frequencies ($\omega^2 \ll \omega_p^2$) as a nearly perfect conductor except in the sheath region where the electron density is very low. If the plasma is represented as a conductor of radius $z = 1 - \sigma$ and a vacuum sheath of thickness σ then the logarithmic derivative at $z = 1$ is

$$\frac{\phi_1'}{\phi_1} = \frac{1 - \sigma + \frac{1}{2}\sigma^2}{\sigma - \frac{1}{2}\sigma^2} \quad . \tag{III.67}$$

Let $L \equiv \phi'/\phi \ (\omega = 0)$ be the logarithmic derivative calculated at zero frequency. Then an effective sheath thickness can be defined from Eqn. III.67

$$\sigma = 1 - \sqrt{\frac{L-1}{L+1}} \quad . \tag{III.68}$$

The numbers L and σ are given in Table III for several values of r_w^2/λ_{DO}^2. Also given is $\sigma\, r_w/\lambda_{DO}$ which measures the effective sheath thickness in Debye lengths. Since $\sigma\, r_w/\lambda_{DO}$ is nearly constant, the effective sheath thickness σ is a measure of the Debye length λ_{DO}. The effective sheath thickness defined by Eqn. III.68 differs by almost a factor of 3 from the sheath thickness defined in Section 2.3 but this is not surprising since σ should measure the thickness of the region where charge separation is almost complete where the definition of Section 2.3 includes the region from 1% charge separation on. If the values of $f(1 - \sigma)$ are compared for various

Debye lengths, it is apparent that for the purposes of defining σ the beginning of the sheath could be defined as the point where the electron density had been reduced by a factor of e^{-2}.

TABLE III -- EFFECTIVE SHEATH THICKNESS

r_w^2/λ_D^2	L	σ	$\sigma\, r_w/\lambda_{DO}$
72	2.383	0.296	6.46
194	3.393	0.262	6.60
515	4.989	0.184	6.71
1580	8.073	0.117	6.73

Discussion. The primary purpose of this investigation is to test the validity of the hypothesis that the observed spectrum of resonances is the result of a nonuniform density distribution in the plasma column. To this end a comparison has been made between the theoretical predictions and the measurements of Nickel (20). Both dipole (Figure 11) and quadrupole (Figure 12) exciting fields were used and the resonant frequencies were determined by measuring the energy absorbed from the exciting fields. In this manner the three lowest resonant frequencies for the dipole and quadrupole modes were found as a function of the average electron density in the column. In order to plot the experimental results versus r_w^2/λ_D^2 the electron temperature must be known. The temperature was not measured by Nickel

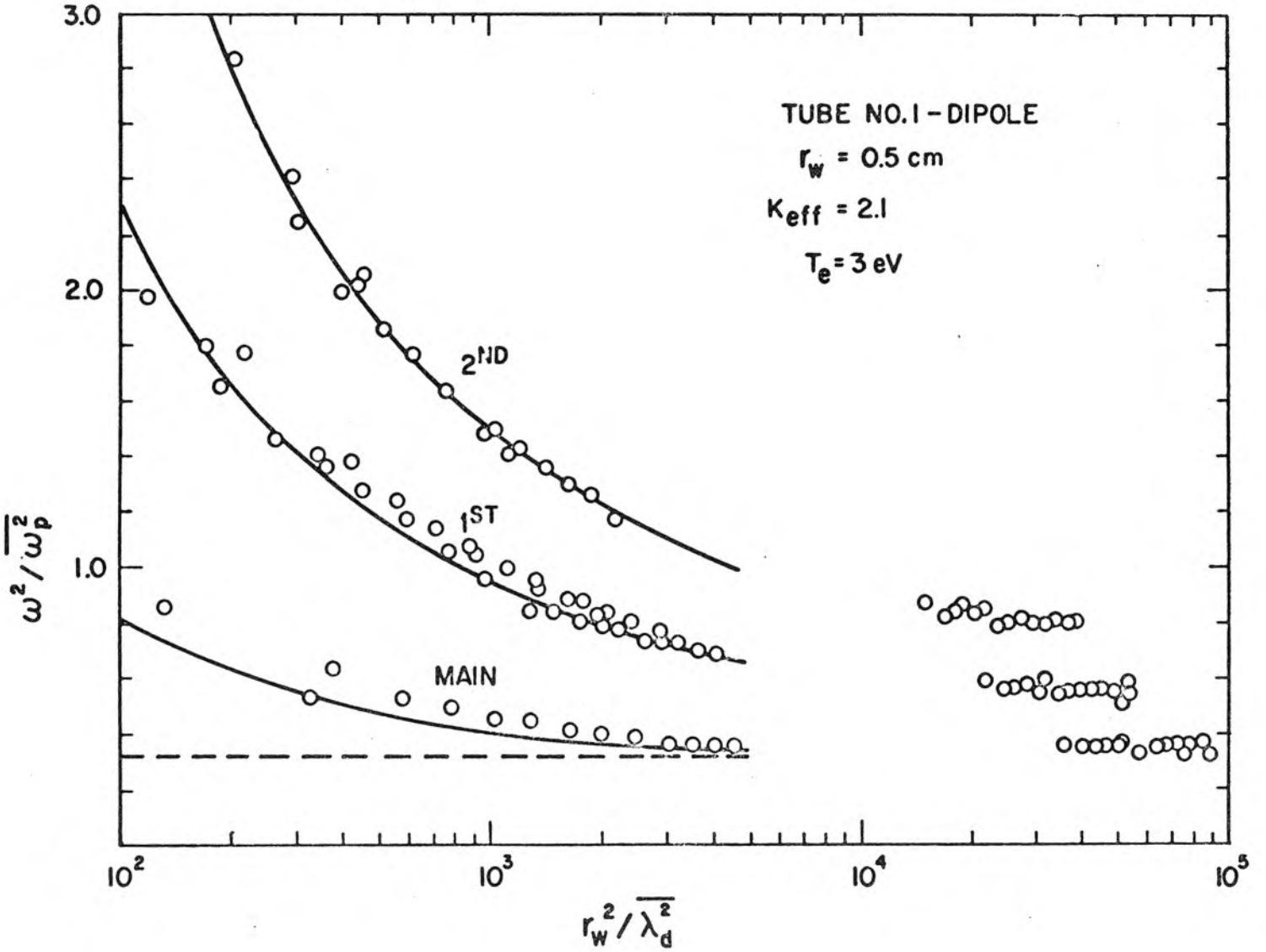

Fig. 11 - COMPARISON OF THEORY AND EXPERIMENT FOR DIPOLE FIELDS

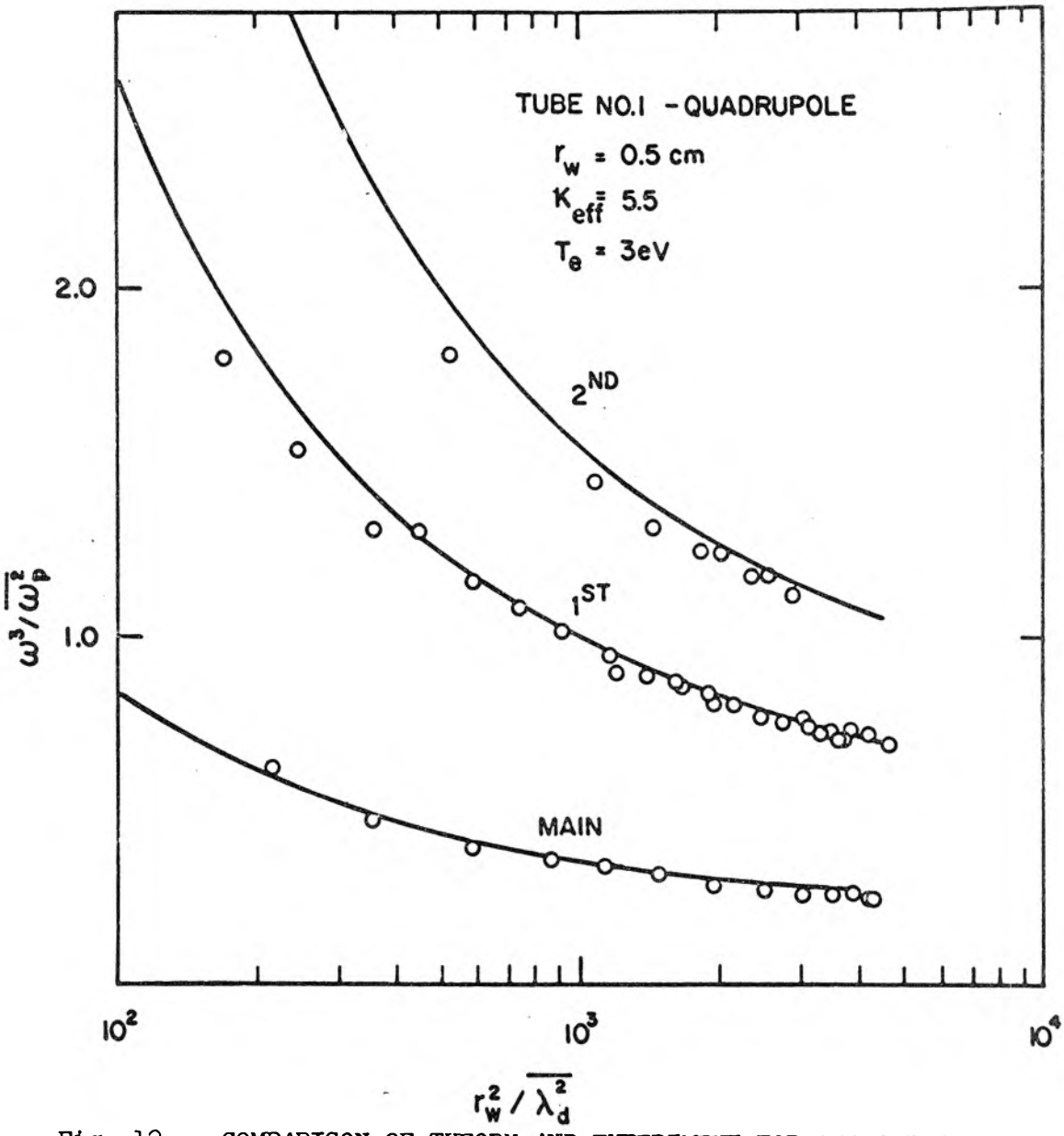

Fig. 12 - COMPARISON OF THEORY AND EXPERIMENT FOR QUADRUPOLE FIELDS

so it has been considered a disposable parameter and the best fit* value of $kT = 3$ e.v. has been used. It is encouraging that this best fit value is in good agreement with Langmuir probe measurements made on similar mercury discharges.

The excellent quantitative agreement between theory and experiment leaves no doubt that the wide spacing of the resonant frequencies is really due to the nonuniform electron density. The manner in which the nonuniform plasma causes such a large separation of the resonant frequencies is illustrated in Figures 13 and 14 which are plots of N_1 versus z. Figure 13 shows the density fluctuations which occur at the lowest resonant frequencies, ω_i^2 $(i = 0,1,2,3)$, for a fixed value of $r_w^2 / \overline{\lambda_D^2} = 1580$. It can be seen that each higher resonance contains one more half-wavelength of the plasma wave. Since it requires greater radial distance in which to fit this extra half-wave, one must raise the incident frequency until more of the plasma can propagate waves (the point r_c indicates the radius where wave propagation ceases, i.e., $\omega^2 = \omega_p^2 = f(r_e)\omega_{po}^2$). Figure 14 illustrates the effect of sheath thickness upon a resonance. Here the electron density fluctuations are shown for the resonance ω_1 for various values of $r_w^2 / \overline{\lambda_D^2}$. As this parameter increases, the thickness of the propagating region (the sheath region) decreases; this does not, however, result in a compensating rise in the frequency

*Obtaining a best fit temperature is particularly easy when $r_w^2 / \overline{\lambda_D^2}$ is plotted on a logarithmic scale because an increase (decrease) in the temperature simply displaces all the experimental points to the left (right) an equal amount.

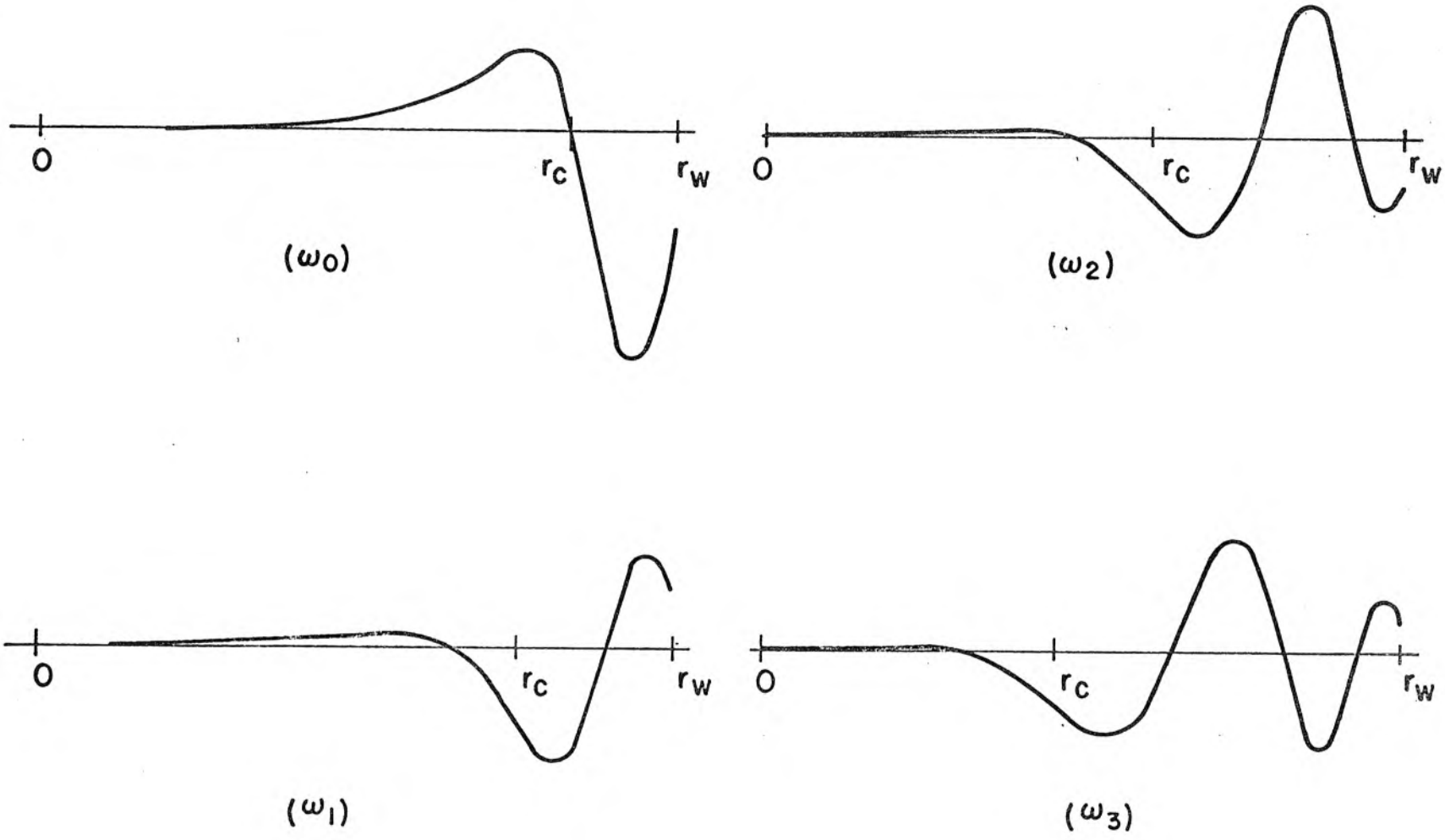

Fig. 13 – Electron Density $N_1(r)$ at the Resonances $\omega_0 - \omega_3$

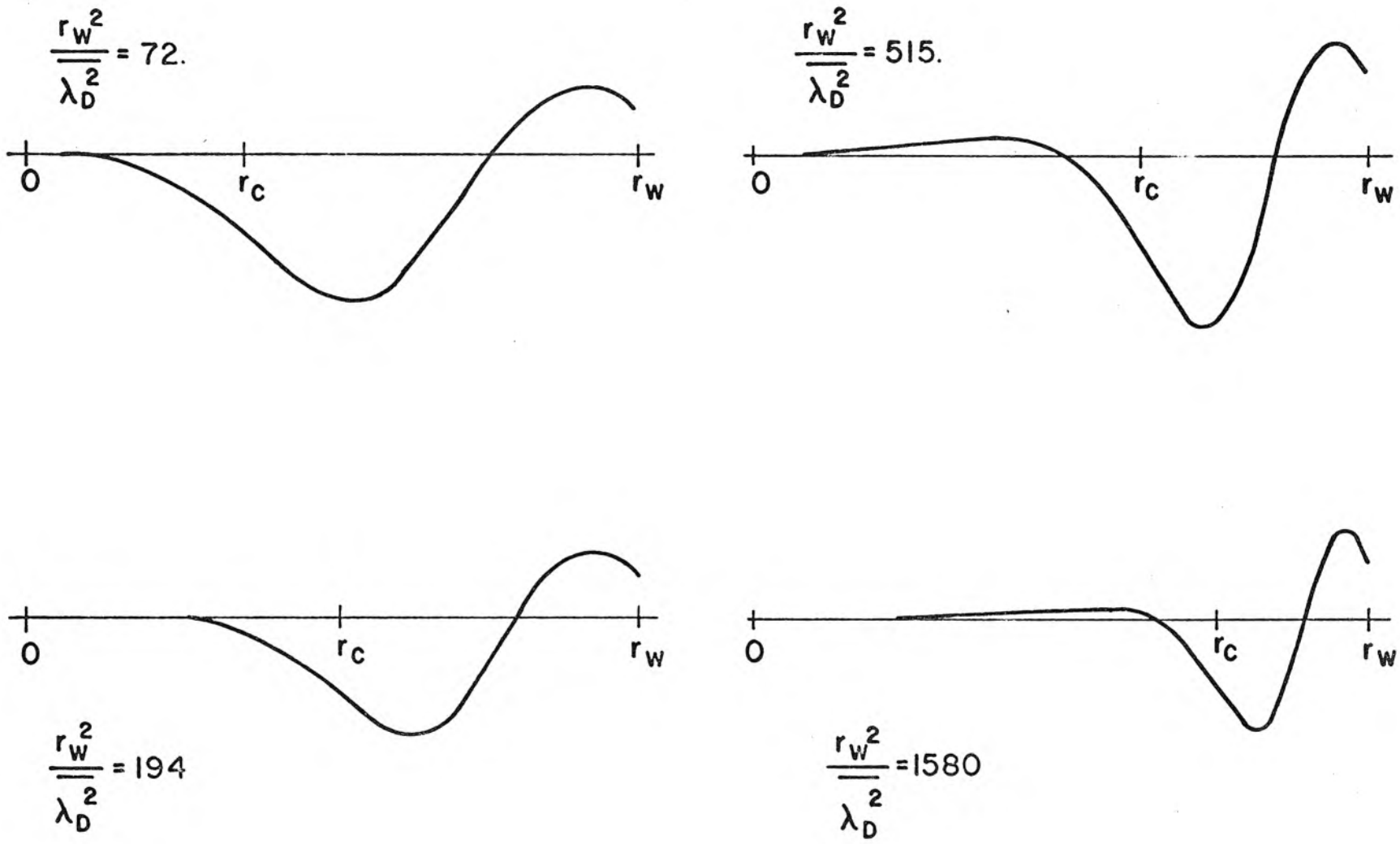

Fig. 14 – Electron Density $N_1(r)$ for the Resonance ω_1

$\omega^2/\overline{\omega_p^2}$, since the wavelength of the plasma wave also decreases as $r_w^2/\overline{\lambda_D^2}$ increases. These two effects combine to hold the frequency $\omega^2/\overline{\omega_p^2}$ nearly constant as the oscillation is restricted to an increasingly narrow region near the wall.

In addition to verifying the importance of the electron density profile, the excellent agreement also yields increased confidence in the assumptions made in deriving both the theory of the static electron density and the theory of plasma-electromagnetic interaction. Independent confirmation of the electron density profiles has come from Crawford (22) who reports probe measurements of the density profiles which agree to about 10% with the calculated curves.

The results of this analysis will extend the usefulness of a commonly used diagnostic method for determining average electron density. In the past the relation

$$\omega_o^2 = \overline{\omega_p^2}/1 + K_{eff} \qquad \text{(III.69)}$$

has been used as a convenient means of determining the average electron density by a simple measurement of the lowest resonant frequency. A line $\omega^2/\overline{\omega_p^2} = 1/1 + K_{eff}$ is shown in Figure 11. It is apparent that Eqn. III.69 is not valid for small values of $r_w^2/\overline{\lambda_D^2}$, that is, for low densities or high temperatures. By using the results of this section it is possible to relate the frequency ω_o to the average electron density over a much wider range of electron densities. In fact, by using ω_1 rather than ω_o it is possible to obtain the average electron density quite accurately without knowing K_{eff}

because the resonance ω_1 is not affected greatly by the surroundings of the plasma.

Analysis of the numerical computations has also shown that a simple determination of sheath thickness and Debye length may be possible if measurements of ϕ'/ϕ for $\omega^2 \ll \omega_p^2$ are feasible.

3.4 Alternate Formulations of the Theory

Although the theory of Section 3.1 has been shown to predict the resonant frequency spectrum with good results, some question can nonetheless be raised concerning its validity. For example, the lack of temperature measurements in the experimental work of Nickel leaves open the possibility that a modification to the theory would yield equally good agreement with experiment at a different electron temperature. It is also interesting to know how sensitive the results obtained here are to changes in some of the assumptions made in deriving the theory.

The ideal test of the approximations made in deriving Eqn. III.26 would be to solve the Boltzmann equation itself. This has proven impossible to date for the cylindrical plasma. Gould (8) has integrated the Boltzmann equation in slab geometry for the special case of a uniform plasma. He solved the problem of boundary conditions by repeating the slab plasma throughout space and requiring that the solutions to the full space problem had a periodicity $2d$. For a nonuniform slab plasma, however, this procedure is not feasible because the resulting full space problem is not a uniform plasma and the Boltzmann equation cannot be integrated. This procedure is even

less effective in the cylindrical plasma where the generalization to a full space problem is impossible. Any attempt to solve the Boltzmann equation using orbit theory is complicated by the static potential in the plasma which causes a particle to change its velocity class as it moves. Short of a completely new method of attack upon the Boltzmann equation, the velocity moment approach seems the only feasible one.

Tensor Pressure Theory. Once the velocity moment approach is adopted, the question of terminating the chain of moment equations arises. It is shown in Appendix II that the use of successive moments of the Boltzmann equation is equivalent to an expansion of the Landau dispersion equation in an asymptotic series and that for a strongly nonuniform plasma the accuracy will not be improved by including moments beyond the tensor pressure. It is possible, however, that eliminating the approximation made in Section 3.1, where the tensor pressure was replaced by a scalar pressure, would improve the theory.

To determine whether this was the case, Eqns. III.9-10 were combined with the third moment equation

$$(P = 2) \qquad n_e \frac{\partial M^2_{ij}}{\partial t} + M^2_{ik} \cdot \nabla u_j + (M_{ik} \cdot \nabla u_j)^{\dagger *} + u \cdot \nabla M^2_{ij} - M^2_{ij} \frac{\partial n_e}{\partial t} + u \cdot \nabla n_e \qquad \text{(III.70)}$$

---

* The superscript $\dagger$ indicates the operation of transposition.

in which the heat flux tensor M^{3}_{ijk} has been set equal to zero and the resulting sixth order differential equation was integrated for a few values of $r_w^2/\overline{\lambda_D^2}$ so that a comparison could be made with experiment. Since the derivation is rather involved, it will be omitted here; reference can be made to the work of Vandenplas (23) for details. The final set of six coupled first order differential equations is

$$\Phi' = \Phi^*/z \tag{III.71}$$

$$\Phi^{*\prime} = A f z N_1 + m^2 \Phi / z \tag{III.72}$$

$$v_r' = \frac{1}{3}\left[Q_{rr} - \frac{f'}{f} v_r - (v_r + m v_\theta)/z \right] \tag{III.73}$$

$$v_\theta' = Q_{r\theta} + (m v_r + v_\theta)/z \tag{III.74}$$

$$Q_{rr}' = \frac{f'}{f}(N_1 - Q_{rr}) - (Q_{rr} + m Q_{r\theta} - Q_{\theta\theta} - \Phi^*)/z - AB v_r \tag{III.75}$$

$$Q'_{r\theta} = -\frac{f'}{f} Q_{r\theta} + \left[m Q_{\theta\theta} - m\Phi - 2Q_{r\theta} \right]/z - AB v_\theta \tag{III.76}$$

where $N_1 = v_r' + \frac{f'}{f} v_r + (v_r + m v_\theta)/z$ is no longer a dependent variable and one of the components of the tensor equation III.70 yields a simple algebraic relation for $Q_{\theta\theta}$.

$$Q_{\theta\theta} = N_1 + 2(v_r + m v_\theta)/z \quad . \tag{III.77}$$

The dimensionless variables $(z, v_r, v_\theta, \Phi, \Phi^*)$ have the same definitions as before (Section 3.3) and the dimensionless pressure

components $\underset{\approx}{Q}$ are related to the pressure tensor by

$$m_e M_{ij}^2 = P_{ij} = n_{eo} f\, kT\, Q_{ij} \tag{III.78}$$

Since this system of equations exhibits a singular point at $z = 0$ a power series solution about $z = 0$ is necessary. The same matrix recursion method used on the fourth order equation in Section 3.3 can be applied here. Define the vector function

$$y(z) = (\Phi, \Phi^*, v_r, v_\theta, Q_{rr}, Q_{r\theta})^\dagger \tag{III.79}$$

and the power series

$$y(z) = z^{t}\, z^{(t+1)} \sum_{j=0}^{\infty} A_j z^j \tag{III.80}$$

where $t^{(t+1)}$ indicates that the variables v_r and v_θ should be multiplied by $z^{(t+1)}$ and the others by z^t. The coefficients A_j are given by the recursion relation

$$J\, A_j = J2\, A_{j-2} + J4\, A_{j-4} \tag{III.81}$$

where the matrices J, $J2$, and $J4$ are determined by inserting definitions II.80 into Eqns. III.71-76 and using the small argument expressions for f and f'/f given by Eqns. III.59-57. The matrices are

$$J = \begin{pmatrix} j+t & -1 & 0 & 0 & 0 & 0 \\ -m^2 & j+t & 0 & 0 & 0 & 0 \\ 0 & 0 & 3(j+t)+4 & m & -1 & 0 \\ 0 & 0 & -m & j+t & 0 & -1 \\ 0 & -1 & -(j+t+4) & -3m & j+t+1 & m \\ m & 0 & -m(j+t+4) & -3m^2 & 0 & j+t+2 \end{pmatrix} \quad \text{(III.82)}$$

$$J2 = \begin{pmatrix} 0 & 0 & 0 & 0 & 0 & 0 \\ 0 & 0 & (j+t)A & mA & 0 & 0 \\ 0 & 0 & 2\alpha & 0 & 0 & 0 \\ 0 & 0 & 0 & 0 & 0 & 0 \\ 0 & 0 & -AB & -2\alpha m & 2\alpha & 0 \\ 0 & 0 & -2\alpha(j+t+1) & -AB & 0 & 2\alpha \end{pmatrix} \quad \text{(III.83)}$$

$$J4 = \begin{pmatrix} 0 & 0 & 0 & 0 & 0 & 0 \\ 0 & 0 & -(j+t)\alpha A & -\alpha mA & 0 & 0 \\ 0 & 0 & 2\alpha^2 & 0 & 0 & 0 \\ 0 & 0 & 0 & 0 & 0 & 0 \\ 0 & 0 & -2\alpha^2(j+t-3) & -2\alpha^2 m & 2\alpha^2 & 0 \\ 0 & 0 & -2\alpha^2 m & 0 & 0 & 2\alpha^2 \end{pmatrix} \quad \text{(III.84)}$$

The indicial equation for t is $\text{Det } J = 0$ for $j = 0$; the roots are $t = \pm m, \pm m, \pm m-2$. The $-m$ roots all correspond to solutions of the differential equation singular at the origin and must be discarded. For each of the roots $t = m, m, m-2$, there must be an initial vector A_0 which satisfies

$$J\ A_o = 0 \quad (j=0) \tag{III.85}$$

and because $t = m$ is a degenerate root, the choice of A_o's will not be unique. A pair of simple vectors for $t = m$ ($m = 1$ or 2) are

m	A_{01}	A_{02}
1	0,0,0,1,1,1	$1,1,\frac{1}{8},\frac{1}{8},1,0$
2	0,0,1,-5,0,-12	$1,2,0,\frac{1}{2},1,1$

Determining the third initial vector for $t = m-2$ is complicated by the fact that Det J vanishes not only for $j = 0$ but also for $j = 2$. Besides the singular equation III.85 a second condition must be satisfied

$$J\ A_2 = J2\ A_o \qquad (j = 2) \quad . \tag{III.86}$$

The initial conditions for the third solution require that both A_o and A_2 be specified.

m	A_{03}	A_{23}
1	0,0,1,-1,0,0	$-AB-2\alpha, -AB-2\alpha, -AB/4, -2\alpha, -7AB/4-4\alpha, AB/4-2\alpha$
2	0,0,1,-1,2,-2	$-AB-2\alpha, -AB-4\alpha, -3AB/20, \alpha, -\frac{3}{2}AB, 3AB/10+2\alpha$

Integration of Eqns. III.71-76 is accomplished with the fourth order RK formula, Eqn. III.33. Each independent solution is evaluated at $z = .02$ using the power series and integrated from there to the

boundary at $z = 1$. After the three solutions have been found the boundary conditions are applied to determine the correct linear combination and ϕ'/ϕ is calculated. Because there are now three solutions, an extra boundary condition in addition to $v_r(1) = 0$ is needed. Since $v_r(1) = 0$ is equivalent to a reflection of each electron's radial velocity at the wall, a natural extension would be to assume specular reflection. That is, in addition to $v_r \rightarrow -v_r$, also $v_\theta \rightarrow v_\theta$. In particular this means that at the wall there is no force in the θ direction on a surface whose normal is in the radial direction. But this is the definition of the tensor pressure component $P_{r\theta}$ so the extra boundary condition is simply $Q_{r\theta} = 0$.

Only dipole mode calculations have been carried out for the tensor pressure theory. The difference between the tensor and scalar pressure theories is shown graphically in Figure A3-4 where ϕ'/ϕ calculated for $r_w^2/\overline{\lambda_D^2} = 1580$ using the tensor theory is shown as a dashed line. In order to compare the tensor and scalar pressure theories, the resonant frequencies predicted by the tensor theory for $K_{eff} = 2.1$ have been plotted in Figure 15 along with the experimental data of Nickel used earlier. The best fit electron temperature is now 3.5 e.v. rather than 3 e.v. Comparison of Figures 11 and 15 seems to imply that the tensor pressure theory is equally successful in predicting the resonant frequencies, but this is not completely true. Experimental results for several more plasma columns with different values of r_w and K_{eff} fit the scalar pressure theory noticeably better. The only conclusions which can be reached from these data are

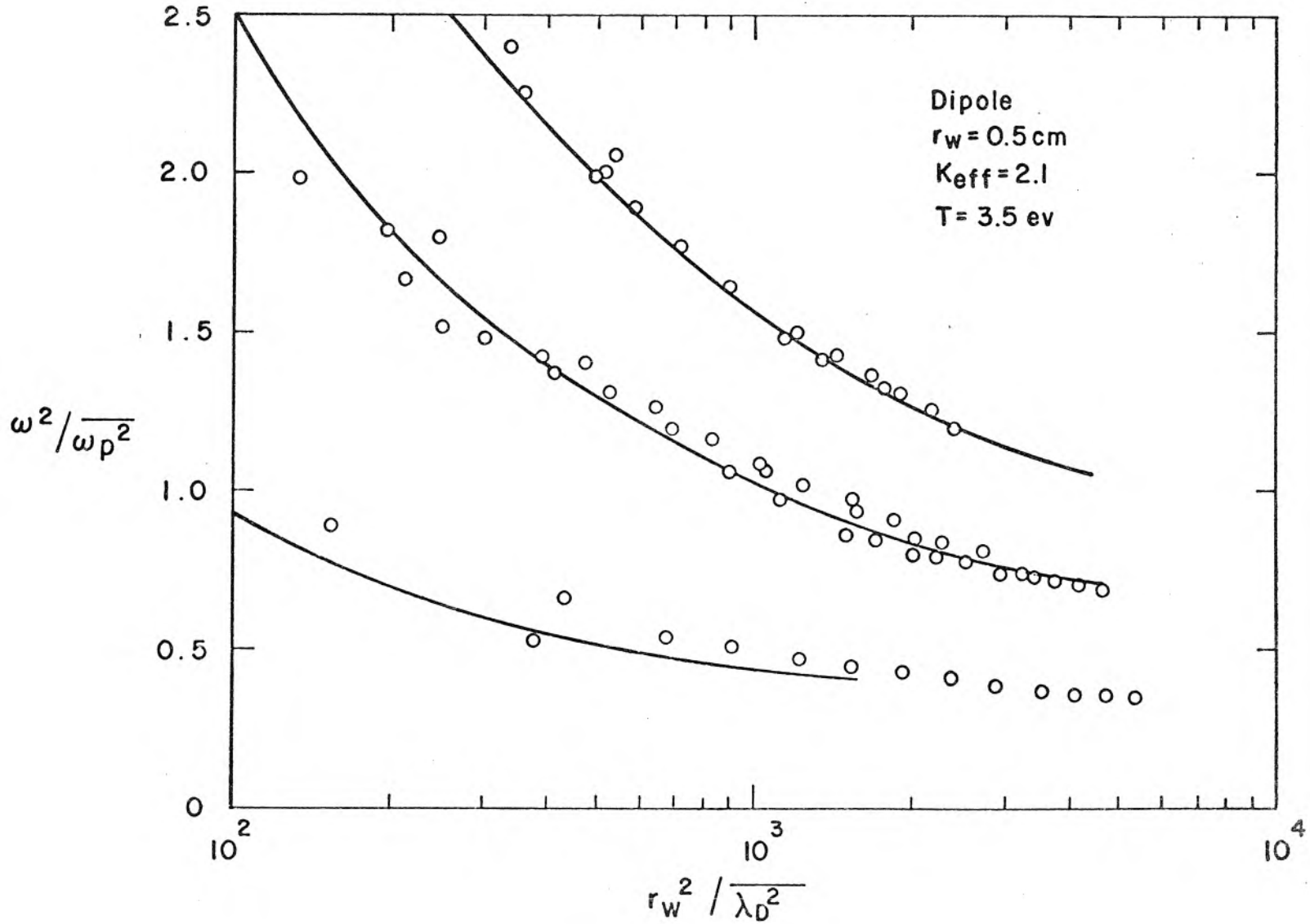

Fig. 15 – Comparison of Tensor Theory With Experiment

these: (1) the tensor pressure theory does not agree with experiment quite as well as the scalar theory, (2) the best fit electron temperature is slightly higher than would be expected for a mercury discharge and (3) any final choice between the two theories must wait until a measurement of electron temperature is made in conjunction with measurements of the resonant frequencies. Even if more complete measurements do not favor the scalar pressure theory, it will still prove very useful because it is computationally faster and cheaper.

Energy Conservation. In the study of beam-plasma interactions and coupled mode interactions in a uniform plasma, the concept of an energy conservation theorem for the time-varying energies has proven quite useful. Such a theorem has the form

$$\frac{\partial}{\partial t}\,[\text{energy density}] + \nabla\cdot[\text{energy flux}] = 0 \qquad \text{(III.87)}$$

and is usually derived by writing an equation for $\underset{\sim}{J}\cdot\underset{\sim}{E}_1$, the rate at which the electric field $\underset{\sim}{E}_1$ does work on the plasma, and then applying Maxwell's equations to obtain $\underset{\sim}{J}\cdot\underset{\sim}{E}_1$ as a time derivative. Since $\underset{\sim}{J} = en_o f\,\underset{\sim}{u}_1$, it is simple to write the equation for $\underset{\sim}{J}\cdot\underset{\sim}{E}_1$ for the scalar pressure theory by dotting $\underset{\sim}{E}_1$ into Eqn. III-23. The resulting equation can be easily manipulated into the form of Eqn. III.87 with the exception of one term.

$$\frac{\partial}{\partial t}\left[\frac{1}{2}\epsilon_o E_1^2 + \frac{1}{2} m_e n_{eo} f\,\underset{\sim}{u}_1^2 + \frac{1}{2}\frac{\gamma kT}{n_o f} n_1^2\right] + \nabla\cdot(\gamma kT\, n_1\,\underset{\sim}{u}_1) =$$

$$(\gamma - 1)en_1\,\underset{\sim}{u}_1\cdot\underset{\sim}{E}_o \quad . \qquad \text{(III.88)}$$

The extraneous term which is evident on the r.h.s. of Eqn. III.88 corresponds to an energy source derived from the motion of the plasma against the static electric field*. A simple modification of the equations describing the plasma will cause this extra term to vanish and leads to a description of the plasma which obeys an energy conservation theorem. This modification, which sets the term $(1-\gamma)\frac{f'}{f}N_1 = 0$ in Eqn. III.52, was made, and the resulting equations were integrated as before. The results were in poor agreement with experiment, indicating that an energy conservation theorem is not possible for the nonuniform plasma.

Boundary Conditions. Having discussed the various approximations made in deriving the equations describing the response of the plasma, the only remaining question concerns the boundary conditions to be used with those equations. Although superficially the boundary condition $u_r(1) = 0$ seems to be well justified for an insulating wall, it can be called into doubt. If, for example, the insulating wall were to alternately accumulate and lose a surface charge on each half-cycle, then the current at the wall would not necessarily be zero. It has been argued on physical grounds that setting the acceleration equal to zero at the wall should be a better boundary condition. However, in a linearized theory the acceleration $\underset{\sim}{a}_1$ is given by

$$\underset{\sim}{a}_1 = \frac{\partial \underset{\sim}{u}_1}{\partial t} + (\underset{\sim}{u}\cdot\nabla)\underset{\sim}{u}\ , \qquad \text{(III.89)}$$

*Note that $\underset{\sim}{E}_0 = 0$ in a uniform plasma so that the conservation law is valid in that case.

and since $(\underset{\sim}{u}_1 \cdot \nabla)\underset{\sim}{u}_1$ is a second order quantity, $a_1 = 0$ implies $u_1 = 0$. It was pointed out by Leavens (24) that for the slab problem another type of boundary condition is available. Leavens argues as follows: When the equations describing the electric field in a slab plasma are put in WKB form the analog of the potential energy function is (Eqn. III.44)

$$U(x) = \frac{1}{\gamma}\frac{d^2}{\lambda_{DO}^2} f(x) + \frac{7}{4}\left(\frac{f'}{\gamma f}\right)^2 - \frac{1}{2}\frac{f''}{f} \quad . \tag{III.90}$$

Near the wall the electron density and hence f is very small so that f'/f becomes large and $U(x)$ may exceed k^2. This means that there is another turning point in the problem besides the expected one at $f(x) = \omega^2/\omega_{po}^2$ and that the function $\psi(x)$ must have exponential behavior near the wall. If this exponential region were infinitely long there would be a second boundary condition requiring only the decaying exponential solution to be present. Although the exponential region is not infinitely thick, it may be several e-folding distances thick so that the requirement of decaying exponential behavior is still an approximate boundary condition.

This argument is probably invalid. The only equation which can be put in WKB form is Eqn. III.29 with $C = 0$. But specifying, $C = 0$ is a boundary condition in itself and uniquely determines the resonant frequencies, thus the WKB boundary condition is redundant. It appears therefore that $u_1 = 0$ is the only boundary condition which has a reasonable justification. A more detailed study of the sheath-wall region would certainly be required before any alternative

boundary condition could be proposed.

SECTION IV - PLASMA WAVE RESONANCES WITH AN AXIAL MAGNETIC FIELD

4.1 Comments

It has been well verified experimentally that an axial magnetic field imposed upon a plasma column has the effect of splitting the lowest frequency resonance ω_o into two two distinct resonances whose frequencies depend upon the strength of the magnetic field (29). Several investigators (25,29), however, have failed to observe a splitting of the higher resonances. Recently Nickel (20) has observed such splittings in low density plasmas.

The splitting of the resonances is not unexpected because the zero magnetic field problem exhibits a two-fold angular degeneracy, i.e., when the angular dependence of the various functions is separated out by the substitutions Eqn. III.50, the resulting coupled equations III.51-54 are quadratic in m. Therefore the right and left handed modes of oscillation characterized by $e^{\pm i|m|\theta}$ are degenerate. Physically this results from the lack of a preferred axis which would allow the sense of rotation to be defined. However, when an axial magnetic field is applied, a preferred direction is defined and the degeneracy is broken.

Previous theoretical investigations of the effect of an axial magnetic field have been limited to the lowest frequency resonance because electron temperatures have been ignored. Crawford (25), for example, has assumed $T_e = 0$ and used a tensor dielectric constant

to describe the plasma. He finds two resonant frequencies, $\omega_{o+}(B_o)$ and $\omega_{o-}(B_o)$, which depend upon the magnetic field strength and obey the relations

$$\omega_{o+}\,\omega_{o-} = \omega_o^2 \tag{IV.1}$$

$$\omega_{o+} - \omega_{o-} = \omega_c \tag{IV.2}$$

where $\omega_c = eB_o/m$ is the electron cyclotron frequency. Nothing can be learned about the higher resonances in this way since they exist only when $T \neq 0$. To predict the effects of a magnetic field upon the higher resonances with reasonable accuracy requires that the theory derived in Sections II and III be modified to take account of the magnetic field.

4.2 Effect of the Magnetic Field upon the Static Density Profile

If a strong axial magnetic field is imposed upon the plasma column, most of the assumptions underlying the calculation of the static electron density profiles in Section II will be invalidated. In particular, the electrons will be tied to magnetic field lines and the electron current transverse to the field will be reduced. Also the ions will be deflected from a straight line motion toward the walls which will change the form of the integral expression for the ion density. These facts seem to indicate that a new calculation of the static electron density will be required before the resonances can be investigated. In certain limits, however, the static density profiles derived earlier are still approximately valid.

For example, it is experimentally observed that the resonances of a low density plasma column subject to an axial magnetic field are strongly damped when the magnetic field exceeds 50-100 gauss. If for this reason investigations are restricted to fields of less than 50 gauss, the problem of ion trajectories is eliminated. The high mass and low velocity of the ions require fields of kilogauss to appreciably affect their motion.

The electron motion provides a more severe limitation. It is reasonable to expect the transverse electron current to remain substantially unaffected as long as the cyclotron radius is larger than the radius of the plasma column. This is the case if $B < 10$ gauss for the experiments of Nickel (20). A more careful calculation of the reduction in the transverse electron current gives the following results. If J_o is the current density at $B = 0$ and the approximation $r_L \ll r_w$ is made, then $J \sim J_o/3$ at 40 gauss and for an ion density of 10^{10} cm^{-3}. At a lower density of $n_I = 10^9$ cm^{-3} the current suffers a more drastic reduction; $J \approx J_o/600$.

For small changes in the radial current J the major modification in the results of Section II is a change in the point s_w where the ion and electron currents are equal. If $n_I \sim 10^{10}$ cm^{-3} then $\beta^2 \sim 10^4$ and a change of 3 in the current causes a change of less than 1% in s_w . In summary, it can be expected that calculations made using the static electron densities calculated for zero magnetic field will be valid for fields such that $r_L \geq r_w$ and for larger fields when the ion densities are high enough. For example,

experiments conducted on a mercury discharge with $r_w \sim .5$ cm will have a range of validity of 0-10 gauss when $n_I \sim 10^9$ cm^{-3} and 0-40 gauss when $n_I \sim 10^{10}$ cm^{-3} .

4.3 Theory

The equations developed in Section III to describe the response of the plasma to an applied electromagnetic wave require only a minor modification to include the effects of a magnetic field. This modification adds to the acceleration $\underset{\sim}{A} = ne\,\underset{\sim}{E}/m_e$ the effect of the magnetic field:

$$\underset{\sim}{A} = \frac{ne}{m}\underset{\sim}{E} + \frac{ne}{m}\underset{\sim}{u} \times \underset{\sim}{B}_o \quad . \tag{IV.4}$$

Except for this change, the derivations in Section 3.1 and 3.3 follow exactly as before*. A new dimensionless parameter C related to the magnetic field is introduced into the problem. It is defined as

$$C = \omega_c^2/\omega_{po}^2 \quad . \tag{IV.5}$$

The final dimensionless equations describing the plasma response are

$$v_r' = N_1\left[1 - \frac{\gamma m^2}{ABz^2}\right] + \frac{m^2}{ABz^2}\,\Phi - \left[\frac{(1-D)}{z} + \frac{f'}{f}\right] v_r \tag{IV.6}$$

*The linearizing assumptions Eqn. III.15-18 are still valid in the presence of a magnetic field. In particular there is no static drift velocity in the θ direction as might be expected from the $\underset{\sim}{E} \times \underset{\sim}{B}/B^2$ drift. This drift is cancelled by an oppositely directed velocity arising from the electron density gradient.

$$N_1' = \frac{1}{\gamma}\left[\Phi^*/z - A(B-C)v_r + \left\{(1-\gamma)\frac{f'}{f} - \frac{\gamma D}{z}\right\} N_1 + \frac{D}{z}\Phi\right] \qquad \text{(IV.7)}$$

$$\Phi^{*\prime} = Afz\, N_1 + m^2 \Phi/z \qquad \text{(IV.8)}$$

$$\Phi' = \Phi^*/z \qquad \text{(IV.9)}$$

where D is a combination of the previously defined dimensionless parameters (The definitions of v_t, N_1, Φ^*, Φ are similar to those in Eqn. III.50 except $\cos m\theta \rightarrow e^{im\theta}$ and $\sin m\theta \rightarrow -ie^{im\theta}$).

$$D = m\left(\frac{C}{B}\right)^{1/2} = \frac{m\,\omega_c\omega}{\omega_{po}^2} \quad . \qquad \text{(IV.10)}$$

Note that Eqns. IV.6-9 depend upon m now as well as m^2 through the factor D and that m occurs only in the combination $m\,\omega_c$ making the equations invariant to reflections along the axis as they should be. The boundary conditions used previously are unaffected by the addition of a magnetic field and do not need to be discussed further. Similarly, the numerical methods used to solve Eqns. IV.6-9 are identical to those used before and the calculations proceed in the same fashion: power series, numerical integration, and boundary conditions. The results of the calculations are considerably more difficult to present, however, because of the additional parameter ω_c^2/ω_{po}^2. Rather than attempting to give general curves of ϕ_1'/ϕ_1 $(\omega^2/\omega_p^2$, ω_c^2/ω_p^2, $r_w^2/\lambda_D^2)$ which would allow the resonant frequencies to be determined for any experimental situation, a value of K_{eff} will be assumed which is typical of the values encountered in practice, and the

resulting resonant frequencies $\omega_i^2/\overline{\omega_p^2}$ will be plotted as a function of $\omega_c/\sqrt{\overline{\omega_p^2}}$. This is done in Figures A3.11-13 for $K_{eff} = 2.1$ and for the values of $r_w^2/\overline{\lambda_D^2}$ indicated on each figure. The curves marked +(-) correspond go the right (left) handed polarization or $m = +1(-1)$.

4.4 Results of Numerical Evaluation of the Theory

The lowest resonance behaves approximately in the manner predicted by the simple dielectric theory. The dependence of the resonant frequencies ω_o^+ and ω_o^- upon the magnetic field can be expressed approximately by

$$\omega_o^+ \omega_o^- = \omega_o^2 \qquad \text{(IV.11)}$$

$$\omega_o^+ - \omega_o^- = \lambda \omega_c \qquad \text{(IV.12)}$$

The constant λ depends upon the shape of the electron density profile or equivalently upon $r_w^2/\overline{\lambda_D^2}$. Values of λ for the results shown in Figures A3.11-13 are given in Table IV

TABLE IV

$r_w^2/\overline{\lambda_D^2}$	72	194	515	1580	4530
λ	0.89	0.83	0.79	0.76	0.74

It is somewhat surprising that λ is not equal to 1 as Larmor's theorem would seem to imply it should be. However, for perturbation in

a plasma with finite electron temperature, Larmor's theorem is not applicable. This follows from the fact that charge separation ($n_e \neq n_i$) can take place and in particular can occur in both ways, i.e., $n_e > n_i$ and $n_e < n_i$. But this is equivalent in the perturbation equations to having charges of both $+\frac{e}{m}$ and $-\frac{e}{m}$ whereas Larmor's theorem assumes that all particles have the same $\frac{e}{m}$ ratio. From a microscopic point of view the discrepancy is a result of the positive ions which have $\frac{e}{m}$ different from the electrons. Examination of Figures A3.11-13 shows that the values of λ are much less than 1 for the higher resonances. This is in agreement with the above argument, since the charge separation throughout the cutoff region ($\omega_p^2 > \omega^2$) is always of the same sign and it is only in the propagation region where $\omega^2 > \omega_p^2$ that any charge of opposite sign can arise. The propagating region is, of course, much larger for the higher resonances and hence the deviation from $\lambda = 1$ is greater.

The higher resonances, only one of which is shown in Figures A3.11-13, exhibit an unexpected behavior as a function of B_o. For very weak magnetic fields a splitting results which is similar to that observed for the lowest frequency resonance. At higher fields however, the (-) polarized resonance begins to move to higher frequencies until both (+) and (-) resonant frequencies are increasing in frequency while maintaining nearly constant separation. That this behavior is correct can be seen easily from the differential equation in the limit of high magnetic field.

If Eqns. IV.6-9 are combined into a single differential equation for Φ and the limit $\omega_c \gg \omega_{po}$, $\omega_c \gg \omega$ is taken, then Φ

is found to satisfy the equation

$$\nabla^2\Phi - \frac{Af}{1 - \frac{Af}{f'}\frac{\omega\omega_c}{\omega_{po}^2}\frac{z}{m}}\Phi = 0 \quad . \tag{IV.13}$$

Eqn. IV.13 is a wave equation $(\nabla^2 + k^2)\Phi = 0$ where k^2 is given by the function

$$k^2 = -\frac{Af}{1 + \frac{Af}{|f'|}\frac{\omega\omega_c}{\omega_{po}^2}\frac{z}{m}} \tag{IV.14}$$

in which all the quantities are positive numbers except m which is $\pm |m|$ depending upon the polarization of the applied field. If $m = +|m|$ then k^2 is strictly negative for all z and the function $\Phi(z)$ will have an exponential character, $\Phi(z) \propto \exp(kz)$, and hence $\Phi^*/\Phi z = \phi_1'/\phi_1 = k$ will be positive. This means that no resonances can occur for $m = +|m|$ and $\omega \ll \omega_c$ which agrees with the numerical results. If $m = -|m|$ the situation is more complicated. The magnitudes of the various quantities are: $Af \approx 5 - 5000$ and $Afz/|f'| \approx 1 - 150$ depending on $r_w^2/\overline{\lambda_D^2}$ and the value of z considered. Now if

$$\frac{Afz}{|f'|}\frac{\omega\omega_c}{\omega_{po}^2} \gg 1 \qquad m = -|m| \tag{IV.15}$$

then

$$k^2 = + \frac{|f'|\ \omega_{po}^2}{\omega\ \omega_c z} \ll |f'|/z \qquad \text{(IV.16)}$$

and although k^2 is positive, it is so small ($\frac{f'}{z} = 3$) that it would be impossible for Φ to undergo even one half-wave of oscillation in the region $0 \leq z \leq 1$. There is, however, one exception to this statement and that occurs if

$$1 + \Delta > \frac{Afz}{|f'|} \frac{\omega \omega_e}{\omega_{po}^2} > 1 \qquad m = -|m| \qquad \text{(IV.17)}$$

for a range of values of z. Then $k^2 \approx Af/\Delta$ which is a large number. More detailed examination of the values of k^2 obtainable and the ranges of z where k is positive, show that it is possible to obtain only a fraction of a wavelength of oscillation even though k^2 is large so that a resonance occurring by this means must be identified with the ω_o^- mode which has less than a half-wavelength of oscillation. For this mode Eqn. IV.17 requires that

$$\frac{\omega}{\omega_{po}} \approx \frac{|f'|}{Afz} \Big/ \frac{\omega_c}{\omega_{po}} \qquad \text{(IV.18)}$$

or that $\omega \propto \omega_c^{-1}$ which agrees with the calculated behavior of the ω_o^- mode.

Recent experiments by Nickel (20) have verified qualitatively this theoretically predicted behavior. In particular he has observed a splitting of the ω_1 resonance into two resonances whose spacing depends upon the magnetic field for weak fields (0-10 Gauss) and becomes independent of the magnetic field as it is increased.

SECTION V - SUMMARY AND CONCLUSIONS

It has been observed experimentally that if a beam of microwaves is incident upon a plasma column perpendicular to its axis and with the incident electric vector transverse to the column, a series of resonances are observed in the scattering at frequencies near the plasma frequency. It has been the purpose of this investigation to provide a quantitative theory explaining the origin of the resonances and to provide detailed calculations of the resonant frequencies. The theory advanced here differs from previous work in taking into account the variation of electron density with radius in the plasma column.

Since it is proposed that the radial variations in electron density are important to these resonances and the theory is expected to provide quantitative information about the resonances, it is apparent that some physically reasonable electron density profiles must be used. This has been accomplished by numerically solving the equation proposed by Tonks and Langmuir as a description of the static behavior of a collisionless plasma in an insulating cylinder. The equation describing the static electron density takes into account the formation of a sheath region near the wall which depends upon the electron temperature. As a result a family of curves is obtained which gives the variation of electron density with radius as a function of the parameter r_w^2/λ_{DO}^2 .

The electron density profiles are used in conjunction with the first two velocity moments of the Boltzmann equation to describe the response of the static plasma column to a perturbing RF electric field oriented transverse to the column. In deriving the equations

describing the response of the plasma an assumption was made concerning the electron pressure, namely, that it was a scalar quantity related to the electron density. The equation derived in this manner is a fourth order differential equation for the electric potential $\phi_1(r)$. In its dimensionless form this equation depends upon the two parameters r_w^2/λ_{DO}^2 and ω^2/ω_{po}^2 .

Extensive numerical integration of the differential equation for $\phi_1(r)$ was carried out and is presented in the form of curves of $\phi_1'/\phi_1(r_w)$ versus ω^2/ω_p^2 for five values of the parameter $r_w^2/\overline{\lambda_D^2}$. In addition, comparisons have been made with the work of Nickel (20) which have shown an excellent agreement between theory and experiment. From this agreement several conclusions may be drawn. First, the non-uniformity of the electron density in the plasma column is essential in determining the spectrum of resonant frequencies observed. Second, the electron density profiles computed are in reasonable agreement with the actual electron density profiles existing in mercury discharges. Finally, the assumptions made in reducing the Boltzmann equation to a soluble differential equation are approximately valid.

Whether the assumptions made in reducing the Boltzmann equation are the best that could be made was also investigated. For example, trial computations were made using a theory which replaced the simple scalar electron pressure with a more complicated tensor electron pressure. It was concluded that the resonances predicted using the tensor pressure are in nearly as good agreement as those predicted using the scalar pressure except that a 15% higher electron temperature was

needed to obtain a proper fit to the experimental data. Measurements of electron temperature in a mercury plasma tend to favor the lower temperature given by the scalar pressure theory, but more extensive experimental measurements need to be made before either assumption can be discarded. An attempt was made to derive a theory which contained an energy conservation theorem, but it was not successful.

In the last section the effects of an axial magnetic field upon the resonant frequencies was studied. It was shown that weak magnetic fields ($B_o < 40$ Gauss) had little effect upon the static electron density so that only the theory of the plasma response required modification. This modification was simply the addition of the term $e\underset{\sim}{V} \times B_o$ to the force acting on an electron. Preliminary numerical solutions were obtained for this modified theory with the following results. The lowest frequency resonance is split into two resonances which move monotonically to higher and lower frequencies as the magnetic field is increased. This general behavior was expected from a simplified theory due to Crawford (27). However, the details of the amount of splitting as a function of B_o do not agree with his conclusions. In particular, his expression for the splitting of the resonances $\omega^+ - \omega^- = \omega_c$ was found to be only an approximation to $\omega^+ - \omega^- = \lambda\, \omega_c$ where λ is a slowly varying function of r_w^2 / λ_{DO}^2.

The higher frequency resonances exhibit a marked difference in their behavior from the lowest resonances. Each higher resonance splits into two resonances at very weak fields, but as the magnetic field is increased, the resonance which had begun to decrease in fre-

quency reverses its behavior so that eventually both modes ω^+ and ω^- are increasing in frequency as the magnetic field increases. This behavior has been shown to be consistent with the equations describing the plasma response in the limit $\omega_c \gg \omega$, $\omega_c \gg \omega_{po}$. Physically, it can be explained by noting that the motion of the plasma for the two lowest frequency resonant modes ω_o^+ and ω_o^- correspond to a uniform right and left handed rotation, so that the magnetic field affects them differently. Conversely, each higher resonant mode, since it exhibits waves in the sheath region, is a mixture of right and left handed rotation and hence is affected in the same manner by the magnetic field.

In addition to demonstrating that the nonuniformity of the plasma electron density is the crucial factor in determining the resonant scattering frequencies of a plasma column, the results presented in this work provide a valuable diagnostic tool for the rapid determination of average electron density. With a simple measurement of a dipole resonant frequency* and a knowledge of the electron temperature, the average electron density can be obtained in the following way. Using the graphs of ϕ'/ϕ versus $\omega^2/\overline{\omega_p^2}$ (Figures A3.1-5), construct a figure similar to Figure 11. Since $r_w^2/\overline{\lambda_D^2} = (r_w^2\, e^2/\epsilon_o kT)\bar{n}$ and $\omega^2/\overline{\omega_p^2} = (\epsilon_o m/e^2)\omega^2/\bar{n}$, this plot is essentially one of resonant frequencies over average density versus

---

* ω_1 is convenient because it is usually easily observed and its frequency is relatively independent of K_{eff} .

average density. If the measured resonant frequency is ω_{lm} then the intersection of the curve $\omega_{lm}^2/\bar{n}$ versus $\bar{n}$ will give the true average electron density and also the effective Debye length $r_w^2/\overline{\lambda_D^2}$. With this information and Tables I and II it is also possible to obtain n_o and the sheath thickness ($\sim 18\ \lambda_{DO}$) .

As is usually the case, this investigation has raised as many new questions as it has resolved. Certainly additional calculations should be made in order to investigate the resonant scattering from plasmas with different ionic species, for example H_2 or H_e . It was also pointed out previously that experimental checks need to be made into the agreement between best fit electron temperatures and experimental electron temperatures. The most interesting theoretical question raised concerns the effect of damping upon the resonances. The experimentally observed resonances have a finite amplitude and width and it would be interesting to know whether the major cause of damping was collisional or Landau damping. In this way the diagnostic uses of the plasma wave resonances might be expanded to include studies of Landau damping in nonuniform plasmas or measurements of the electron collision frequency.

APPENDIX I

DETAILS OF THE TECHNIQUES USED IN THE NUMERICAL SOLUTION OF EQUATION II.7

As outlined in Section 2.2, a predictor corrector method is used to build a table of the function $\eta(s)$ at some interval h. This table is begun at the origin by calculating the first 12 values of η using a power series solution to Eqn. II.7.

The power series is derived in the following way. $\eta(s)$ may be expanded in a power series about the origin as*

$$\eta(s) = as^2 + bs^4 + cs^6 + \cdots \quad . \tag{A1.1}$$

Regrettably the integral in Eqn. II.7 cannot be evaluated when a power series occurs within the square root. The alternative is to invert the series A1.1 to obtain a series expansion of s in powers of η. These new series are

$$s = \left(\frac{\eta}{a}\right)^{1/2} - \frac{1}{2}\frac{b}{a}\left(\frac{\eta}{a}\right)^{3/2} + \cdots \tag{A1.2}$$

$$s^2 = \frac{\eta}{a} - \frac{b}{a}\left(\frac{\eta}{a}\right)^2 + \cdots \quad . \tag{A1.3}$$

The integral which must be done is

---

*The odd powers of s all vanish because the square root in the integral generates half integral powers of s when odd terms are included and no half integral powers occur in the rest of the equation.

$$I = \frac{1}{2}\int_0^s \frac{e^{-\eta(\sigma)}\, d\sigma^2}{\sqrt{\eta(s) - \eta(\sigma)}} \quad . \tag{A1.4}$$

If the definitions $\eta(\sigma) \equiv \eta$ and $\eta(s) = \eta_s$ are made and Eqn. A1.3 is substituted into A1.4, then

$$I \approx \frac{1}{2}\int_0^{\eta_s} \frac{(1 - \eta + \frac{\eta^2}{2} - \cdots)(\frac{1}{a} - \frac{2b}{a}\frac{\eta}{a^2} + \cdots)d\eta}{\sqrt{\eta_s - \eta}} \tag{A1.5}$$

or

$$I \simeq \frac{\eta_s^{1/2}}{a} - \frac{4}{3}(\frac{b}{a^3} + \frac{1}{2a})\eta_s^{3/2} - \cdots \quad .$$

A straightforward evaluation of $s\nabla^2 \eta_s$ leads to

$$s\nabla^2 \eta_s = 4a^{1/2}\, \eta_s^{1/2} + 14b(\frac{\eta_s}{a})^{3/2} + \cdots \tag{A1.6}$$

Inserting A1.5-6 into Eqn. II.7 leads to the following relations for a and b.

$$a = (1 + \frac{4a}{\beta^2})^{-2} \tag{A1.7}$$

$$b = \frac{a - \frac{2}{3}a^{1/2}}{\frac{4}{3a^{3/2}} - \frac{1}{2a} + \frac{14}{\beta^2}} \tag{A1.8}$$

Eqn. A1.7 is cubic in a and can be solved most easily by iteration. That is, assume a = 1, evaluate the r.h.s. of Eqn A1.7 to obtain a new value of a and continue until the process converges. Once a is

known, b can be calculated straightforwardly.

The resulting two-term power series has errors of the order $O(s^6)$. If the initial values of η are desired to an accuracy of 10^{-6} then the restriction on s is $s<0.03$. If the power series is used to evaluate the first 12 values of η then $11h < .03$ or $h < .0027$. Once the initial values have been calculated, the predictor corrector method can be used to obtain the remainder of the solution.

The predictor formula is derived using finite difference operators (14). For convenience let $\eta_N \equiv \eta(Nh)$. Then the operator ∇_d is defined as

$$\nabla_d \eta_{N+1} = \eta_{N+1} - \eta_N \tag{A1.9}$$

or rearranging terms

$$\eta_{N+1} = \frac{1}{1-\nabla_d} \eta_N \quad . \tag{A1.10}$$

Expansion of the operator $1/(1-\nabla_d)$ leads to

$$\eta_{N+1} = (1 + \nabla_d + \nabla_d^2 + \nabla_d^3 + \cdots)\eta_N \tag{A1.11}$$

which when truncated after the term ∇_d^4 and applied to η_N gives the predictor formula used.

$$\overset{P}{\eta}_{N+1} = 5\eta_N - 10\eta_{N-1} + 10\eta_{N-2} - 5\eta_{N-3} + \eta_{N-4} \quad . \tag{A1.12}$$

Using the value $\overset{P}{\eta}_{N+1}$ and the table of η_i $(i = 0,1,\cdots N)$ the integral and derivatives occurring in Eqn. II.7 can be evaluated. The

derivatives $d\eta/ds$ and $d^2\eta/ds^2$ are given by the formulas

$$\eta'_{N+1} = \left[\frac{25}{12}\eta_{N+1} - 4\eta_N + 3\eta_{N-1} - \frac{4}{3}\eta_{N-2} + \frac{1}{4}\eta_{N+3}\right]\Big/h \qquad (A1.13)$$

$$\eta''_{N+1} = \left[\frac{35}{12}\eta_{N+1} - \frac{26}{3}\eta_N + \frac{19}{2}\eta_{N-1} - \frac{14}{3}\eta_{N-2} + \frac{11}{12}\eta_{N-3}\right]\Big/h^2 . \qquad (A1.14)$$

The derivation of these equations is a direct result of the finite difference identity

$$\eta_{N+1} = \eta_N + h\,D\,\eta_N + \frac{h^2}{2!}D^2\eta_N + \frac{h^3}{3!}D^3\eta_N + \cdots \equiv e^{hD}\eta_N \qquad (A1.15)$$

where D is a symbolic operator for differentiation. From A1.15 and A1.10 it follows

$$\eta_{N+1} = \frac{1}{1-\nabla_d}\eta_N = e^{hD}\eta_N$$

and hence

$$hD = -\log(1-\nabla_d) = \nabla_d + \frac{1}{2}\nabla_d^2 + \frac{1}{3}\nabla_d^3 + \cdots \qquad (A1.16)$$

giving the operation of differentiation in terms of finite difference operators. A similar expression can be derived for D^2, the second derivative.

For a function tabulated at constant intervals the process of integration in its simplest approximation reduces to forming the sum of all the table entries. A more accurate method of numerical

integration is Gregory integration. The formula for Gregory integration of an arbitrary function F is given by Todd (14) as

$$\int_0^N F_N \, dN = \frac{1}{2} F_o + F_1 + \cdots F_{N-1} + \frac{1}{2} F_N + \frac{1}{12} (\Delta_d F_o - \nabla_d F_N) - \frac{1}{24} (\Delta_d^2 F_o - \nabla_d^2 F_N) + \cdots \quad \text{(A1.16)}$$

where $\Delta_d \eta_o = \eta_1 - \eta_o$. This formula consists of a simple sum of the table entries plus corrections involving differences in the table. In the actual calculation correction terms through ∇_d^5 have been retained. It should be noted that to evaluate $\nabla_d^5 F_N$ and $\Delta_d^5 F_o$ requires the values F_o through F_5 and F_N through F_{N-5} , a minimum of 12 values of F . This is the reason for the seemingly arbitrary choice to evaluate the first 12 points by η by power series.

Equation II.13 illustrates a way of eliminating the singularity in the function which must be integrated. In the actual calculation the subtraction discussed was carried out twice to reduce the error. The actual calculations were performed with the formula

$$\int_0^s \frac{e^{-\eta\sigma} \, d\sigma}{\sqrt{\eta_s - \eta}} = \frac{4}{3} \frac{s \, e^{-\eta_s}}{\sqrt{\eta_s' / s}} \left[1 + \frac{1}{5} s \left(\eta_s' + \frac{\eta_s''}{4\eta_s'} \right) \right] + \int_0^s \left\{ \frac{e^{-\eta\sigma}}{\sqrt{\eta_s - \eta}} - \frac{e^{-\eta_s \sigma}}{\sqrt{\eta_s' (s-\sigma)}} \left[1 + \left(\eta_s' + \frac{\eta_s''}{4\eta_s'} \right) (s-\sigma) \right] \right\} d\sigma \quad \text{(A1.17)}$$

where the integral on the r.h.s. was evaluated using the previously

described Gregory formula.

When the two sides of equation II.7 are evaluated they will not, in general, be equal because η^{P}_{N+1} is not the correct value of η_{N+1}. To find a correction to the value of η^{P}_{N+1} we define the error ψ_o = l.h.s. Eqn. II.7 - r.h.s. Eqn. II.7 . An approximate correction to η^{P}_{N+1} is given by the empirical formula

$$\Delta\eta = \frac{.02\ \psi_o}{(1 + 10^4 s/\beta^2)} \quad . \tag{A1.18}$$

Using the new value $\eta^{c1}_{N+1} = \eta^{P}_{N+1} + \Delta\eta$, the evaluation of Eqn. II.7 is repeated and a new error is defined ψ_1 . Using Newtonian interpolation on the two points (η_{N+1}, ψ_o) and $(\eta^{c1}_{N+1}, \psi_1)$ a new guess η^{c2}_{N+1} is made. If $(\eta^{c1}_{N+1} - \eta^{c2}_{N+1}) < \tau$ then the iteration has converged and the calculation proceeds to the point η_{N+2} . If the test is not satisfied then ψ_2 is calculated using η^{c2}_{N+1} and the iteration is repeated until it converges.

In all calculations $\tau = 2 \times 10^{-8}$ so that the only errors in the calculation are caused by errors in the numerical formulas. These errors depend upon the interval size and for best results the interval should be small; however, the calculation time depends upon $(1/h)^2$ so that too small an interval is costly in computational time. The best compromise was found to be $h = 0.002$. The errors in integration are estimated to be less than 10^{-6} and by using only every other point ($h = .004$) for differentiation, the error there has been kept less than 5×10^{-7} . Even allowing for accumulation of error during the calculation

the results should be accurate to 1 or 2 parts in 10^5 (for random errors of size Δ committed n times, the total error grows as $\sqrt{n}$ which is about 25 times for a typical calculation.)

APPENDIX II

JUSTIFICATION OF THE TERMINATION OF THE VELOCITY MOMENT EQUATIONS

Whether termination of the chain of coupled equations III.8 is justified is logically connected to the question "to what extent are the coupled moment equations equivalent to the Boltzmann equation?" This question can be answered approximately by investigating a uniform plasma for which the Boltzmann equation is soluble by analytic techniques. The results derived by examining the uniform plasma will be approximately valid from point to point in a nonuniform plasma.

The conductivity of a uniform plasma can be found directly from the Boltzmann equation in terms of the well known plasma dispersion function (26).

$$Z\left(\frac{\omega}{kV_e}\right) = \frac{1}{\sqrt{\pi}} \int_{-\infty}^{\infty} \frac{e^{-\xi^2}\, d\xi}{\xi - \frac{\omega}{kV_e}} \qquad \text{(A2.1)}$$

where k is the magnitude of the wave vector for some wave in the plasma, ω is its angular frequency and V_e is the mean thermal velocity. The dispersion relation for longitudinal waves in a uniform plasma can also be written in terms of this function as

$$1 - \frac{\omega_p^2}{k^2 V_e^2} Z'\left(\frac{\omega}{kV_e}\right) = 0 \qquad \text{(A2.2)}$$

where Z' denotes differentiation with respect to the argument. The function Z' can be expanded for large arguments and Eqn. A2.2 can

be rewritten as

$$\omega^2 \simeq \omega_p^2 + \frac{3}{2} k^2 V_e^2 + \frac{15}{4} \frac{k^4 V_e^4}{\omega_p^2} + \cdots \quad . \tag{A2.3}$$

If the same problem of longitudinal plasma oscillations is now considered from the point of view of the coupled moment equations, an interesting comparison can be made to Eqn. A2.3. Referring to Eqn. III.8 if $M_2 = 0$ then the resulting equations can be solved with the result

$$\omega^2 \simeq \omega_p^2 \quad . \tag{A2.4}$$

If $M_2 \neq 0$ but $M_3 = 0$ then the resulting dispersion equation is

$$\omega^2 \simeq \omega_p^2 + \frac{3}{2} k^2 V_e^2 \tag{A2.5}$$

and if $M_2 \neq 0$, $M_3 \neq 0$ but $M_4 = 0$ then

$$\omega^2 \simeq \omega_p^2 + \frac{3}{2} k^2 V_e^2 + \frac{15}{4} \frac{k^4 V_e^4}{\omega_p^2} \quad . \tag{A2.6}$$

Note that each additional moment M_i adds an additional term to the dispersion equation for ω^2 and that this series agrees term by term with the result, Eqn. A2.3, derived by expanding the plasma dispersion function.

It can be shown, however, that the expansion of the plasma dispersion function used to derive Eqn. A2.3 is an asymptotic expansion and by convention should be terminated when the terms begin to

increase. The general formula for Eqn. A2.3 is

$$\omega^2 = \omega_p^2 \sum_{m=0}^{\infty} \frac{1\cdot 3\cdot 5 \cdots 2m+1}{2^m} \left(\frac{kV_e}{\omega}\right)^{2m} \qquad (A2.7)$$

and if the ratio of the m^{th} term to the $m\text{-}1^{th}$ term is to be less than 1, then

$$m \leq \frac{\omega^2}{k^2 V_e^2} - \frac{1}{2} \quad . \qquad (A2.8)$$

In a nonuniform plasma the quantity $\omega^2/k^2V_e^2$ is, of course, a function of position and the number of terms justifiable in the moment equations will depend upon the smallest value of $\omega^2/k^2V_e^2$. This can be estimated as follows:

$$\frac{1}{k^2} \approx \frac{3}{2} \frac{V_e^2}{\omega^2 - \omega_p^2} \qquad (A2.9)$$

$$\frac{\omega^2}{k^2V_e^2} \approx \frac{3}{2} \frac{\omega^2}{\omega^2 - \omega_p^2} \quad . \qquad (A2.10)$$

Since only the propagating region $\omega > \omega_p$ is of concern, the smallest value of Eqn. A2.10 $\omega^2/k^2V_e^2 = \frac{3}{2}$ or $m = 1$. This corresponds to retaining moments as high as the pressure tensor in the moment equations, but any higher moments will not necessarily increase the accuracy of the results.

APPENDIX III

GRAPHS AND TABLES OF NUMERICAL RESULTS

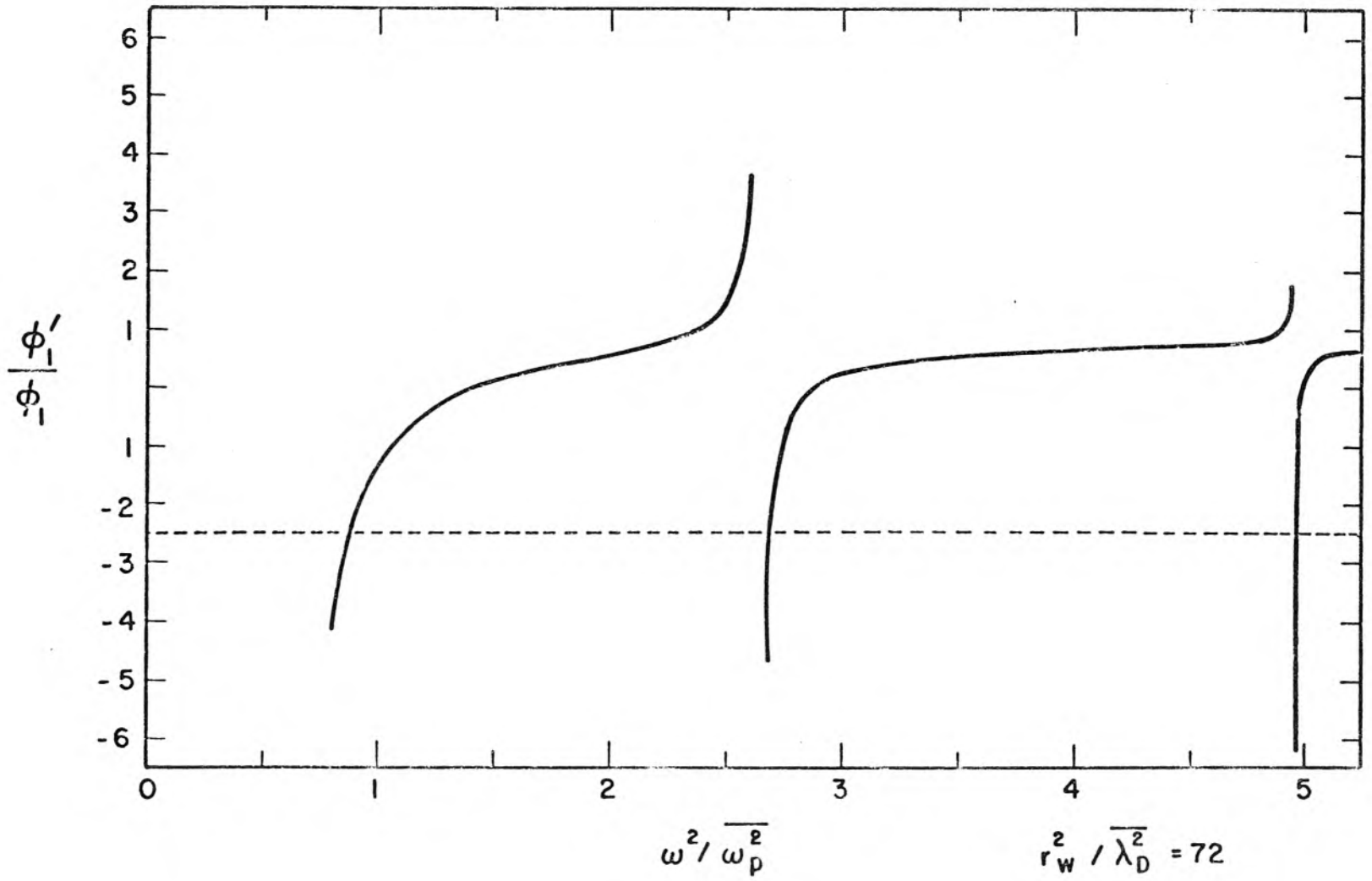
$\frac{\phi_1'}{\phi_1}$
6
5
4
3
2
1
1
-2
-3
-4
-5
-6
0
1
2
3
4
5
$\omega^2 / \overline{\omega_p^2}$
$r_w^2 / \overline{\lambda_D^2} = 72$

Fig. A 3.1

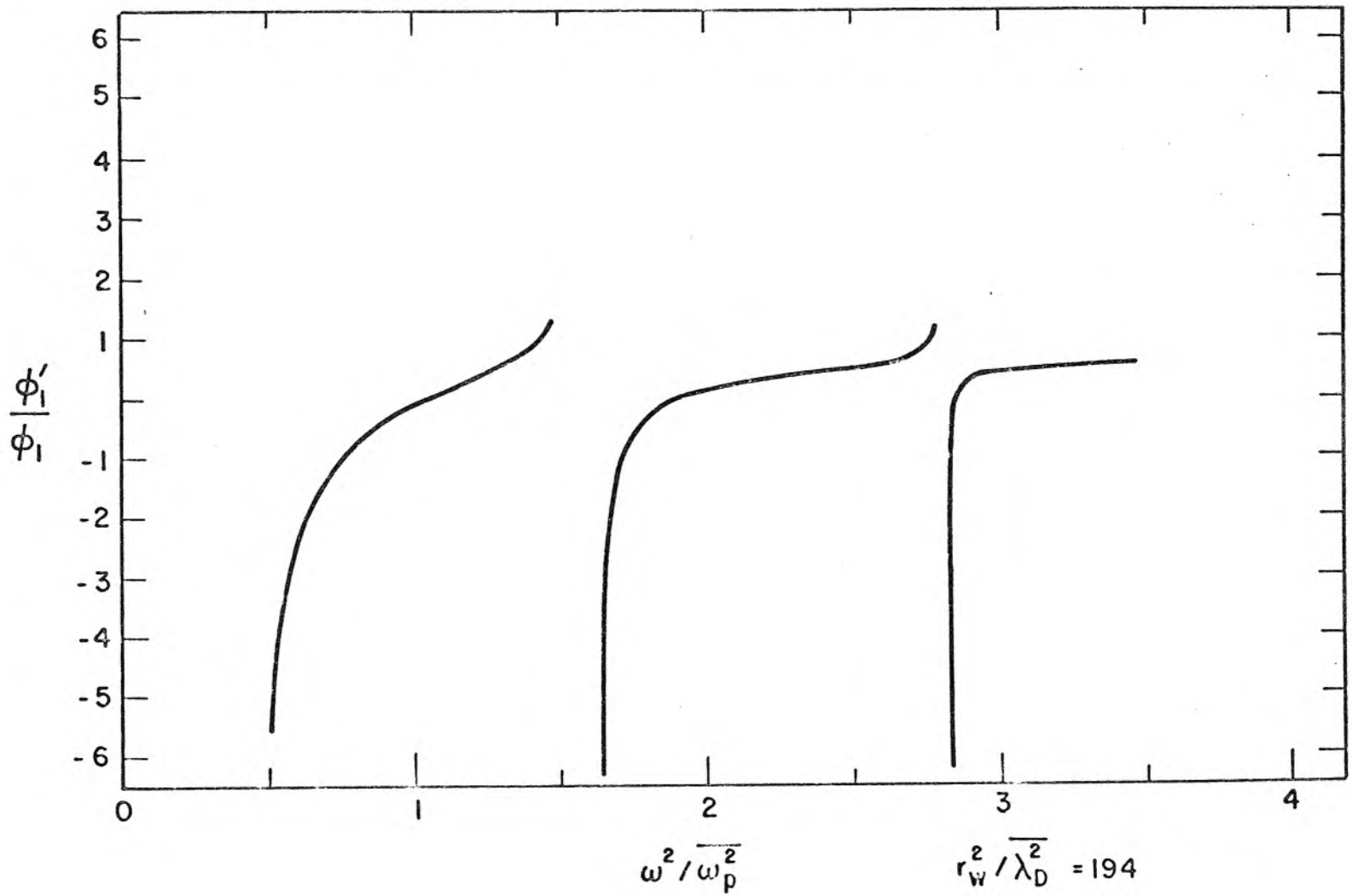
6
5
4
3
2
1
-1
-2
-3
-4
-5
-6
0
1
2
3
4
$\frac{\phi_1'}{\phi_1}$
$\omega^2/\overline{\omega_p^2}$
$r_w^2/\overline{\lambda_D^2} = 194$

Fig. A 3.2

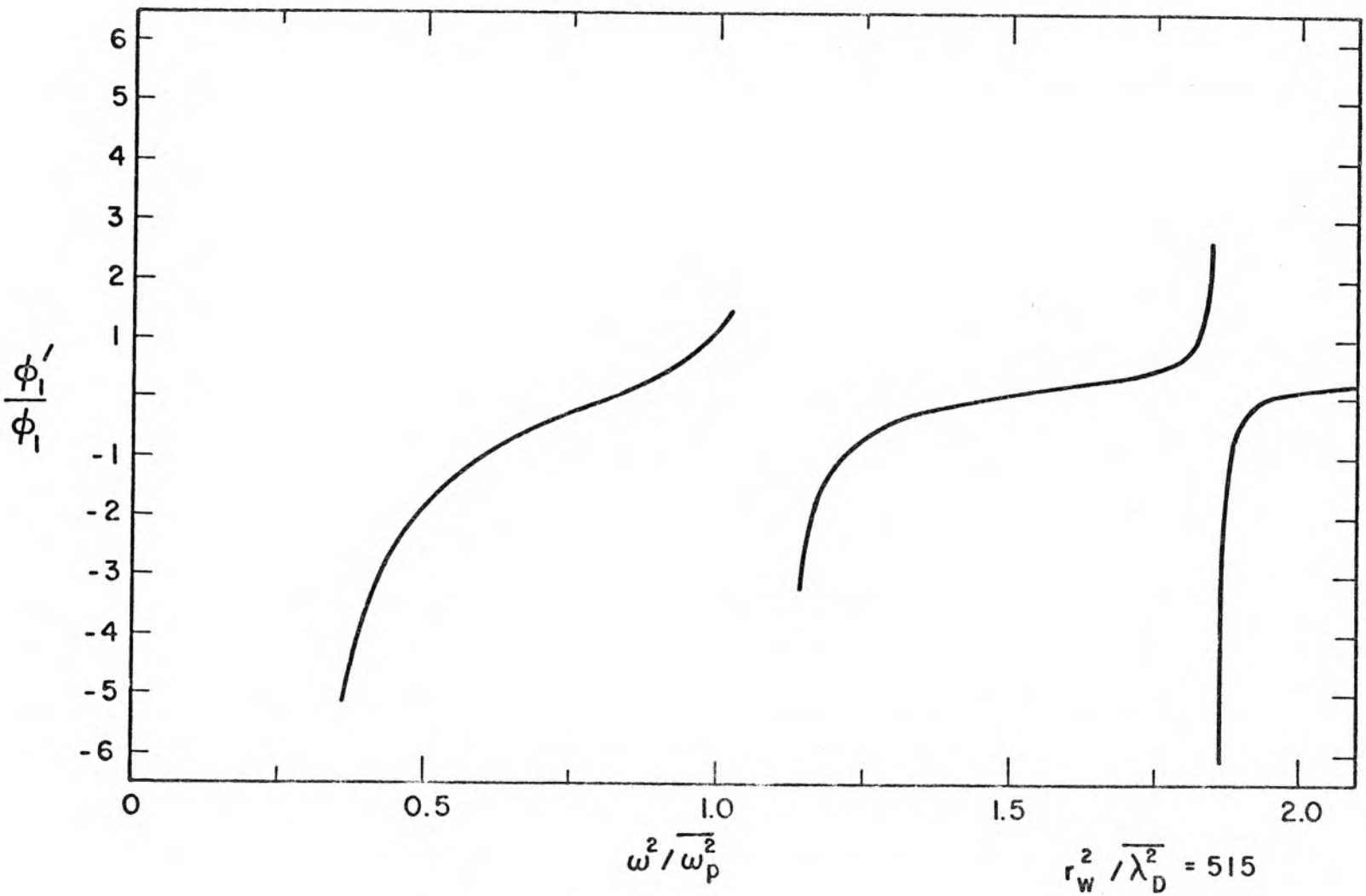
6
5
4
3
2
1
-1
-2
-3
-4
-5
-6
0
0.5
1.0
1.5
2.0
$\frac{\phi_1'}{\phi_1}$
$\omega^2/\overline{\omega_p^2}$
$r_w^2/\overline{\lambda_D^2} = 515$

Fig. A 3.3

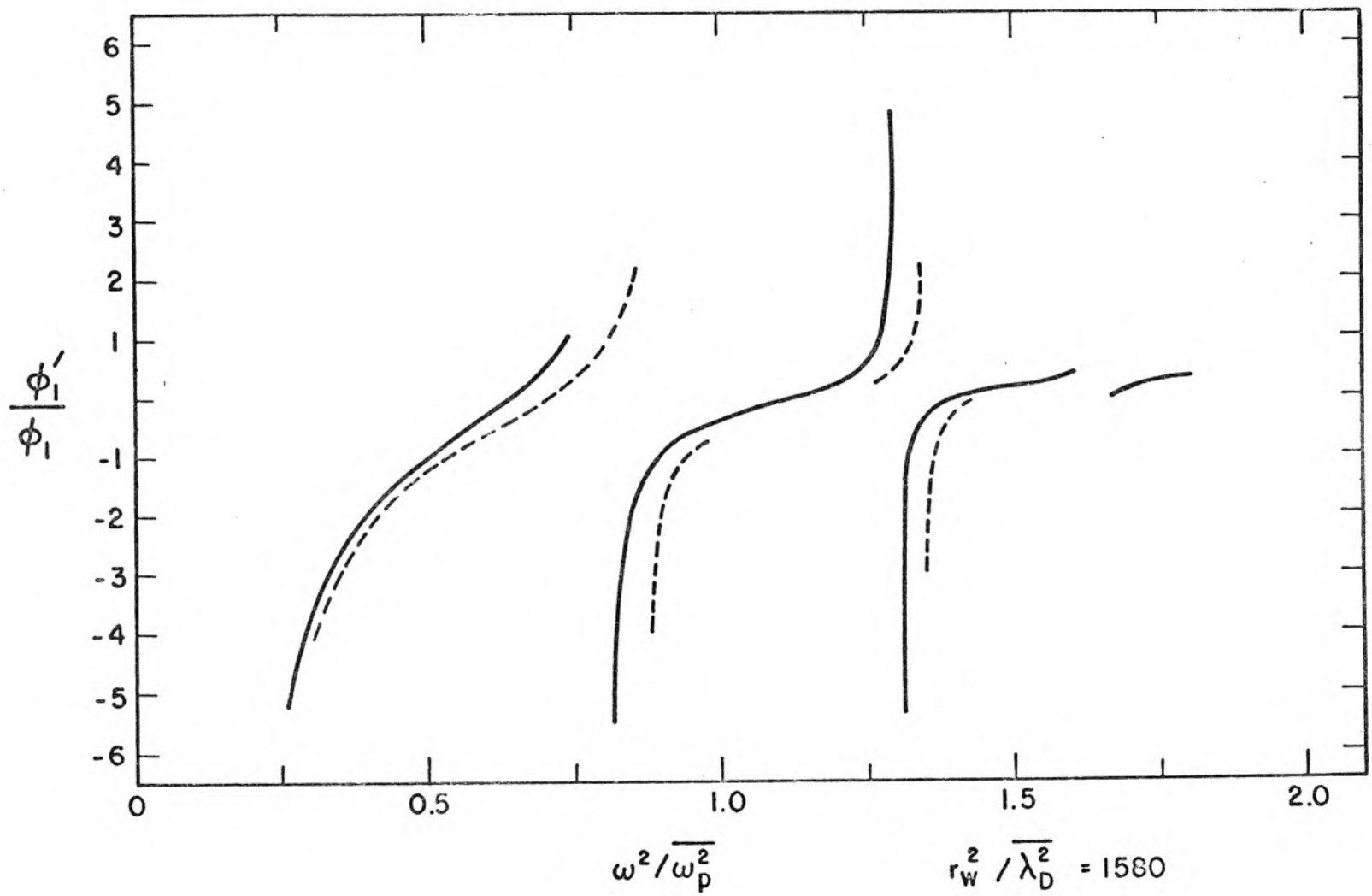
6
5
4
3
2
1
-1
-2
-3
-4
-5
-6
0
0.5
1.0
1.5
2.0
$\frac{\phi_1'}{\phi_1}$
$\omega^2/\overline{\omega_p^2}$
$r_w^2/\overline{\lambda_D^2} = 1580$

Fig. A 3.4

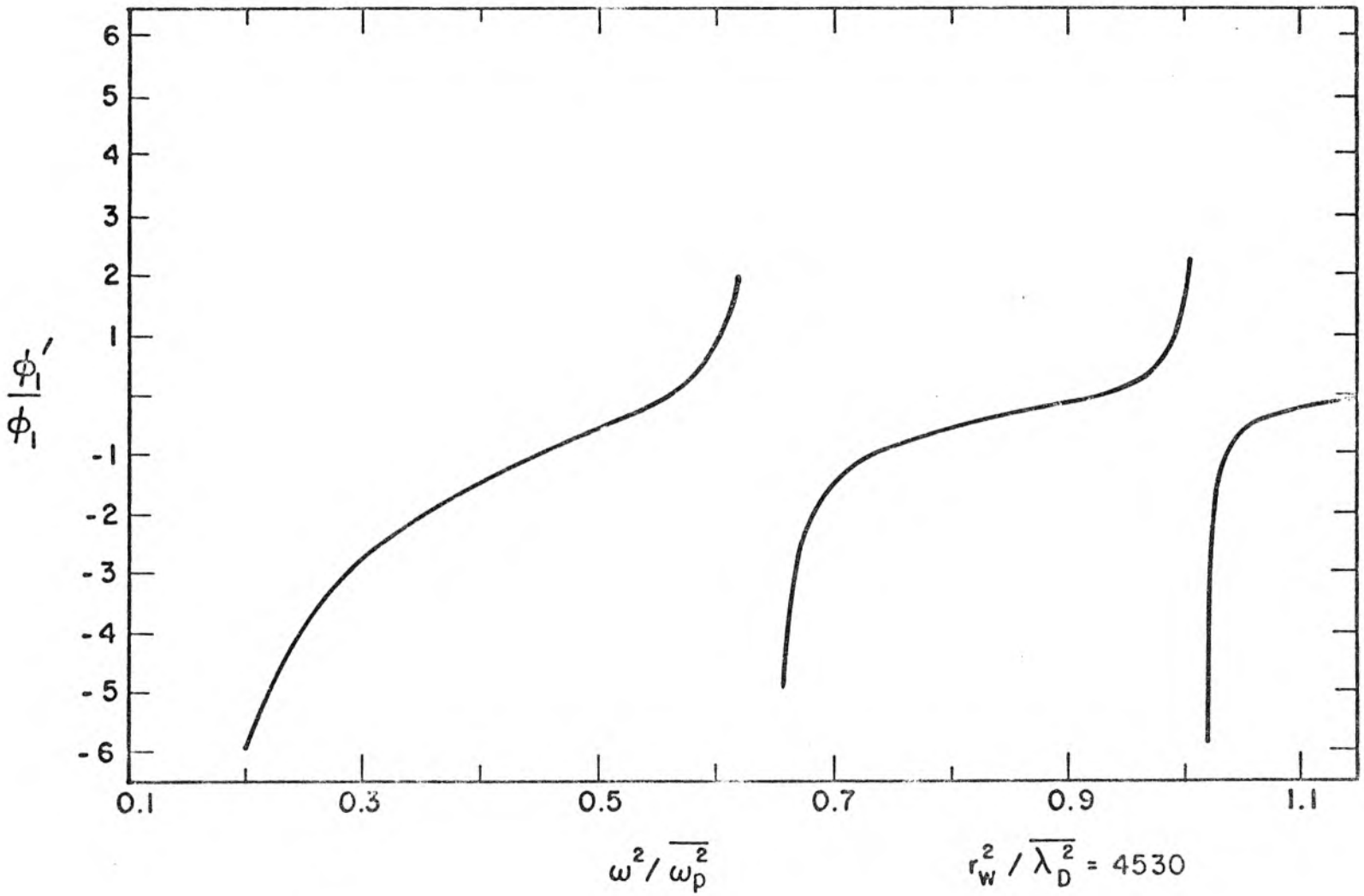
6
5
4
3
2
1
-1
-2
-3
-4
-5
-6
ϕ_1 / ϕ_1'
0.1
0.3
0.5
0.7
0.9
1.1
$\omega^2 / \overline{\omega_p^2}$
$r_w^2 / \overline{\lambda_D^2} = 4530$

Fig. A 3.5

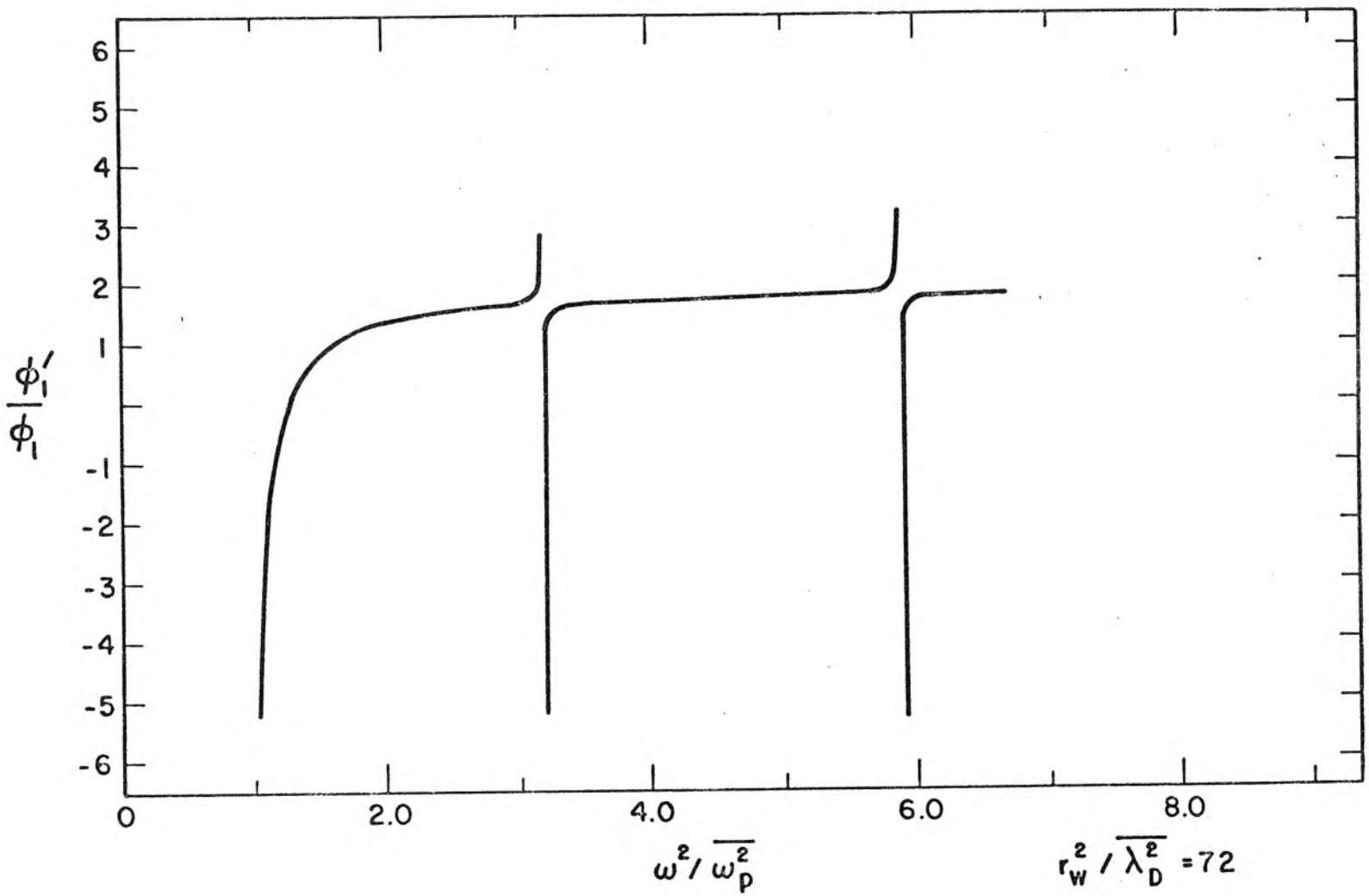
6
5
4
3
2
1
-1
-2
-3
-4
-5
-6
$\frac{\phi_1'}{\phi_-}$
0
2.0
4.0
6.0
8.0
$\omega^2 / \overline{\omega_p^2}$
$r_w^2 / \overline{\lambda_D^2} = 72$

Fig. A 3.6

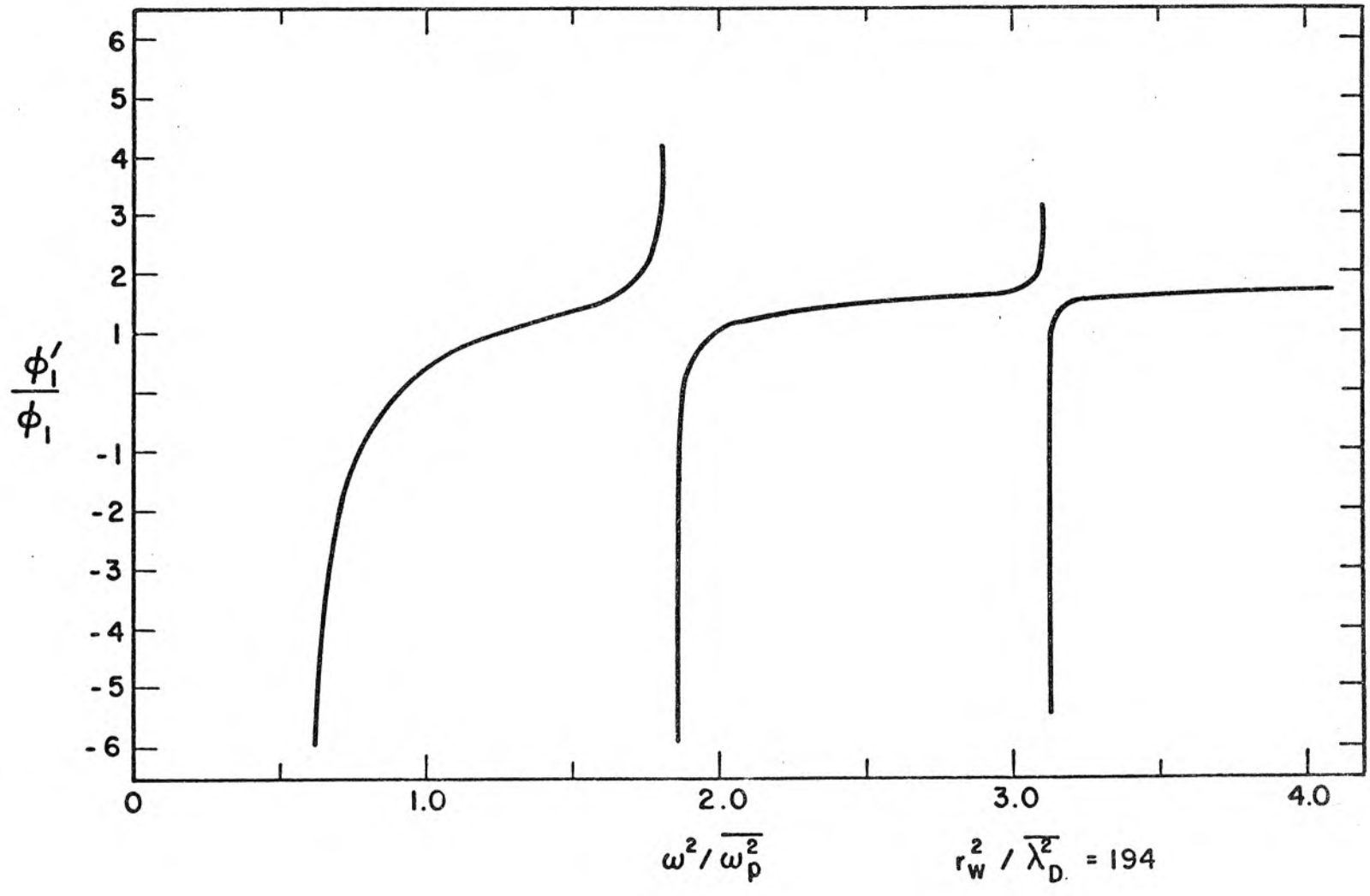
6
5
4
3
2
1
-1
-2
-3
-4
-5
-6
$\frac{\phi_1'}{\phi_1}$
0
1.0
2.0
3.0
4.0
$\omega^2 / \overline{\omega_p^2}$
$r_w^2 / \overline{\lambda_D^2} = 194$

Fig. A 3.7

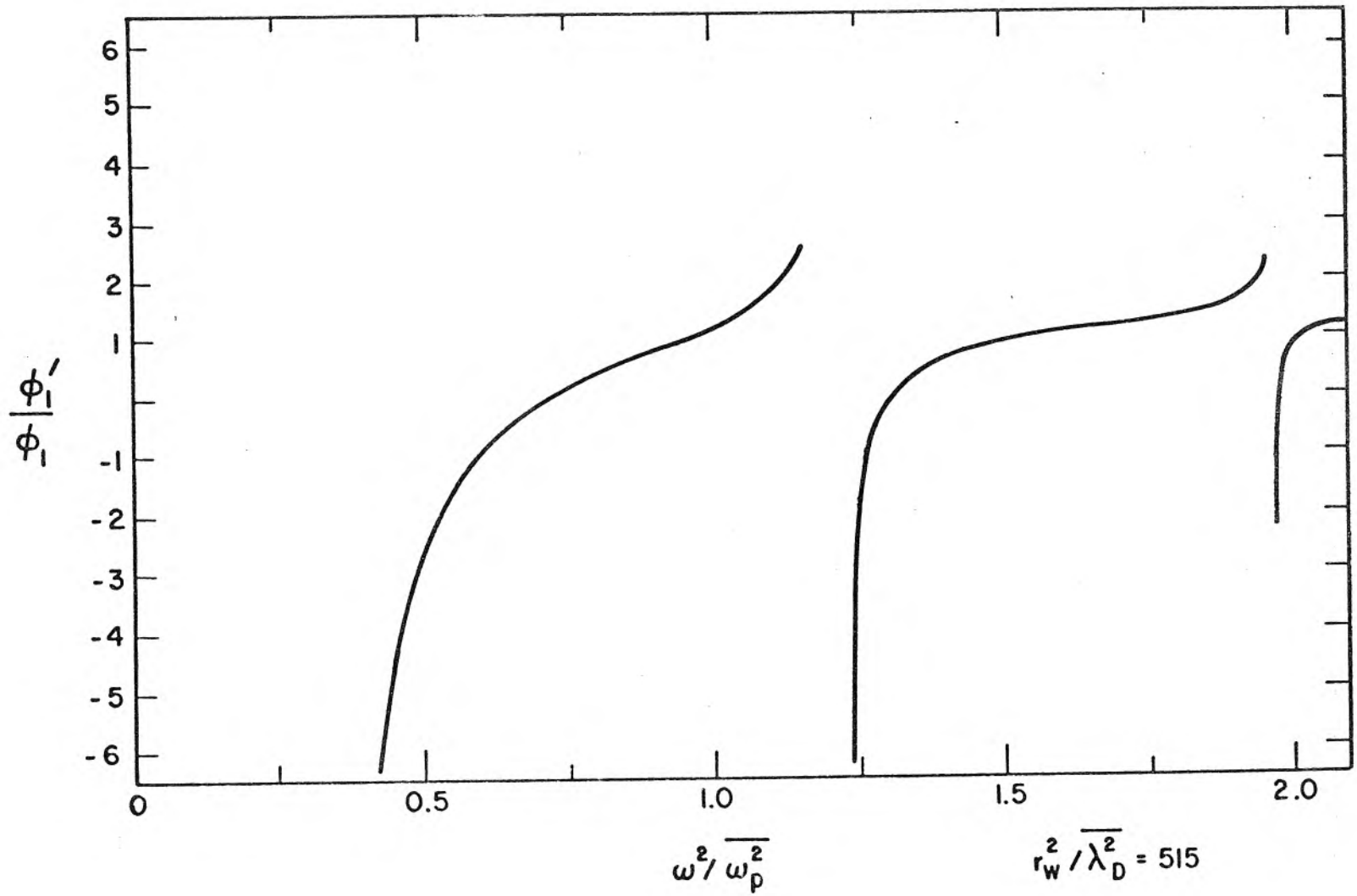
6
5
4
3
2
1
-1
-2
-3
-4
-5
-6
$\frac{\phi_1'}{\phi_1}$
0
0.5
1.0
1.5
2.0
$\omega^2/\overline{\omega_p^2}$
$r_w^2/\overline{\lambda_D^2} = 515$

Fig. A 3.8

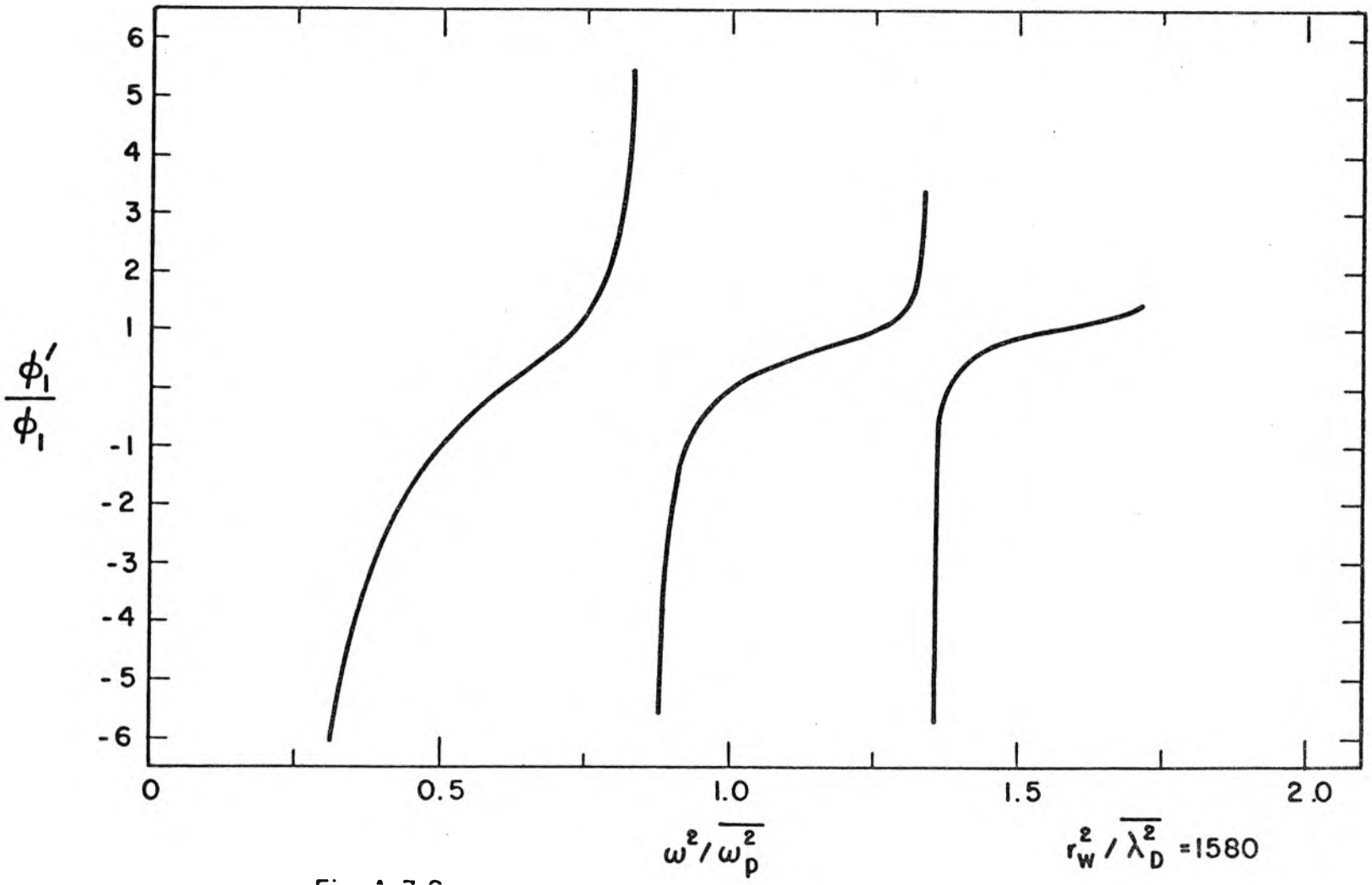
$\frac{\phi_1'}{\phi_1}$
6
5
4
3
2
1
-1
-2
-3
-4
-5
-6
0
0.5
1.0
1.5
2.0
$\omega^2/\overline{\omega_p^2}$
$r_w^2/\overline{\lambda_D^2}$ =1580

Fig. A 3.9

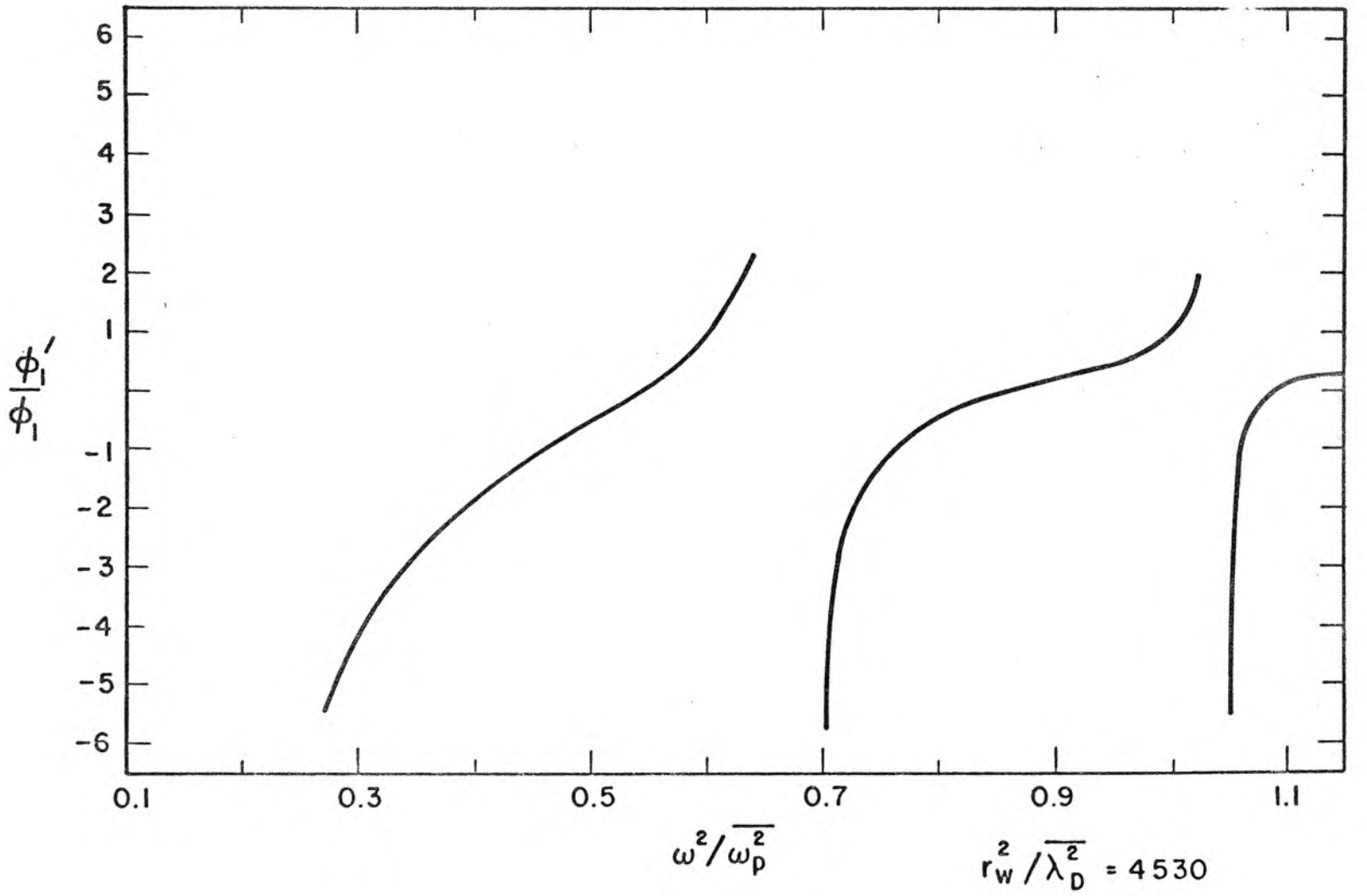
6
5
4
3
2
1
-1
-2
-3
-4
-5
-6
$\frac{\phi_1'}{\phi_1}$
0.1
0.3
0.5
0.7
0.9
1.1
$\omega^2/\overline{\omega_p^2}$
$r_w^2/\overline{\lambda_D^2} = 4530$

Fig. A 3.10

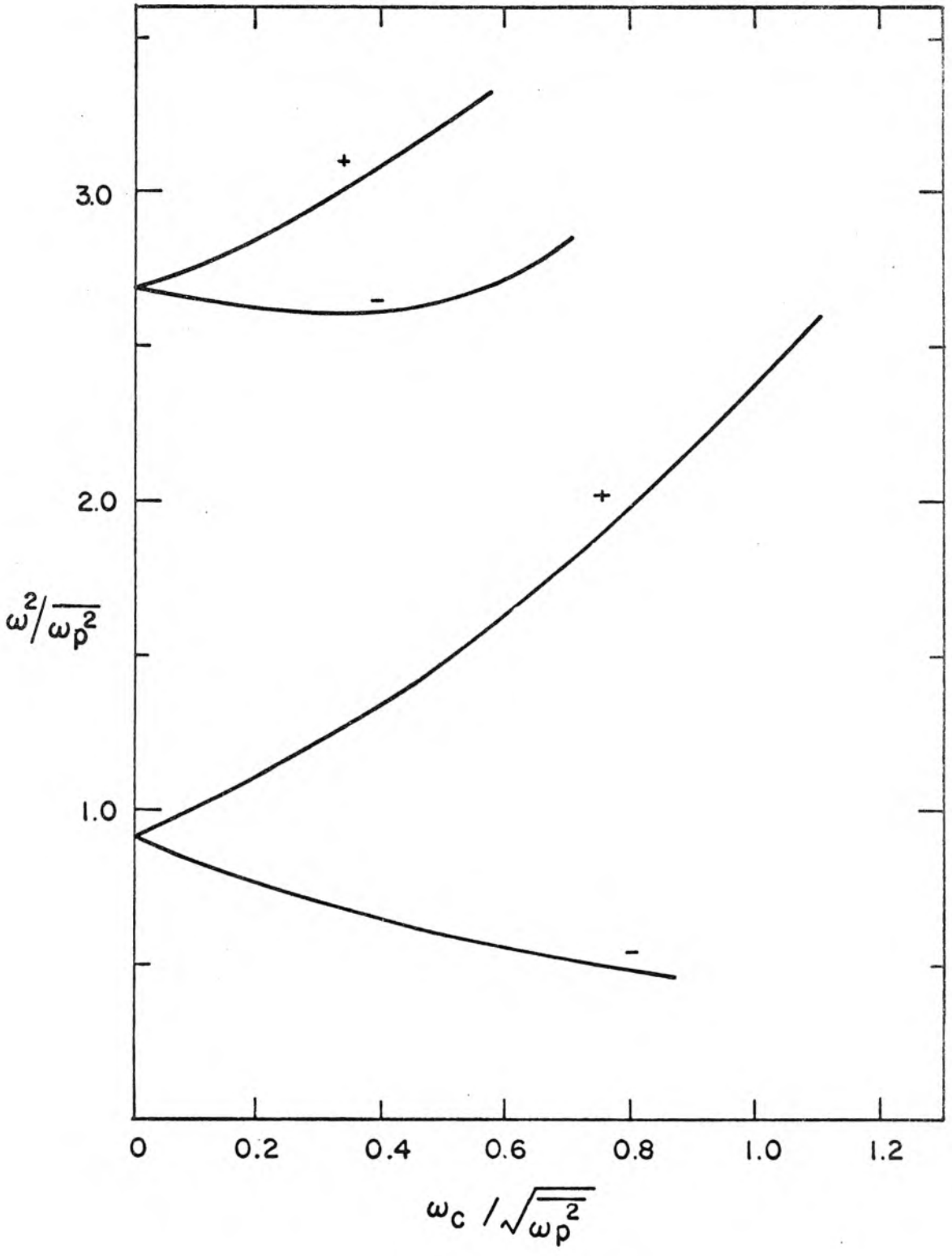

Fig. A3.11

$r_w^2 / \overline{\lambda_D^2} = 72$

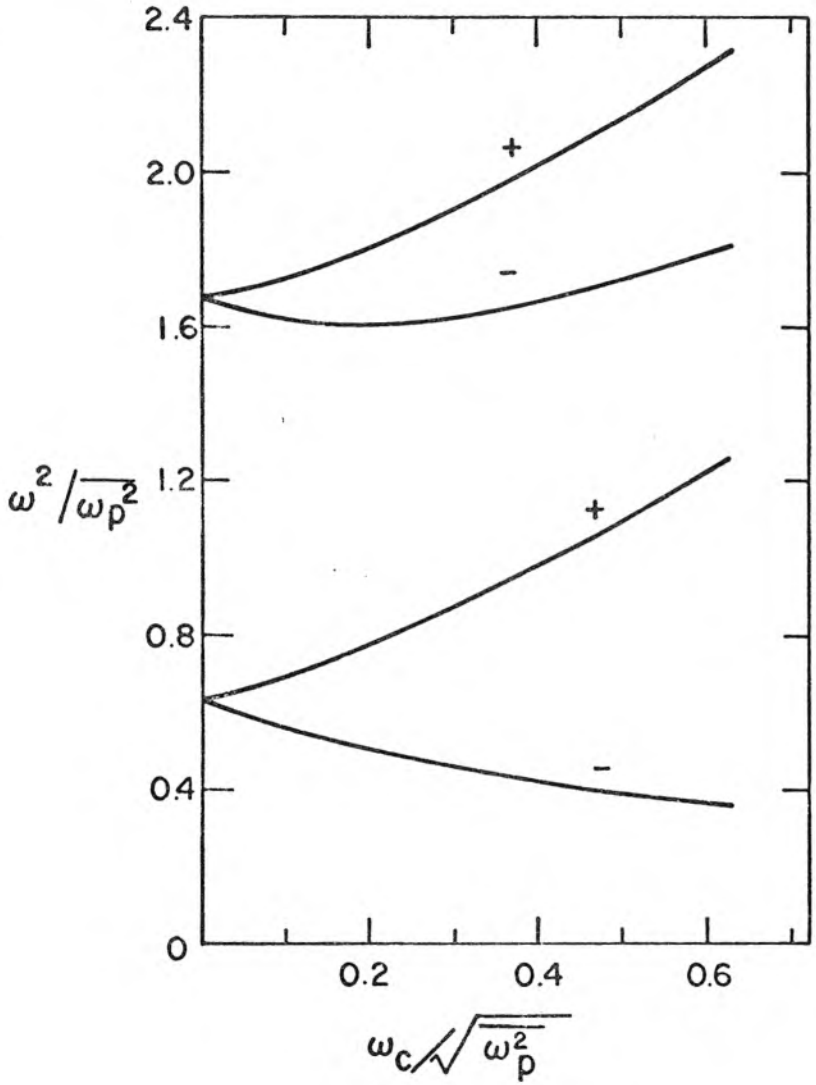

Fig. A3.12 $r_w^2 / \overline{\lambda_D^2} = 194$

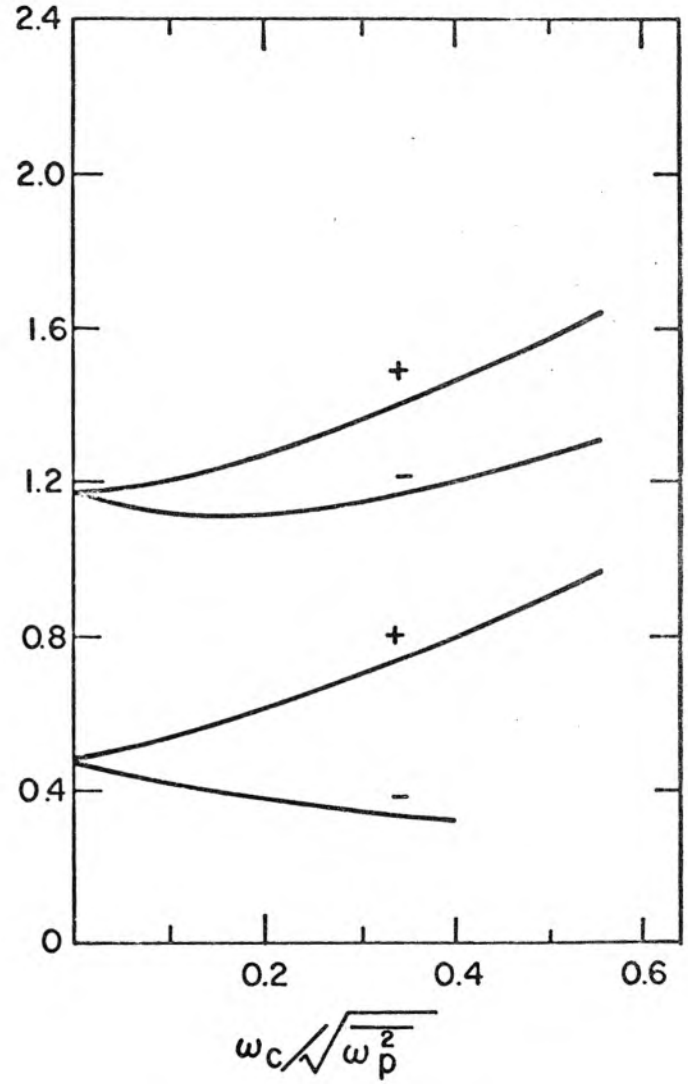

$r_w^2 / \overline{\lambda_D^2} = 515$

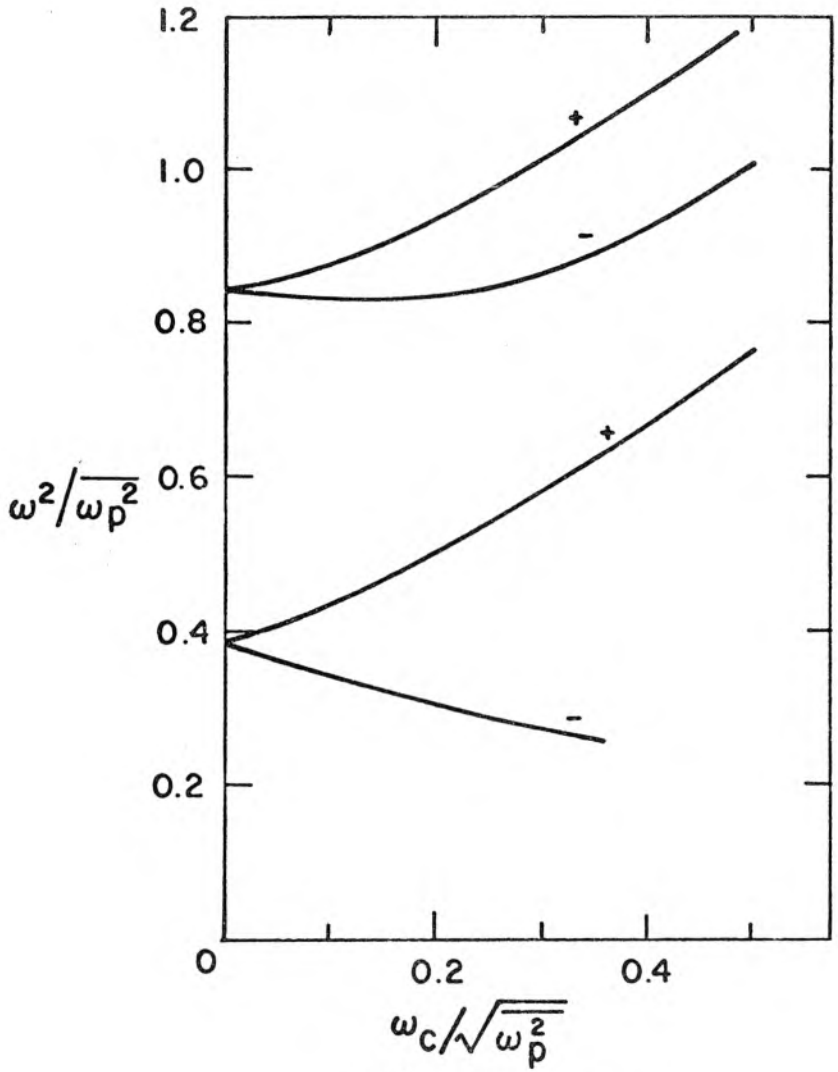

Fig. A3.13 $r_w^2/\overline{\lambda_D^2} = 1580$

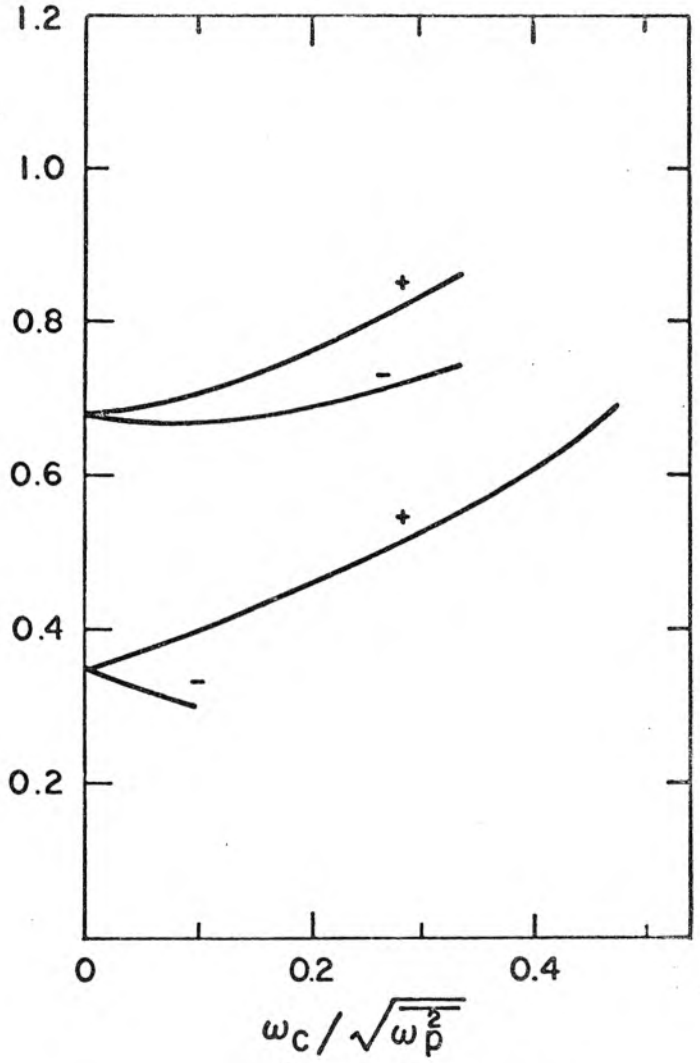

$r_w^2/\overline{\lambda_D^2} = 4530$

$\beta^2 = \infty$

s	$\eta(s)$	$n(s)/n_o$	$\eta'(s)$	$\eta''(s)$
0.00	0.0000	1.0000	0.0000	2.000
0.05	0.0025	0.9975	0.1002	2.012
0.10	0.0100	0.9900	0.2016	2.049
0.15	0.0227	0.9776	0.3056	2.113
0.20	0.0407	0.9602	0.4135	2.210
0.25	0.0641	0.9379	0.5271	2.344
0.30	0.0935	0.9107	0.6487	2.532
0.35	0.1292	0.8788	0.7812	2.784
0.40	0.1719	0.8421	0.9288	3.142
0.45	0.2224	0.8006	1.0974	3.636
0.50	0.2821	0.7542	1.2968	4.385
0.55	0.3529	0.7027	1.5436	5.592
0.60	0.4378	0.6455	1.8698	7.689
0.65	0.5424	0.5814	2.3490	$1.207\ 10^1$
0.70	0.6787	0.5073	3.2105	$2.513\ 10^1$
0.75	0.8901	0.4106	6.0337	$1.378\ 10^2$
0.76	0.9598	0.3830	8.2056	$3.229\ 10^2$
0.77	1.0790	0.3399	$1.9443\ 10^1$	$2.579\ 10^3$

Ion Species	He	Ne	Ar	Cs	Hg
s_{wall}	0.772	0.772	0.772	0.772	0.772
$\frac{\overline{n_e}}{n_o}$	0.698	0.698	0.698	0.698	0.698

Fig. A3.14

$$\beta^2 = 10^6$$

s	$\eta(s)$	$n(s)/n_o$	$\eta'(s)$	$\eta''(s)$
0.00	0.0000	1.0000	0.0000	2.000
0.05	0.0025	0.9975	0.1002	2.012
0.10	0.0100	0.9900	0.2016	2.049
0.15	0.0227	0.9776	0.3056	2.113
0.20	0.0407	0.9602	0.4135	2.210
0.25	0.0641	0.9379	0.5271	2.344
0.30	0.0935	0.9107	0.6487	2.530
0.35	0.1292	0.8788	0.7812	2.785
0.40	0.1719	0.8421	0.9287	3.139
0.45	0.2224	0.8006	1.0974	3.642
0.50	0.2821	0.7541	1.2967	4.388
0.55	0.3529	0.7027	1.5435	5.582
0.60	0.4378	0.6455	1.8696	7.689
0.65	0.5423	0.5814	2.3487	$1.210\ 10^1$
0.70	0.6787	0.5073	3.2089	$2.504\ 10^1$
0.75	0.8897	0.4108	5.9958	$1.336\ 10^2$
0.76	0.9585	0.3835	8.0304	$2.944\ 10^2$
0.77	1.0649	0.3447	$1.4897\ 10^1$	$1.288\ 10^3$
0.78	1.6740	0.1875	$1.9035\ 10^2$	$5.016\ 10^4$
0.79	7.8272	0.0004	$1.0861\ 10^3$	$9.580\ 10^4$

Ion Species	He	Ne	Ar	Cs	Hg
s_{wall}	0.787	0.788	0.788	0.788	0.789
$\frac{\overline{n_e}}{n_o}$	0.681	0.679	0.679	0.679	0.678

Fig. A3.15

$$\beta^2 = 10^5$$

s	$\eta(s)$	$n(s)/n_o$	$\eta(s)$	$\eta''(s)$
0.00	0.0000	1.0000	0.0000	2.000
0.05	0.0025	0.9975	0.1002	2.012
0.10	0.0100	0.9900	0.2016	2.049
0.15	0.0227	0.9776	0.3055	2.113
0.20	0.0407	0.9602	0.4134	2.209
0.25	0.0641	0.9379	0.5271	2.344
0.30	0.0935	0.9107	0.6487	2.528
0.35	0.1292	0.8788	0.7811	2.786
0.40	0.1719	0.8421	0.9286	3.136
0.45	0.2224	0.8006	1.0971	3.640
0.50	0.2821	0.7542	1.2964	4.383
0.55	0.3528	0.7027	1.5429	5.577
0.60	0.4377	0.6455	1.8685	7.663
0.65	0.5421	0.5815	2.3457	$1.203\ 10^1$
0.70	0.6782	0.5076	3.1961	$2.458\ 10^1$
0.75	0.8859	0.4124	5.7419	$1.099\ 10^2$
0.76	0.9500	0.3867	7.2123	$1.918\ 10^2$
0.77	1.0346	0.3554	$1.0057\ 10^1$	$3.998\ 10^2$
0.78	1.1638	0.3123	$1.6805\ 10^1$	$1.026\ 10^3$
0.79	1.4109	0.2439	$3.5808\ 10^1$	$3.006\ 10^3$
0.80	1.9892	0.1368	$8.7328\ 10^1$	$7.630\ 10^3$
0.81	3.3160	0.0363	$1.8502\ 10^2$	$1.170\ 10^4$
0.82	5.7393	0.0032	$2.9878\ 10^2$	$1.066\ 10^4$

Ion Species	He	Ne	Ar	Cs	Hg
s_{wall}	0.816	0.819	0.820	0.822	0.822
$\frac{\bar{n}_e}{n_o}$	0.648	0.643	0.641	0.638	0.637

Fig. A3.16

$$\beta^2 = 10^4$$

s	$\eta(s)$	$n(s)/n_o$	$\eta'(s)$	$\eta''(s)$
0.00	0.0000	1.0000	0.0000	2.000
0.05	0.0025	0.9975	0.1001	2.010
0.10	0.0100	0.9900	0.2014	2.047
0.15	0.0227	0.9776	0.3053	2.111
0.20	0.0406	0.9602	0.4131	2.207
0.25	0.0641	0.9379	0.5266	2.340
0.30	0.0934	0.9108	0.6480	2.524
0.35	0.1291	0.8789	0.7802	2.777
0.40	0.1717	0.8422	0.9272	3.127
0.45	0.2221	0.8008	1.0951	3.623
0.50	0.2817	0.7545	1.2931	4.351
0.55	0.3522	0.7031	1.5371	5.508
0.60	0.4366	0.6462	1.8571	7.495
0.65	0.5402	0.5826	2.3174	$1.142\ 10^1$
0.70	0.6734	0.5100	3.0918	$2.123\ 10^1$
0.75	0.8643	0.4213	4.8258	$5.646\ 10^1$
0.76	0.9157	0.4002	5.4696	$7.305\ 10^1$
0.77	0.9744	0.3774	6.3123	$9.665\ 10^1$
0.78	1.0429	0.3524	7.4397	$1.305\ 10^2$
0.79	1.1245	0.3248	8.9755	$1.790\ 10^2$
0.80	1.2243	0.2940	$1.1094\ 10^1$	$2.478\ 10^2$
0.81	1.3491	0.2595	$1.4025\ 10^1$	$3.426\ 10^2$
0.82	1.5084	0.2212	$1.8048\ 10^1$	$4.668\ 10^2$
0.83	1.7147	0.1800	$2.3450\ 10^1$	$6.179\ 10^2$
0.84	1.9828	0.1377	$3.0443\ 10^1$	$7.832\ 10^2$
0.85	2.3290	0.0974	$3.9059\ 10^1$	$9.386\ 10^2$
0.86	2.7685	0.0628	$4.9056\ 10^1$	$1.055\ 10^3$
0.87	3.3130	0.0364	$5.9934\ 10^1$	$1.112\ 10^3$
0.88	3.9681	0.0189	$7.1066\ 10^1$	$1.105\ 10^3$
0.89	4.7333	0.0088	$8.1885\ 10^1$	$1.050\ 10^3$
0.90	5.6034	0.0037	$9.2007\ 10^2$	$9.691\ 10^2$
0.91	6.5705	0.0014	$1.0126\ 10^2$	$8.798\ 10^2$

Ion Species	He	Ne	Ar	Cs	Hg
s_{wall}	0.888	0.897	0.901	0.908	0.910
$\frac{\overline{n_e}}{n_o}$	0.574	0.562	0.557	0.550	0.547

Fig. A3.17

$$\beta^2 = 10^3$$

s	$\eta(s)$	$n(s)/n_o$	$\eta'(s)$	$\eta''(s)$
0.00	0.0000	1.0000	0.0000	1.984
0.05	0.0025	0.9975	0.0994	1.996
0.10	0.0100	0.9901	0.2000	2.031
0.15	0.0225	0.9777	0.3029	2.092
0.20	0.0403	0.9605	0.4097	2.183
0.25	0.0636	0.9384	0.5218	2.310
0.30	0.0926	0.9115	0.6413	2.482
0.35	0.1279	0.8800	0.7709	2.715
0.40	0.1699	0.8437	0.9140	3.032
0.45	0.2196	0.8028	1.0756	3.464
0.50	0.2779	0.7574	1.2630	4.076
0.55	0.3465	0.7072	1.4875	4.966
0.60	0.4276	0.6521	1.7671	6.322
0.65	0.5246	0.5918	2.1329	8.490
0.70	0.6432	0.5256	2.6394	$1.209\ 10^1$
0.75	0.7925	0.4527	3.3854	$1.832\ 10^1$
0.80	0.9886	0.3721	4.5452	$2.901\ 10^1$
0.85	1.2585	0.2841	6.3932	$4.607\ 10^1$
0.90	1.6448	0.1931	9.2490	$6.875\ 10^1$
0.95	2.2027	0.1105	$1.3249\ 10^1$	$9.014\ 10^1$
1.00	2.9834	0.0506	$1.8059\ 10^1$	$9.964\ 10^1$
1.05	4.0098	0.0181	$2.2947\ 10^1$	$9.367\ 10^1$
1.06	4.2440	0.0144	$2.3870\ 10^1$	$9.108\ 10^1$
1.07	4.4871	0.0112	$2.4767\ 10^1$	$8.822\ 10^1$
1.08	4.7392	0.0087	$2.5634\ 10^1$	$8.514\ 10^1$
1.09	4.9997	0.0067	$2.6469\ 10^1$	$8.196\ 10^1$
1.10	5.2685	0.0052	$2.7272\ 10^1$	$7.868\ 10^1$
1.11	5.5451	0.0039	$2.8042\ 10^1$	$7.534\ 10^1$
1.12	5.8292	0.0029	$2.8779\ 10^1$	$7.203\ 10^1$
1.13	6.1205	0.0022	$2.9482\ 10^1$	$6.875\ 10^1$
1.14	6.4188	0.0016	$3.0154\ 10^1$	$6.556\ 10^1$

Ion Species	He	Ne	Ar	Cs	Hg
s_{wall}	1.075	1.107	1.119	1.140	1.147
$\frac{\overline{n_e}}{n_o}$	0.445	0.420	0.411	0.396	0.392

Fig. A3.18

$\beta^2 = 10^2$

s	$\eta(s)$	$n(s)/n_o$	$\eta'(s)$	$\eta''(s)$
0.00	0.0000	1.0000	0.0000	1.860
0.05	0.0023	0.9977	0.0931	1.867
0.10	0.0093	0.9907	0.1870	1.891
0.15	0.0210	0.9792	0.2825	1.932
0.20	0.0376	0.9631	0.3805	1.991
0.25	0.0591	0.9426	0.4819	2.071
0.30	0.0859	0.9177	0.5879	2.172
0.35	0.1180	0.8887	0.6995	2.301
0.40	0.1560	0.8556	0.8183	2.460
0.45	0.2000	0.8187	0.9459	2.652
0.50	0.2507	0.7782	1.0841	2.887
0.55	0.3086	0.7344	1.2353	3.170
0.60	0.3745	0.6876	1.4019	3.507
0.65	0.4491	0.6382	1.5869	3.908
0.70	0.5336	0.5865	1.7934	4.374
0.75	0.6289	0.5332	2.0251	4.906
0.80	0.7365	0.4788	2.2848	5.502
0.85	0.8579	0.4240	2.5760	6.154
0.90	0.9947	0.3698	2.9004	6.840
0.95	1.1485	0.3171	3.2590	7.518
1.00	1.3212	0.2668	3.6510	8.158
1.05	1.5141	0.2200	4.0723	8.710
1.10	1.7288	0.1775	4.5186	9.120
1.15	1.9662	0.1400	4.9806	9.358
1.20	2.2270	0.1078	5.4505	9.418
1.25	2.5112	0.0812	5.9175	9.268
1.30	2.8186	0.0597	6.3724	8.926
1.35	3.1481	0.0429	6.8060	8.434
1.40	3.4987	0.0302	7.2120	7.838
1.45	3.8688	0.0209	7.5861	7.182
1.50	4.2568	0.0142	7.9265	6.467
1.55	4.6608	0.0095	8.2309	5.782
1.60	5.0794	0.0062	8.5021	5.096
1.65	5.5103	0.0040	8.735	4.441
1.70	5.9524	0.0026	8.940	3.755
1.75	6.4038	0.0016	9.100	3.100

Ion Species	He	Ne	Ar	Cs	Hg
s_{wall}	1.548	1.649	1.693	1.758	1.787
$\frac{\overline{n_e}}{n_o}$	0.299	0.264	0.250	0.232	0.225

Fig. A3.19

References

(1) L. Tonks, Phys. Rev. 37, 1458 (1931).

(2) L. Tonks, Phys. Rev. 38, 1219 (1931).

(3) S. Denno, H. Prime, J. Craggs, Proc. Phys. Soc. B63, 726 (1950).

(4) D. Romell, Nature 167, 243 (1951).

(5) A. Dattner, Ericsson Technics 2, 309 (1957); Ericsson Technics 8, 1 (1963).

(6) N. Herlofson, Arkiv Fysik 3, 247 (1951).

(7) R. I. Boley, Nature 182, 790 (1958).

(8) R. W. Gould, Proc. Linde Conf. on Plasma Oscillations, Indianapolis, 167 (June 1959).

(9) R. W. Gould, CIT Report No. 1, Contract DA36-039 SC-85317, April 1960.

(10) P. Weissglas, Phys. Rev. Letters 10, 206 (1963).

(11) L. Tonks, I. Langmuir, Phys. Rev. 34, 876 (1929).

(12) I. Langmuir, H. M. Mott-Smith, Jr., Gen. Elec. Rev. 27, 449 (1924).

(13) S. Self, Phys. Fluids 6, 1762 (1963).

(14) J. Todd, Editor, Survey of Numerical Analysis (McGraw-Hill Book Co., New York, 1962).

(15) J. C. Nickel, J. V. Parker, R. W. Gould, Phys. Rev. Letters 11, 183 (1963).

(16) W. Panofsky, M. Phillips, Classical Electricity and Magnetism, (Addison-Wesley Publishing Co., Reading, Mass., 1956).

(17) T. R. Kaiser, R. L. Closs, Phil. Mag. 43, 1 (1952).

(18) P. M. Morse, H. Feshbach, Methods of Mathematical Physics, Part III, (McGraw-Hill Book Co., New York, 1953).

(19) F. Crawford, G. Kino, S. Self, J. Spalter, Microwave Laboratory Report No. 961, Stanford University (October 1961).

(20) J. C. Nickel, Ph.D. Thesis, California Institute of Technology, (June 1964).

(21) R. W. Gould, Private Communication

(22) F. Crawford, Private Communication

(23) P. Vandenplas, R. W. Gould, Electron Tube and Microwave Lab. Report No. 3, California Institute of Technology (July 1960).

(24) W. Leavens, Private Communication

(25) F. Crawford, G. Kino, A. Cannara, Jour. Appl. Phys. 34, 3168 (1963).

(26) B. D. Fried, S. Conte, The Plasma Dispersion Function, (Academic Press, New York, 1961).

(27) R. W. Gould, Electron Tube and Microwave Lab. Report No. 1, California Institute of Technology, April 1960.

(28) P. Vandenplas, VI International Conference on Ionization Phenomena in Gases, Paris, 1963.

(29) Messien, P. Vandenplas, Physica 28, 537 (1962).

DISTRIBUTION LIST

Chief of Naval Research 2
Navy Department - CODE 427
Washington 25, D. C.

Director, Naval Research Lab.
Washington 25, D. C.
Attn: CODE 5240 1
CODE 7130 1
CODE 2000 6
CODE 5430 1

Commanding Officer 1
ONR Branch Office
1000 Geary Street
San Francisco, California

Scientific Liaison Officer 25
ONR, London
c/o Navy 100, Box 39, FPO
New York, New York

Commanding Officer 1
ONR Branch Office
1030 E. Green Street
Pasadena, California

Commanding Officer 1
ONR Branch Office
The John Crerar Library Bldg.
86 E. Randolph Street
Chicago 1, Illinois

Commanding Officer 1
ONR Branch Office
346 Broadway
New York 13, New York

Officer-in-Charge 3
Office of Naval Research
Navy 100, FPO
New York, New York

Chief, Bureau Aeronautics EL4 1
Navy Department EL43 1
Washington 25, D. C. EL45 1

Chief, Bureau of Ordnance
Navy Department Re 4 1
Washington 25, D. C. Re 9 1

Chief of Naval Operations Op20X 1
Navy Department Op421 1
Washington 25, D. C. Op 55 1

Director, Naval Ordnance Lab. 1
White Oak, Maryland

Director, Naval Electronics Lab 1
San Diego 52, California

Professor Norman L. Oleson 1
Department of Physics
U.S. Naval Postgraduate School
Monterey, California

Commander CODE 366 1
Naval Air Missile Test Center
Point Mugu, California

U.S. Naval Proving Ground 1
Attn: W. H. Benson
Dahlgren, Virginia

Commander 1
U.S.Naval Air Development Center
Johnsville, Pennsylvania

Thermionics Branch 5
Signal Corps Eng. Labs.
Evans Signal Lab, Bldg.42
Belmar, New Jersey

Defense Documentation Center 20
Cameron Station, Bldg. 5
5010 Duke Street
Alexandria, Virginia 22314

Ballistics Research Labs 2
Aberdeen Proving Ground
Maryland
Attn: D.W.H. Delsasso

Chief, Ordnance Develop. Div. 2
Natl.Bureau of Standards
Connecticut Av, Van Ness St.NW
Washington 25, D. C.

Naval Research Laboratory 6
Washington 25, D. C.

Committee on Electronics 1
Research and Development Board
Department of Defense
Washington 25, D. C.

Director, Natl.Bureau of Stds. 1
Washington 25, D. C.
Attn: Div.14.0 CRPL, Librarian

Commanding Officer 1
Engineering Res. and Dev. Lab
Fort Belvoir, Virginia

Commanding Officer 1
Frankford Arsenal
Bridesburg, Philadelphia, Pa.

Eitel-McCullough, Inc. 1
301 Industrial Way
San Carlos, California
ATTN: Research Library

Commanding General WCLC 1
Wright Air Devel.Center WCLRC 1
Wright-Patterson AF Base, Ohio

Commanding General, CRRE 1
A.F. Cambridge Research Center
230 Albany Street
Cambridge 39, Massachusetts

Commanding General RCRW 1
Rome Air Development Center
Griffiss Air Force Base
Rome, New York

Chief, West Coast Office 1
Signal Corps Eng. Labs
75 So. Grand Avenue
Pasadena 2, California

Signal Corps Resident Engineer 1
Electronic Defense Laboratory
P.O. Box 205
Mountain View, California

Chief, Bureau of Ships 816 1
Department of the Navy 820 1
Washington, D. C. 340 1

Material Lab. Library 912B 1
New York Naval Shipyard
Brooklyn 1, New York

Office of Technical Services 1
Department of Commerce
Washington 25, D. C.

Director CR4582 1
Air University Library
Maxwell A.F. Base, Alabama

Chief, Western Division 1
Office of Aerospace Research
Office of Scientific Research
P.O.Box 2035, Pasadena, Calif.

Technical Library 1
Research and Development Board
Pentagon Building
Washington 25, D. C.

Advisory Group on Electron Tubes 1
346 Broadway (8th Floor)
New York 13, New York

Dr. G. E. Barlow 1
Australian Joint Service Staff
Box 4837
Washington 8, D. C.

Microwave Library 1
W. W. Hansen Labs. of Physics
Stanford University
Stanford, California

Engineering Library 1
Stanford University
Stanford, California

Electronics Lab. Library 1
Stanford University
Stanford, California

Technical Library 1
General Electric Microwave Lab.
601 California Avenue
Palo Alto, California

General Electric Company 1
Electronic Components Div.
Power Tube Department
Microwave Lab at Stanford
Palo Alto, California

Dr. E. D. McArthur 1
Electron Tube Laboratory
General Electric Company
Schenectady, New York

University of Michigan 1
Electron Tube Laboratory
Ann Arbor, Michigan
Attn: J. Rowe

Johns Hopkins University 1
Radiation Laboratory
1315 St. Paul Street
Baltimore 2, Maryland
Attn: M.Poole, Librarian

Research Lab. of Electronics 1
Massachusetts Inst. of Tech.
Cambridge 39, Massachusetts

Sloane Physics Laboratory 1
Yale University
New Haven, Connecticut
Attn: R. Beringer

Mr. H. J. Reich 1
Department of Electrical Eng.
Yale University
New Haven, Connecticut

Laboratory for Insulation Res. 1
Massachusetts Inst. of Tech.
Cambridge 39, Massachusetts
Attn: A. von Hippel

Lincoln Laboratory 1
Massachusetts Inst. of Tech.
Cambridge 39, Massachusetts

Dr. J. M. Lafferty, Manager 1
Physical Studies
General Electric Company
P.O. Box 1088
Schenectady, New York

General Electric Company 1
One River Road
Schenectady 5, New York
Attn: Miss W. Crain, Librarian

Technical Report Collection 1
303A Pierce Hall
Harvard University
Cambridge 38, Massachusetts

Electron Tube Section 1
Electrical Engineering Dept.
University of Illinois
Champaign, Illinois

Chairman, Div.of Elec. Eng. 1
University of California
Berkeley 4, California

Radiation Laboratory 1
Tech. Information Division
University of California
Berkeley 4, California

Dr. A. W. Trivelpiece 1
Department of Elec. Eng.
University of California
Berkeley 4, California

Periodicals Librarian 1
General Library
California Inst. of Technology
Pasadena, California

Dr. Z. Kaprielian 1
Electrical Engineering Dept.
University of Southern Calif.
Los Angeles 7, California

Supervisor of Research Lab. 1
Electrical Engineering Bldg.
Purdue University
Lafayette, Indiana

Georgia Institute of Techn. 1
Atlanta, Georgia
ATTN: Librarian

W. E. Lear 1
University of Florida
Department of Electrical Eng.
Gainesville, Florida

Director Electronics Defense 1
Engineering Research Inst.
University of Michigan
Ann Arbor, Michigan

Cornell Aeronautical Lab 1
Cornell Research Foundation
Buffalo 21, New York

Director, Microwave Res.Inst. 1
Polytechnic Inst.of Brooklyn
55 Johnson Street
Brooklyn 1, New York

University of Washington
Department of Elec. Eng.
Seattle, Washington
ATTN: E. A. Harrison 1
A. V. Eastman 1

University of Colorado 1
Department of Elec. Eng.
Boulder, Colorado

University of Colorado 1
Engineering Experiment Sta.
Boulder, Colorado
ATTN: W. G. Worcester

Electrical Engineering Dept. 1
Princeton University
Princeton, New Jersey

Professor W. P. Dyke 1
Linfield College
McMinnville, Oregon

Research Lab.of Electronics 1
Chalmers Institute of Tech.
Gothenburg, Sweden
ATTN: Librarian

Columbia Radiation Lab. 1
538 W. 120th Street
New York 27, New York

Cascade Research 1
5245 San Fernando Road
Los Angeles 39, California

Fred D. Wilimek 1
Varian Associates
611 Hansen Way
Palo Alto, California

John Dyer 1
Airborne Instrument Lab
Mineola, New York

Bell Telephone Laboratories 1
Murray Hill, New Jersey
ATTN: J. R. Pierce

Hughes Aircraft Company 1
Culver City, California
ATTN: Mr. Milek, Librarian

Hughes Aircraft Company 1
Microwave Laboratory
Culver City, California
ATTN: Dr. A. D. Berk

Bell Telephone Laboratories 1
Technical Information Library
463 W. Street
New York 14, New York

RCA Laboratories 1
Princeton, New Jersey
ATTN: Dr. W. M. Webster

Federal Telecommunic. Labs 1
500 Washington Avenue
Nutley, New Jersey
ATTN: W. Derrick 1
K. Wing 1

Countermeasures Laboratory 1
Gilfillan Brothers, Inc.
1815 Venice Boulevard
Los Angeles, California

The Rand Corporation 1
1700 Main Street
Santa Monica, California
ATTN: Librarian

Motorola Riverside Res. Lab. 1
8330 Indiana Avenue
Riverside, California
ATTN: Mr. John Byrne

Ramo-Wooldridge Corporation 1
Control Systems Division
P.O. Box 9008
Hawthorne, California
ATTN: Librarian

Dr. James E. Shepherd 1
General Manager
Sperry Rand Research Center
P.O. Box 400
Sudbury, Massachusetts

W. L. Maxson Corporation 1
460 West 34th Street
New York 1, New York
ATTN: M. Simpson

Bertram G. Ryland, Manager 1
Spencer Laboratory
Raytheon Manufacturing Co.
Burlington, Massachusetts

Westinghouse Electric Corp. 1
Electronic Tube Division
Elmira, New York
ATTN: Mr. S.S.King, Librarian

Mr. Gilbert Kelton 1
Security Officer
Philips Laboratories
Irvington-on-Hudson, New York

R. E. McGuire, Librarian 1
Boeing Airplane Company
P.O. Box 3707
Seattle 24, Washington

A. Simon 1
General Atomic
P. O. Box 608
San Diego, California

Image Instruments, Inc. 1
2300 Washington Street
Newton Lower Falls 62, Mass.

Sylvania Electric Prod. Inc. 1
Waltham, Massachusetts
ATTN: Charles A. Thornhill

Research Division Library 1
Raytheon Company
28 Seyon Street
Waltham 54, Massachusetts

ITT Laboratories 1
15151 Bledsoe Street
San Fernando, California

Technical Research Group Inc. 1
2 Aerial Way
Syosset, New York

Advanced Techniques Branch 1
Electronics Technology Lab.
Aeronautical Systems Division
Wright-Patterson AFB, Ohio

Microwave Physics Laboratory 1
Sylvania Electric Products
P.O. Box 1296
Mountain View, California

U. S. Atomic Energy Commission 1
Tech. Information Service Ext.
P.O. Box 62
Oak Ridge, Tennessee

Electromagnetic Research Corp
5001 College Avenue 1
College Park, Maryland 20740
ATTN: R. E. Skinner

Bomac Laboratories, Inc. 1
Salem Road
Beverly, Massachusetts
ATTN: Arthur McCoubrey

Aerospace Corporation 1
Post Office Box 95085
Los Angeles 45, California
Attn: F. L. Vernon, Jr.

Space-General Corp 1
9200 E. Flair Drive
El Monte, California
ATTN: Bruce Ferrell, Lib.

Northern Electric Co. Ltd. 1
Research and Devel. Labs.
Library, Dept. 8421
P.O. Box 3511, Station C
Ottawa, Ontario, Canada

Dalmo Victor Company 1
Division of Textron, Inc.
Belmont, California
ATTN: Librarian

Dr. W. E. Drummond 1
General Atomic
P. O. Box 608
San Diego 12, California

Dr. M. Gottlieb 1
Princeton University
Plasma Physics Laboratory
Princeton, New Jersey

Dr. R. F. Post 1
Radiation Laboratory
Livermore, California

Dr. W. Kunkel 1
U.C. Radiation Laboratory
Berkeley, California

Dr. R. J. Mackin 1
Jet Propulsion Laboratory
Pasadena, California

Dr. M. Allen 1
Microwave Associates
Burlington, Massachusetts

Dr. Irving Kaufman 1
Space Technology Laboratories
1 Space Park
Redondo Beach, Calif.

Prof. J. Van Bladel 1
Technicum der Rijksuniversiteit
Sint-Pietersnieuwstraat
Gent, Belgium

Prof. C. C. Johnson 1
Electrical Engineering Dept.
University of Utah
Salt Lake City 12, Utah